To the Graduate Council:

I am submitting herewith a thesis written by Thang Q. Dam entitled " Nanoparticle Measurement Methods in Internal Combustion Engines". I have examined the final paper copy of this thesis for form and content and recommend that it be accepted in partial fulfillment of the requirements for the degree of Master of Science, with a major in Engineering Science.

David K. Irick, Major Professor

We have read this thesis
and recommend its acceptance:

Dr. Jeffrey W. Hodgson

Dr. Ke Nguyen

Dr. John M. Storey

Accepted for the Council:

Vice Provost and Dean of Graduate Studies

Nanoparticle Measurement Methods in Internal Combustion Engines

A Thesis
Presented for the
Master of Science
Degree
The University of Tennessee, Knoxville

Thang Quoc Dam

December 2001

This thesis is dedicated to my parents, sisters, and brothers.

ACKNOWLEDGEMENTS

Throughout my time at the University of Tennessee I have gained a tremendous amount of support, help, and advice from my colleagues and friends. I would like to take this opportunity to thank the main actors in shaping my thesis.

I would like to thank Dr. John Storey, Oak Ridge National Laboratory (ORNL), for the support, guidance, and excellent supervision that he has given to me throughout every stage of my research. His real world experience provided me with more knowledge than whatever I have learned from books. He made my graduate study an important contribution work to the field of particulate emissions from engines in the future.

I would like to thank to Dr. David Irick, my faculty advisor, and Dr. Jeffrey Hodgson for encouraging me to join Graduate Automotive Technology Education (GATE) program at University of Tennessee at Knoxville (UTK) and set up my graduate research assistantship at ORNL. I appreciate all of the lively discussions with them about dilution device and aerosol technology.

Dr. Ke Nguyen in Mechanical and Aerospace Engineering and Engineering Science Department (MAES), UTK, for his valuable advising on designing micro dilution devices made me feel very encouraged.

Dr. Meng Dang Cheng, Environment Sciences Division, ORNL, for his help in evaluating the dilutors before they were used in this project.

I would like to thank to Mr. Gurpreet Singh, team leader of Engines and Emission Control Technologies, and Mr. Stephen Goguen, team leader of Advanced Fuels, in the Oak Ridge National Laboratory (ORNL) and the Office of Heavy Vehicle Technologies, were strong supporters of these effort for funding this research.

Special thanks to Dr. Robert Wagner, Mr. Ron Meyers, Mr. Norberto Domingo and the staff in the Advanced Propulsion Technology Center (APTC), ORNL who have provided a fun friendly working atmosphere.

Especially, I would like to thank Mr. Sidney V. McCulloch, machine shop technician, APTC, for his outstanding professional skill, helped me to build the dilutors.

Dr. Joseph Norbeck, Director of College of Engineering-Center of Environmental Research and Technology (CE-CERT), the University of California at Riverside, taught me fundamental automotive emissions and encouraged me to go further in education.

I wish to give special thanks to all my relatives, brothers and sisters. Their love and support have kept me going through rough times, and they seemed to always believe I would finish even when I did not believe it.

Especially my parents, Mr. Dam Huu Phuc and Ms. Nguyen Thi Dau, for their wish, encouraging, and invaluable support made me more persistent in achieving my goals.

Thanks to my youngest brother, Tuan Dam, for his emotional and financial support throughout my entire career as a student. I am sure he will be glad that this career is over.

Finally, I would like to thank my friend, Jenny Nguyen, for her love, support, and sacrifice.

ABSTRACT

The primary objective of this study is to investigate the characteristics of nanoparticle formation in dilute exhaust streams from diesel engines. Nanoparticle formation may be due to condensation, homogenous nucleation, coagulation and adsorption from low temperature, sulfate and water in exhaust system. After being released from the tail pipe, new nanoparticles also might be formed due to nucleation growth from low dilution ratio and long residence time. On the other hand, nanoparticles might be formed from dilution tunnels themselves. The artifact formation in dilution tunnels is due to specific problems that may occur in a dilution device, such as dilution ratio, dilution air temperature, dilution air pressure, residence time and critical flow orifice.

The experimental apparatus consists of a variable residence time, micro dilution system for exhaust dilution. Particle detection instruments consist of a scanning mobility particle sizer (SMPS), a condensation particle counter (CPC), and a NOx analyzer. Exhaust from modern diesel and gasoline engines was analyzed.

Two dilution devices were designed to simulate the process of engine exhaust into the atmosphere. For high dilution ratio from 5 to 10,000:1 and variable long residence time of 50 to 2000 ms, a first dilutor, Dilutor I, was used. For low dilution ratio from 5 to 300:1 and short fixed residence time of 50 ms, a second dilutor, Dilutor II, was used. Temperature, dilution ratio, and residence time were controllable. A NOx analyzer was used to check dilution ratio. A series of experiments was done to calibrate the dilutors. The results showed that the dilution devices alter particle size if particles were not solid.

Particle size measurements were taken upstream and downstream of a diesel particulate filter (DPF) with residence time changing from 50 ms to 700 ms, which increased nanoparticle concentrations by up to two orders of magnitude. Nanoparticles below about 20 nm in diameter were higher than in Microwave Regeneration Particulate Filter (MRPF) exhaust engine out during DPF regeneration.

The research should help for any future measurements of nanoparticles. The nanoparticle formation and growth under different dilution conditions needs to be investigated further. A nanoparticle formation model could be built to understand homogenous nucleation. Due to the

complex nature of the atmospheric dilution process, a dilution system could be developed in the laboratory to imitate the atmospheric processes.

The University of Tennessee, Knoxville (UTK) and the Oak Ridge National Laboratory have joined in this research. The Graduate Automotive Technology Education (GATE) Center of UTK, sponsored by U.S. Department of Energy (DOE), was the main participant, and the research was be conducted at Advanced Propulsion Technology Center (APTC), a research and evaluation laboratory for new internal combustion engines and emissions controls technologies. The DOE Office of Heavy Vehicle Technologies sponsored the research.

TABLE OF CONTENTS

CHAPTER 1 INTRODUCTION **1**

1.1 PARTICULATE MATTER IN THE ENVIRONMENT 1
1.1.1 Health Concerns 1
1.1.2 Particulate Matter Regulation 2
1.1.3 Nanoparticle Formation 3
1.1.4 Particle Measurement System 7
1.2 AEROSOL MECHANICS 9
1.2.1 Brownian Motion and Diffusion 9
1.2.2 Gravitational Settling 13
1.2.3 Inertial Impaction 13
1.3 GAS TO PARTICLE CONVERSION AND GROWTH 18
1.3.1 Nanoparticle Characteristics 18
1.3.2 Nucleation 23
1.3.3 Growth by Condensation 24
1.3.4 Growth by Coagulation 26

CHAPTER 2 MICRO-DILUTION DEVICE **28**

2.1 MICRO DILUTION DEVICE 29
2.1.1 Two-Staged Micro Dilution Device, Dilutor I 30
2.1.2 One-Staged Micro Dilution Device, Dilutor II 32
2.2 TRANSFER AND PROBES 32
2.3 EJECTOR 35
2.4 HEATING SYSTEM 36
2.5 MIXING PROFILES 36
2.6 ORIFICE 40

CHAPTER 3 RESEARCH METHOD **41**

3.1 APPARATUS 41
3.1.1 Scanning Mobility Particle Sizer (SMPS) 42
3.1.4 Condensation Nucleus Counter (CNC) 45
3.1.4 Electrospray Aerosol Generator (EAG) 45
3.1.5 Nitrogen Oxides Analyzer 48
3.1.6 Tapered Element Oscillating Micro-balance (TEOM) Detector 48
3.1.7 Flow System 48
3.1.10 Dilutor Cleaner (DC) 49
3.2 EXPERIMENTAL PROCEDURES 52
3.2.1 Dilution Calibration with NaCl and DOP Aerosols 52
3.2.2 Experiments on Engine Dynamometer Tests and Dilutors 53
3.2.2 Diesel Particulate Filter 55
3.2.3 Heavy-Duty Diesel 55
3.2.4 Light-Duty Diesel 55
3.2.5 Spark-Ignited Direct Injection Gasoline Engine 57

CHAPTER 4 EXPERIMENT RESULTS AND ANALYSIS **60**

4.1 DILUTION DEVICE CALIBRATION 60

4.2 INFLUENCE OF DILUTION RATIO 63
4.3 INFLUENCE OF RESIDENCE TIME 63
4.4 INFLUENCE OF DIESEL PARTICULATE FILTERS 66
4.5 INFLUENCE OF SULFUR FUEL 67
4.6 INFLUENCE OF ENGINE TECHNOLOGY 67
4.6 INFLUENCE OF EXHAUST GAS TEMPERATURE 70

CHAPTER 5 SUMMARY AND CONCLUSION 75

5.1 RECOMMENDATION FOR FUTURE RESEARCH 76

REFERENCES 77

APPENDICES 82

A AEROSOL CALCULATIONS 83
B PARTICLE MEASUREMENT SYSTEMS 84
C DILUTION RATIO 84
D HOW TO OPERATE THE DILUTORS 97
E UNITS OF GAS 99

VITA 101

LIST OF FIGURES

Figure 1.1 The human respiratory system (A) and penetration of fine particles into the alveoli (B) (Adapted from Hinds and Sher)..... 4
Figure 1.2 Schematic of four phases that could happen during exhaust process..... 6
(Adapted from Khalek *et. al.* [7])..... 6
Figure 1.3 Ultra-fine particles formation process (Adapted from Lipkea, *et al.*)..... 6
Figure 1.4 Particulate composition and structure (Adapted from Heywood [8])..... 7
Figure 1.5 Above figure is orifice inserted in sampling line and below figure is ejector and main sampling line setup..... 17
Figure1.6 Typical engine exhaust sizes distribution both mass and number weightings are shown (Kittelson).[31] 20
Figure 1.7 Typical engine exhaust sizes distribution both mass and number weightings are shown 21
Figure 1.8 Even though mass of spherule A is the same as mass of spherule B, but number 22
of size concentration and surface area of spherule A is less than spherule B..... 22
Figure 1.9 The differences between supersaturation and condensation which affect formation of particles (Adapted from Hinds) 23
Figure 2.1 Schematic of Mini Dilution device constructed by Abdul-Khalek *et al.* (Redrawn from SAE980525) 29
Figure 2.2 A schematic of one stage dilution device. 31
Figure 2.3 Dilutor I is two staged micro dilution device 33
Figure 2.4 Dilutor I is one staged micro dilution device 34
Figure 2.5 Sampling line and probe in Dilutor I and II..... 35
Figure 2.6 Basic structure of ejector. 37
Figure 2.7 Photograph of heated line which is used 38
to connect from the dilutor to exhaust gas system. 38
Figure 2.8 Photograph of heating tapes, thermocouple, and mixing chamber..... 38
Figure 3.1 Schematic of experimental apparatus. 41
Figure 3.2 TSI Model 3949 SMPS system : 3071 Electrostatic Classifier and 3025 CPC. 43
Figure 3.3 Schematic of a TSI Model 3934 SMPS..... 44
Figure 3.4. A diagram of the central rod..... 44
Figure 3.5 The above picture is TSI Model 3936 SMPS and the bottom picture is the schematic of 3936 SMPS. 46
Figure 3.6 Schematic of TSI Model 3025 CNC..... 47
Figure 3.7 The above picture is Model 3480 Electrospray Aerosol Generator. The below picture shows the process in which a neutralized monodisperse aerosol is formed. 47
Figure 3.8 Photograph of NOx and HC analyzers 49
Figure 3.9 TEOM measurement..... 50
Figure 3.10 Two different HEPA filters and one regulator were installed on the Dilutor I. 50
Figure 3.11 Mass Flow system consists of a HEPA filter, a Mass Flow Controller HFC-230 (above picture) and a Mass Flowmeter HFM-201 (bottom picture)..... 51

Figure 3.12 Photograph of dilutor cleaner. 51
Figure 3.14 Diesel particulate filter 56
Figure 3.15 Microwave regenerated particulate filter 56
Figure 3.16 Heavy duty Diesel Detroit Series (DDS) 50 engine 58
Figure 3.17 Volkswagen 1.9 liter engine 58
Figure 3.18 Mitsubishi 4G9 Series 1.9 liters 59
Figure 4.1 NaCl aerosol distribution (A), coefficient of variation by particle size (B), and coefficient of skewness (C) before and after dilutor. (source from Cheng *et al.*[50]).. 61
Figure 4.2 DOP aerosol distribution (A), coefficient of variation by particle size (B), and coefficient of skewness (C) for DOP aerosol comparison before and after dilutor. (source from Cheng *et al.*[50]) 62
Figure 4.3 Number concentration difference for different dilution ratio (DDS engine, 1950 rpm, 37% load, 3ppm S fuel, engine out). 64
Figure 4.4 Number concentration distributions for different residence times . The volume in the nuclei mode grows considerably with residence time (DDS engine, 1950 rpm, 37% load, 40ppm S fuel, engine out). 65
Figure 4.5 Influence of catalyzed diesel particulate filter exhaust in engine out and catalyst out in DR = 10 and RT = 700 ms (DDS engine, 1950 rpm, 37% load, 40ppm S fuel). 68
Figure 4.6 Comparison between CR-DPF and CDPF in effect on number concentrations (DDS engine, idle, 40ppm S fuel) 68
Figure 4.7 Number concentration difference between regeneration process (o), engine out (Δ), and MRPF out (□) (VW 1.9 L engine, 1491 rpm, 150ppm S fuel). 69
Figure 4.8 Comparison between two different sulfur fuels: 3 ppm and 40 ppm operated in DDS engine and DPF from Engelhard (DDS engine, 2100 rpm, full load). 69
Figure 4.9 Influence of EGR in engine technology, a increasing in load only effect the range of diameter size larger than 50 nm. The nuclei mode did not happen. 71
Figure 4.10 Size distribution and number concentration in heavy duty Detroit diesel engine . (2100 rpm, 37% load, 3ppm S fuel, engine out). 71
Figure 4.11 Size distribution and number concentration in light duty Volkswagen 1.9 L diesel engine (1991 rpm, 150ppm S fuel, engine out). 72
Figure 4.12 Size distribution and number concentration in light duty Mitsubishi SIDI gasoline engine (1950 rpm, 40% load, indolene fuel, engine out). 72
Figure 4.13 Shows the trend of increasing the number concentration at low exhaust temperature (SIDI engine, 3400 rpm, Indolene fuel, engine out). 73
Figure C1 Effect of saturation ratio for two condensable species at two exhaust temperatures (Kittelson and Dolan, 1980) 85
Figure C.2 Air supply and air consumption for the ejector. 95
Figure D1 Main components need to be checked. 98
Figure D2 Orifice sampler 98
Figure D3 Orifice box with different orifice samplers 98

LIST OF TABLES

Table 1.1 Diffusion coefficients for gas or airborne particles @ 1.0 atm and 20 °C 17
Table 1.2. Definitions of some technical terms [17] 21
Table 1.3 Properties of Coagulation, Condensation, and Nucleation [34] 27
Table 2.1 Specifications of one-stage micro dilution device 31
Table 2.2 Specification of ID 2.5" and ID 2" tubes 31
Table 2.3 Transfer line and probe characteristics 35
Table 2.4 Configuration of ejector TD110HSS manufactured by Air Vac Engineering Company Inc. 37
Table 2.5 Specifications of the heating system: 37
Table 3.1 Specifications of the engines used in this project 54
Table 3.2 Experiment Conditions 54
Table 3.3 Summary of three different modes 54
Table 3.4 Composition of Fuels 54
Table 3.5 Summary of test conditions on heavy duty diesel 57
Table 3.6 Summary of test conditions on light duty diesel 57
Table 3.7 Summary of test conditions on light duty gasoline 57
Table 4.1 Testing Conditions 64
Table 4.2 Summary of the three engine test conditions. 70
Table A.1 Calculated properties on the size of 0.01-nm particles at 293 K* 83
Table C1 Relationship between sonic velocity and orifice sizes. 88
Table C2 Summary of the orifice sizes and dilution ratios used in the dilutors. 89
Table C3 Residence time calculation: Dilutor I and II 91
Table C4 Relationship between pressure and air flow correction factor of the flowmeter 95
Table C5 Relationship between mass air flow correction factor of the Mass Flowmeter (HFM-201) and controller (HFC-203) 96
Table E1 Mass concentration of several main pollutants at different temperatures. 100

LIST OF NONMENCLATURE

A	area, cross-sectional area (m^2)
A_p	cross-sectional area of a particle(m^2)
A_s	surface area (m^2)
Al_2O_3	aluminum trioxide
b	empirical constant (dimensionless)
C_x	*f* pollutant concentration point x (mg/m^3)
C_0	pollutant concentration at x ‹ 0 (mg/m^3)
C_c	Cunningham slip correction, dimensionless
$C_{i;in}$	concentration of pollutant i entering the dilutor (g/m^3)
$C_{i;out}$	concentration of pollutant i leaving the dilutor (g/m^3)
C_{iv}	pollutant concentration in the inlet ventilation air (mg/m^3)
CO	carbon monoxide
CO_2	carbon dioxide
d_c	diameter of cylinder
d_d	droplet diameter
d_s	Stokes diameter
dn/dx	concentration gradient
D	particle diffusion coefficient
D_j	impactor jet diameter
D_s	sampling probe diameter
DOP	dioctyl phthalate
DPM	diesel particulate matter
f	fraction; frequency; frequency of light
f	fanning friction factor
F	correction factor (dimensionless)
F_D	force of gravity
F_G	drag force
g	gravity
HCs	hydrocarbons
H_2SO_4	sulfuric acid

J	diffusion flux
k	Boltzmann's constant
K_t	dimensionless thermophoretic constant
K	turbulence kinetic energy (m^2/s^2)
Kn	Knudsen number
K_R	Kelvin ratio
L	molecule weight
n	number of molecules per unit volume
NaCl	sodium chloride
NO_2	nitrogen dioxide
NOx	nitrogen oxides
$N(t)$	particle number concentration at time t
N_o	particle number concentraton at time 0
p	partial pressure, pressure
p_A	partial pressure of component A
p_{sv}	saturation vapor pressure
p_∞	partial pressure of vapor at droplet surface
P	penetration
PM	particulate matter
PAHs	polycyclic aromatic or polynuclear aromatic or polyaromatic hydrocarbons
Q	flow rate, air flow rate across the dilutor (m^3/s)
r	radius, cm
R	gas constant
R_b	bend radius
Re	Reynolds number
Re_o	initial Reynolds number
R_i	removal rate of pollutant i out of the dilutor (g/s)
S	stopping distance, Stokes terminal settling velocity, cm/s
Sc	Schmidt number
SR	saturation ratio
S_{tk}	Stokes number
SOF	soluble organic fraction
SO_2	sulfur dioxide

SO_3	sulfur trioxide
SO_4	sulfate
t	time
T	temperature
T_d	temperature at droplet surface
T_∞	temperature away from droplet
TiO_2	titanium dioxide
U	velocity, gas velocity (m/min)
U_e	velocity at x = 0 (m/min)
U^*	friction velocity
$\overline{U}$	average velocity
V	velocity of particle
V_d	deposition velocity
V_t	thermophoretic velocity
V_{st}	settling velocity of a particle
VOC	volatile organic compounds
x_{rms}	rms displacement of particle
x_t	position of particle at time t
β	correction factor for coagulation coefficient
δ	diffusion boundary-layer thickness
ΔC	concentration difference (g/m^3)
Δp	pressure drop
ΔT	temperature gradient
σ	standard deviation
ν	deposition velocity (m/min), kinematic velocity (m2/s)
η	vicosity ($N.s/m^2$)
λ	particle mean free path
μ	deposition parameter for diffusion loss in tubes (dimensionless)
ρ	density of gas, density of particle
τ	relaxation time
δ	diffusion boundary layer
ϕ	bend angle, Fuchs-effect correction factor

CHAPTER 1 INTRODUCTION

Compression ignition (CI) engines such as advanced direct-injection diesel engines are currently the most efficient internal combustion engines. CI engines are considered as the best candidate to combine with electric motors in hybrid electric vehicles (HEVs) in order to achieve the 80 miles per gallon goal (mpg) for the Partnership for a New Generation of Vehicles (PNGV). However, CI engines can emit high levels of particulate matter (PM) and oxides of nitrogen (NOx). It is likely that hybrid electric vehicle (HEV) engines will start and stop frequently, and go from start to a high fuel efficiency mode rapidly. This has the potential for particulate generation. Although technological improvements have reduced diesel particulate mass emissions, the new technologies may alter the chemical and physical character of diesel particulate matter (DPM) to high number concentration and surface area of small particles, especially, ultrafine particles (< 100 nm) and nanoparticles (<50 nm).[1] The decreasing size of these small particles has currently become an important issue because of the following: 1) impact of ultrafine particles on human health, 2) particulate matter emission regulation, 3) nanoparticle characteristics and activity, and 4) particulate matter measurement method. Any one of these issues could affect the future regulation of diesel engines.

1.1 PARTICULATE MATTER IN THE ENVIRONMENT

1.1.1 Health Concerns

Particulate matter is one of six criteria pollutants which are regulated by the U.S. government because of its impact on human health. Particulates are fine solids (dust or soot) or liquid particles (mist or fog) suspended in air. Their sizes are from 0.0002 to 500 μm (0.2 nm to 500,000 nm).[1] The size of the particles strongly affect their impaction the human respiratory system. While large particles can be kept by the hairs and lining of the nose, fine particles less than 250 nm can be transported deeply into the tracheobronchial system and held by mucus. Particles larger than 10 μm are often removed in the upper respiratory system. Particles less than 10 μm, PM_{10}, are small enough to reach the lung when they are deposited in there by sedimentation.[2] Particulate emissions from motor vehicles are generally fine particles, $PM_{2.5}$.

Nanoparticles (≤ 50 nm) are more dangerous to human health due to their small size. They tend to reach the alveoli regions of the lung where they are deposited due to diffusion. There are three main problems: 1) the overall gas exchange surface area of the alveoli is reduced, 2) alveoli cells die from volatile organic compounds adsorbed on particles, and 3) cancer can form in the lung cells. **Figure 1.1** shows the penetration of ultrtrafine particles into the alveoli. Recently, inhalation experiments conducted on rats using inert nanoparticles (21 nm) of titanium dioxide (TiO_2) and aluminum trioxide (Al_2O_3) showed deeper lung penetration and higher inflammatory lung response when compared with larger size particles (250 nm).[3] In addition, ultrafine particles may be the cause of excess deaths and asthma in children living near roadways.[4] Cheng, *et al.* .[5] also have been testing the impact of nanoparticles on human lung tissue and found an inflammatory response after exposure. In 2001, Annette, *et al.*[6] at Harvard School of Public Health reported that the more fine particles $PM_{2.5}$ in the air, the greater the risk of having a heart attack (48 percent greater risk). Older people with chronic heart or lung disease are affected the most. People also suffer more heart attacks on hot and hazy days of summer. It appears that there is a relationship between nanoparticle exposure and human health.

1.1.2 Particulate Matter Regulation

The U.S. government currently has focused on regulating particulate mass emission and limited fine particle mass concentration ($PM_{2.5}$) in the ambient atmosphere. The $PM_{2.5}$ is a concentration based emission regulation for particles less than 2.5 μm. The $PM_{2.5}$ national annual average ambient air quality standard is 15 mg/m^3. Heavy and light-duty diesel engine diesel particulate matter emission standard is 0.13 g/kWh (0.10 g/bhp.hr). Currently, light-duty spark-ignited gasoline engines do not currently have a PM emission standard. Engine manufacturers have developed low-emission engines to meet these standard requirements. However, the new modern engines with direct high-pressure injection system create small fuel droplets which may result in a high number of nanoparticles which have a low mass. Low concentration of soot agglomerates may help for nucleation growth by adsorption or condensations of volatile materials. In the case of the engine and dilution system tested here the volatile materials are the soluble organic fraction (SOF) or sulfuric acid. Therefore, government agencies and engine manufactures have been interesting in finding the size distribution and number concentrations emitted from the engines.

Depending on how much nanoparticles affect human health, particles number and particle surface could be included in emission regulation in the future.

1.1.3 Nanoparticle Formation

Nanoparticle emission formation in diesel engines are complex processes. They form in combustion process, exhaust process, and dilution process. Modern low emission engines produce low concentration of soot agglomerates. The absence of these agglomerates to act as sites for adsorption or condensations of volatile materials make nucleation and high number emissions more likely.[7]

There are three phases of particle growth that could occur in diesel combustion process. The first phase begins during combustion with black carbon particles (soot), which are formed in fuel rich regions in the combustion chamber. Heywood [8] and Amann *et. al* [9] described in detail how soot is formed in combustion engine. Decreasing the duration of diffusion combustion and promoting soot oxidation during the expansion stroke can reduce formation of soot agglomerates. Increasing the fuel injection rate enhances both of these effects. The primary means of accomplishing this is by increasing fuel injection pressure. Increased injection pressure can significantly reduce soot emissions (mass), but can increase particle emissions (number). It can also increase combustion temperatures and cause an increase in NOx emissions. Another primary combustion product results from fuel sulfur. During combustion, sulfur compounds present in the fuel are oxidized to sulfur dioxide (SO_2). Approximately 1% to 4% of fuel sulfur is oxidized to SO_3, which combines with water vapor in the exhaust to form sulfuric acid (H_2SO_4).

The second phase of particle growth begins during the expansion stroke as a result of cooling of hot exhaust products. In this phase, gas phase metallic from lube oil may either adsorb onto soot particles or act as nucleation sites to form new particles. The third phase of particle growth occurs as a result of cooling and diluting hot exhaust emissions with atmospheric air. In this phase, the hot exhaust which consists of unburned fuel, partially burned fuel, lube oil and existing nucleation particles is cooled and diluted with air. Semi-volatile components can condense into particles. The existing nucleation particles could be formed in the second phase. There are two events that may happen in this phase. First, the volatile particles could adsorb onto existing

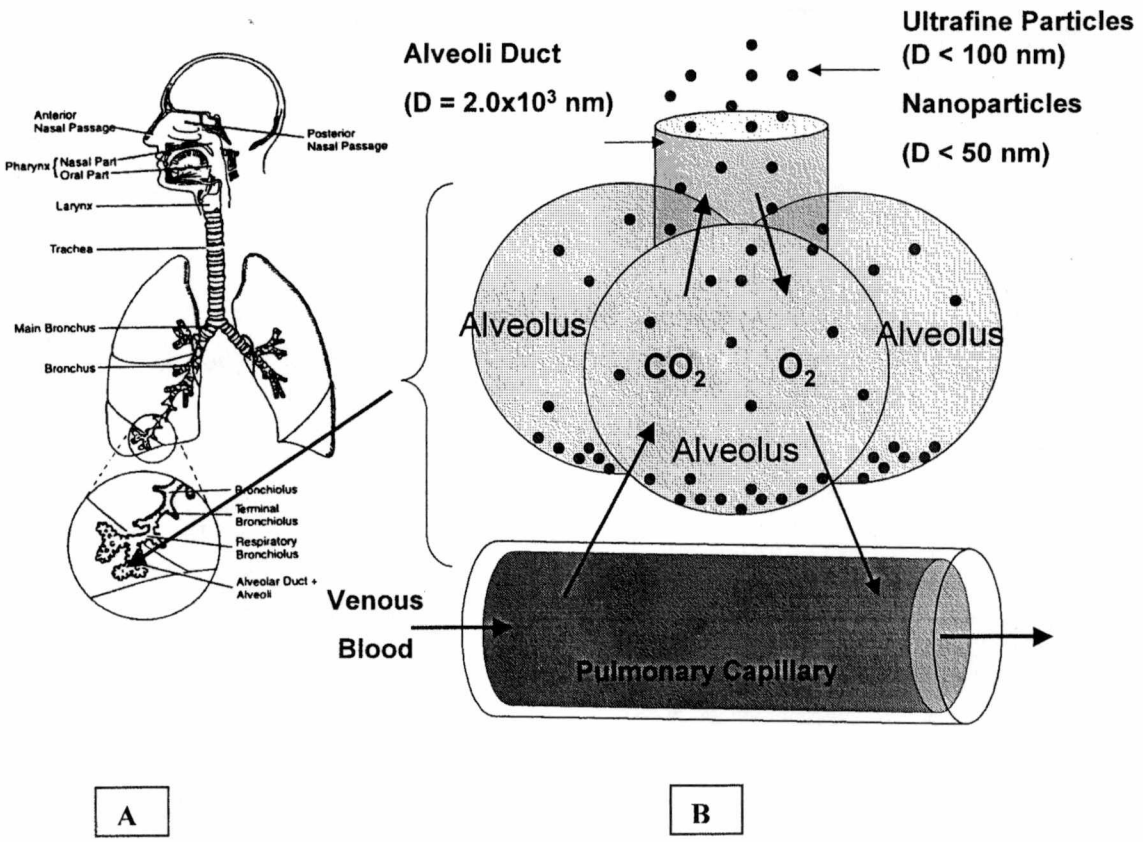


Figure 1.1 The human respiratory system (A) and penetration of fine particles into the alveoli (B) (Adapted from Hinds and Sher).

particles, consequently, the mass of particulate increases while the number concentrations stay the same. Second, self-nucleation (homogenous nucleation) may play a role. Because of this, both mass and number concentrations will increase. Finally, sulfate in the exhaust dilution may nucleate with water and create higher particle number concentrations as well. **Figure 1.2** and **1.3** shows four phases that could happen in the formation of nanoparticles during exhaust process.

Diesel exhaust is a complex mixture of particles and gases with hundreds of chemical compounds, including many organic compounds, present in the particles and in the gases. There are more than 10,000 chemical compounds which could be identified.[10] The particles are very small (a mean aerodynamic diameter of about 100 nm) and have an elemental carbon core.

Therefore, they are highly respirable. The small particles have a large surface area on which many organic compounds are adsorbed. The organic compounds contribute from 10% to 30% of particle weight. The gases have both inorganic and organic constituents (e.g., sulfur dioxide, nitrogen oxides, benzene, ethylene, toluene, aldehydes, olefins, and low molecular-mass polyaromatic hydrocarbon (PAHs). The individual particles are principally clusters of many small spheres or spherules of carbon at temperatures about 500°C. These spherule's diameters are about 15 to 30 nm. **Figure 1.4** show as temperatures decrease below 500°C, the particles become coated with adsorbed and condensed high molecular weight organic compounds which include: unburned hydrocarbons (HC), oxygenated HC (ketones, esters, ethers, organic acids) and polynuclear aromatic HCs (PAHs). The condensed material also includes inorganic species such as sulfur dioxide (SO_2), nitrogen dioxide (NO_2), and sulfuric acid (H_2SO_4) or sulfate. By maintaining exhaust temperature above 300°C, Storey [11] reported that a catalyzed soot filter (CSF) excellently removes the soot sized PM and increases in number density the smallest ultrafine PM. The CSF is known to desorb sulfur compounds and promote the oxidation of SO_2 to SO_3. As a consequence, H_2SO_4 droplets will form faster due to high sulfate concentration. Since vapor saturation pressure is dependent on temperature, as the temperature decreases, the saturation ratio increases. As a result, condensation occurs. In summary, there are two ways to describe nucleation growth: 1) number concentration is unchanged with surface growth only, 2) number concentration is changed due to new particle growth.

In 1996, the Health Effect Institute (HEI) showed that a modern high-pressure direct injection diesel engine emits at least one order of magnitude higher number concentration than older technology engines.[12] Furthermore, the University of Minnesota (UMN) has also demonstrated that diesel engine aftertreatment devices such as particulate traps and catalytic converters might result in very high number concentrations of particles [6].

Kato *et al.*[13] investigated particulate formation of a DI diesel engine with direct sampling from combustion chamber. The concentrations of total particulate matter (TPM) and of its two components, the Soluble Organic Fractions (SOF) and the Insoluble Fractions (ISF), were found at sampling positions along the spray flame axis. The concentrations of SOF and ISF were higher at sampling positions closer to the wall than away from the wall. Their results suggested that SOF formation is significantly affected by wall quenching. Also, PM concentrations were much higher in the combustion chamber than in the exhaust.

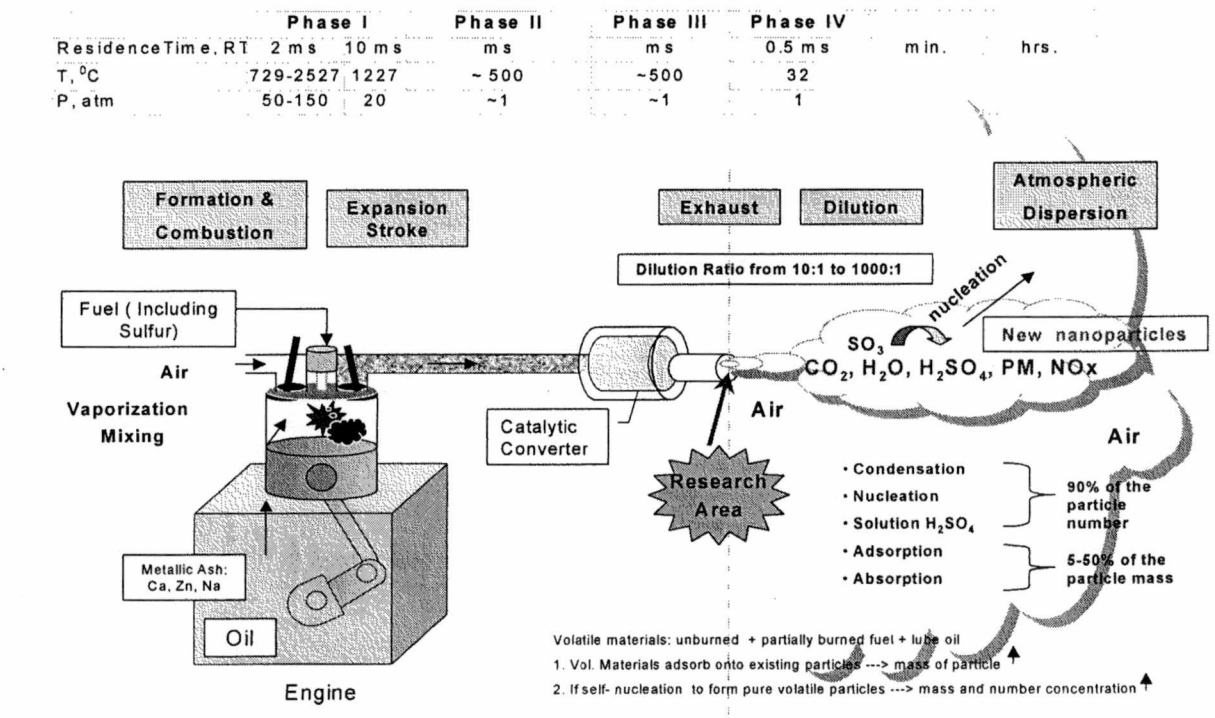


Figure 1.2 Schematic of four phases that could happen during exhaust process (Adapted from Khalek *et. al.* [7])

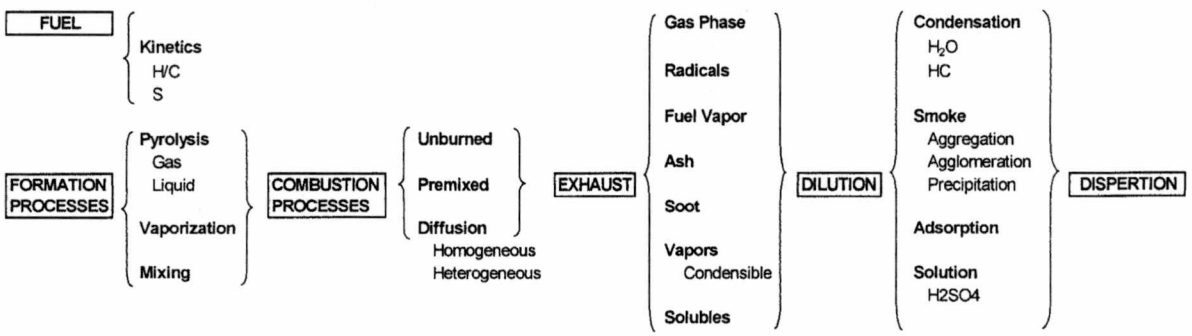


Figure 1.3 Ultra-fine particles formation process (Adapted from Lipkea, *et al.* [14])

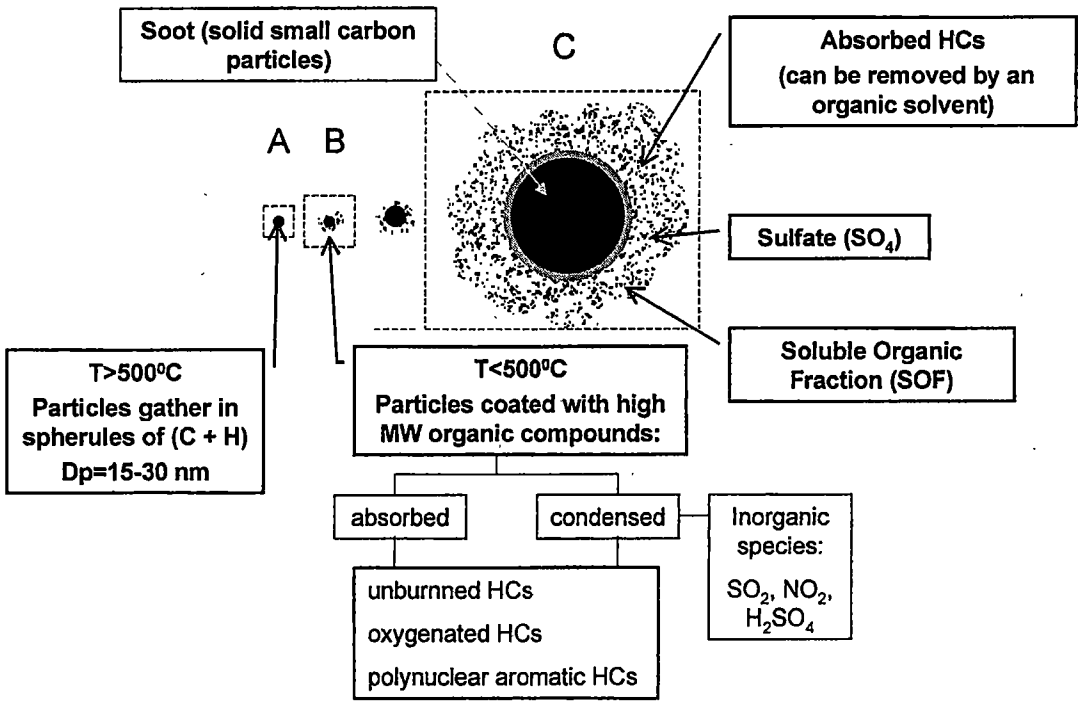


Figure 1.4 Particulate composition and structure (Adapted from Heywood[8])

Therefore, it is important to understand aerosol formation, transformation, and the processes that have major effects on the aerosol size distribution, which include dilution, nucleation, condensation, adsorption, and coagulation.

1.1.4 Particle Measurement System

Most particulate measurement techniques are used to determine the mass of particulate being emitted to the atmosphere. Most techniques require long sample-collection periods because of low concentration of individual species. The physical conditions during particulate measurements are critical. The emitted species from the process are unstable and may be altered through loss

from surfaces, and changes in size distribution (through collisions). In addition, some dilution devices employ flow through an orifice at sonic velocity which creates turbulence that may set up shear forces strong enough to break apart some types of particles. [15]

Techniques for particulate measurement and characterization range from simple smoke meter opacity readings to analyses using dilution tunnels. Smoke meters do not measure mass directly. In the standard mass emission measurement procedure, dilution tunnels are used to lower the temperature of the exhaust below the dew-point temperature. In the dilution tunnel, the exhaust gases are diluted with ambient air to a temperature of 52°C or less. A sample stream from the diluted exhaust is filtered to remove the particulate and another sample stream is used to count number concentration.[8] Most particle detection instruments used for exhaust particle measurements operate at ambient temperature and pressure. Dilution and cooling of hot exhaust are required in these instruments. This requirement is due to both the high particle number concentration, and the need to lower the dew point of the gases. Most laboratories have standard dilution tunnel devices. Most of the dilutors are designed for mass measurements and have a relatively long residence time, low dilution ratio and high dilution temperature.

Currently, there is no standard dilution system for particle number concentration and size distribution measurements from engines because many dilutors have been used to characterize particulate emissions at different engine operating and dilution conditions.[16] One system in particular, the ejector pump dilutor (micro-dilutor), has been used extensively at the University of Minnesota (UMN). This device is compact and can provide a wide range of dilution conditions. However, little is understood about artifact formation in the micro-dilutor. Artifacts include thermophoretic loss of the small particles to the walls, discrimination by the inlet orifice, shear force from highly compressed air, and velocity change of airflow in diverging-converging duct. There is no published study that investigates the turbulent mixing effect on the particle size distribution as well. The narrow critical flow orifice used to obtain high dilution may preferentially favor the entrainment of nanoparticles and ultrafine particles. The dilution process may artificially cause larger or smaller particle sizes through condensation and coagulation processes. The dilution ratio may influence the amount of exhaust volatile materials adsorbed onto particles. An evaluation of artifacts and measurement procedures is required to use the micro-dilutors effectively.

1.2 AEROSOL MECHANICS

In this section, aerosol mechanics that may be responsible for particle losses such as particle Brownian diffusion, settling, and inertial impaction will be discussed. An understanding of particle movement in a gas is necessary to build a micro-dilution device. The rate of transport of particles across at a point is called the flux at the point.

1.2.1 Brownian Motion and Diffusion

Diffusion is the net transport of aerosol particles undergoing irregular, or Brownian, motion in a concentration gradient from a higher concentration region to a lower concentration region. This is due to the random motion of particles suspended in gas.[17] The diffusion coefficient D relates the flux J of aerosol particles to the concentration gradient. In the absence of any external force, Fick's first law of diffusion is:

$$J = -D\frac{dn}{dx} \tag{1.1}$$

where dn/dx is the concentration gradient

Aerosol diffusion coefficient can be written as:

$$D = \frac{kTC_c}{3\pi\mu d_p} = \frac{x_{rms}^2}{2t} \tag{1.2}$$

and dimensionless deposition parameter, μ,

$$\mu = \frac{4DL}{\pi d_t^2 \overline{U}} = \frac{DL}{Q} \tag{1.3}$$

Another way to describe flux is in term of Brownian motion

$$J = -\frac{(x_{rms})^2}{2t}\frac{dn}{dx} \tag{1.4}$$

where D is the diffusion coefficient

k is the Boltzmann's constant

T is the absolute temperature

C_c is the Cunningham slip correction factor

μ is the dimensionless deposition parameter

d_p is the particle diameter

x_{rms} is the individual displacements with their rms average value

t is the time that the particle moving L is the length of the tube

d_t is the diameter of the tube

$\overline{U}$ is the average velocity

Q is the flow rate

Table 1.1 shows diffusion coefficient for particles and gas molecules. For gas molecules, diffusion coefficients are much larger than those for large particles. Therefore, gas molecules mix much faster than particles in laminar flow. For a polydisperse aerosol mixing with dilution air in laminar flow, dilution ratios vary with the size of particles. Measuring the dilution ratio for a gas to obtain the dilution ratio for particles is not suitable for an aerosol dilution in laminar flow. Gormley *et al.* [18] provided two equations applied to laminar flow (Re<2300) and turbulent flow Re>2300. Under turbulent flow conditions where the Re > 2300, the deposition velocity (V_d) depends on the diffusion coefficient of particles and the thickness of the diffusion boundary layer (δ):

$$V_d = \frac{D}{\delta} \tag{1.5}$$

Fuch [19], and Davis *et al.* [20] realized that the diffusion boundary layer is difficult to predict because the flow and the size of the particles The approximations for different flow conditions have been made V_d can be expressed as [21]:

$$V_d = 0.042Uf^{1/2}Sc^{-2/3} \tag{1.6}$$

$$f = \frac{U^*}{U} = \frac{0.316}{4(\mathrm{Re})^{1/4}} \tag{1.7}$$

$$Sc = \frac{\mu}{\rho D} \tag{1.8}$$

where f is the fanning friction factor

$U^*$is the friction velocity

U is the average velocity of the fluid

Sc is the Schmidt number.

The penetration, P, is the fraction of particles entering a circular cross section. The overall penetration of particles through a tube of length L subjects to losses as a result of turbulent diffusion, assuming constant concentration and deposition velocity. Diffusion losses are most important when sampling through a tube. The overall penetration is defined as:

$$P = \frac{n_{out}}{n_{in}} = \exp\left(\frac{-4V_{dep}L}{d_t\overline{U}}\right) = \exp\left(-\frac{2\pi R_t L V_d}{Q}\right) \tag{1.9}$$

$$P = 1 - 5.50\mu^{2/3} + 3.77\mu \qquad \text{for } \mu < 0.009 \tag{1.10}$$

$$P = 0.819\exp(-11.5\mu) + 0.09751\exp(-70.1\mu) \qquad \text{for } \mu \geq 0.009 \tag{1.11}$$

where Q is the volume flow rate.

Equations 1.10 and 1.11 gives the penetration P as a function of μ (for all value of μ). For example, a 10 nm particle in dilution exhaust of 50°C is sampled at the volume flow rate, Q, at 1 liter per minute (lpm) through inside diameter (ID) 0.186 in. and the tube length of 3.65 in. The

diffusion coefficient, D, is 5.33 x 10^{-4} cm^2/s and the dimensionless deposition parameter, μ, is 0.00029 (See Appendix A).

For $\mu > 0.3$, all particles are lost to the tube walls. For $\mu < 0.001$, particle losses by diffusion to the walls are small. Because the time is too short in turbulence flow, fine particles do not deposition to the walls.

In turbulent tube flows, deposition is a function of the Schmidt and the Reynolds numbers. Malet *et al.* [22]. reported that nanometer size aerosols deposition is found to be enhanced by about 50% for the rough surface tube compared to the other surface roughnesses.

Finally, the other way that particles can be deposited on the walls of sampling lines and probes is temperature gradient, a process called thermophoresis. Due to the temperature difference a thermophorestic force is introduced in addition to the drag, gravity, and Brownian forces. The temperature gradient is high in combustion engines, therefore, the themophoresis force becomes significant. Thermophoresis is also the main driving deposition force for the thermal precipitator used in aerosol sampling.[23] Talbot *et al.*[24] derived an equation for thermophoretic velocity in terms of temperature gradient in the gas with the Stokes drag force and expression for the terminal velocity.

$$Vt = -K_t \upsilon \frac{\nabla T}{T} \tag{1.12}$$

where V_t is the thermophoretic velocity

K_t is the dimensionless thermophoretic constant (between 0.55 and 0.45 for particles in the diesel size range)

ν is the kinematic viscosity of the gas

∇T is the temperature gradient in the gas

T is the average temperature of the gas near the particle

Kato *et al.*[13] investigated of particulate formation of DI diesel engine with direct sampling from combustion chamber. Particulate formation is a function of location along the wall and distance from the wall.

1.2.2 Gravitational Settling

When a particle is released in air, it quickly reaches its terminal settling velocity due to gravitational force. Terminal settling velocity increases rapidly with particle size (proportion to the square of the particle diameter). In the absence of other forces, relatively large particle, ≥ 0.5 μm in diameter, tend to flow with the movement of air. According to Hinds [17] and Agarwal *et al.*[25], if t >> τ, the particle reaches a constant velocity, V_{st} is defined as:

$$V_{st} = \tau g = \frac{1}{18}\frac{C_c \rho_p d_p^2 g}{\mu} \tag{1.13}$$

$$C_c = 1 + \frac{2.514\, l}{D} \qquad \text{(for } 0.1\ \mu m \le D \le 1.5\ \mu m\text{)} \tag{1.14}$$

where V_{st} is the settling velocity of a particle,

$\overline{U}$ is the average gas velocity in the sampling tube

g is the gravity

τ is the relaxation time of a particle

C_C is slip correction factor or Cunningham connection factor

The equation 1.14 for the terminal settling velocity only applies to particles with diameters ≥ 1.5 μm. Agarwal *et al.*[25] reported that if the Reynolds number is larger than 2300, particles (larger than 1 μm) are brought closer to the surface of the wall of a tube. If the Reynolds number exceeds 12,500, the losses affect large particles (>300 nm in diameter). Finally, nanoparticles do not settle via gravity at a significant rate, they undergo turbulent diffusion that affects the losses of nanoparticles. [17]

1.2.3 Inertial Impaction

Impaction, a special case of curvilinear motion, is a mechanism that leads to deposition of particles on the tube wall due to their inertia. Particles whose inertia exceeds a certain value are unable to follow the streamlines and impact on the flat plate. It mostly occurs in bends and

sampling inlet of the particle measurement system. [17] The stopping distance of particles and a characteristic length of a particular geometry affect the Stokes number (S_{tk}). The Stokes number is defined as:

$$S_{tk} = \frac{S}{d_c} = \frac{\tau U_0}{d_c} \qquad \text{for } \mathrm{Re}_0 < 1.0 \qquad (1.14)$$

$$\mathrm{Re}_o = \frac{\rho_g d_p U_o}{\eta}$$

where S is the stopping distance

d_c is the diameter of cylinder

U_o is the undisturbed air velocity well away from the cylinder

Re_o is the initial Reynold number

When Stokes number is larger than 1, particles continue moving in a straight line which leads to particle deposition. When Stokes number is smaller than 1, particles follow the gas streamlines.

An impactor separates aerosol particles into two size ranges. Particles larger than a certain aerodynamic size are removed from the airstream. Particles smaller than the aerodynamic size pass through the impactor. The other Stokes number formula is applied in terms of the nozzle radius $D_j/2$:

$$Stk = \frac{\tau U}{D_j} = \frac{\rho_p d_p^2 U C_c}{9\eta D_j} \qquad (1.15)$$

where S is the stopping distance

ρ_P is the particle density

d_P is the particle diameter

U_o is the undisturbed air velocity away from the cylinder

U is the average nozzle exit velocity

μ is the kinematic viscosity of the gas

Re_0 is inertial Reynold, $\rho_g d_p U_o/\eta$

1.2.3.1 Tube Bend

Particles may be lost in the tubing and fittings between the inlet and the measuring device. Loss in tube bend is not important for particles less than 1 μm in diameter. For laminar flow, the inertial deposition of particles in a tube bend is given by the empirical equation: [17]

Bend loss = (Stk)ϕ

For turbulent flow in a tube bend, an empirical equation by Pui *et al.* [26], and Cheng *et al.* [27] gives

Bend loss = 1 – exp(-2.88(Stk)ϕ)

They also described particle loss in particle penetration (*P*), which is the ratio of downstream concentration in tube bends, in the following equations:

$$P = 1 - \left(1 + \frac{\pi}{2R_0} + \frac{2}{3R_0^2}\right)St \quad \text{for Re} < 5000 \qquad (1.16)$$

$$P = 10^{(-0.963St)} \quad \text{for Re} > 5000 \qquad (1.17)$$

where R_b is the bend radius, R_t is the tube radius, R_o is the ratio of bend radius over tube radius, ϕ is the bend angle in radians

1.2.3.2 Sampling Inlet

Once a sample of aerosol has entered a sampling line and is being drawn along a tube. According to the Davis criteria [20] on particle sampling from free stream, sampling bias due to inertial

impaction become important if $S_{tk} \geq 0.032$. For engine particles of 10 to 100 nm in a diluted exhaust, Stokes numbers are 0.0000018 to 0.000024. The fraction penetration is 99 % (See Appendix A). Inertial forces affect the penetration at a sampling inlet. This typically occurs when sampling from a flowing gas stream via a sampling probe. The following is two different samplings:

- Isokinetic sampling can be defined as sampling by drawing a suspension into a probe at the same linear velocity as that of the bulk of the suspension. It is negligible when sampling particles below 1 μm in diameter. [20]

- Orifice is used to control the dilution ratio the aerosol sample (See Appendix B and C). A steep contraction of the fluid occurs before fluid enters the orifice. This may lead to particle losses via inertial deposition. Yan *et al.* [28] developed a model to predict losses in a similar configuration.

The empirically correlated penetration, which is defined as the ratio of particle concentrations leaving the orifice over the concentration entering the tube, is expressed as:

$$P = \exp(1.721 - 8.557x + 2.227x^2) \tag{1.18}$$

$$x = \frac{\sqrt{St}}{(D_e / D_0)^{0.31}}$$

where D_e is the diameter of the tube

D_0 is the diameter of the orifice

According to Davis *et al* [20] losses in orifices due to particle inertial deposition can be significant for particles above 1 μm in size. **Figure 1.5** shows the structure of orifice in sampling line and ejector.

Table 1.1 Diffusion coefficients for gas or airborne particles @ 1.0 atm and 20 °C

Gas of Airborne Particles (μm)	Diffusion Coefficient (m^2/s)	D_{air}/D
Air (dry)	0.19	1.00
H_2O (vapor)	0.24	0.79
N_2	0.2	0.95
0.01	5.31×10^{-4}	3.578×10^{2}
0.05	2.37×10^{-5}	8.016×10^{3}
0.1	6.84×10^{-6}	2.778×10^{4}
0.5	6.31×10^{-7}	3.011×10^{5}
1.0	2.76×10^{-7}	6.884×10^{5}
5.0	4.89×10^{-8}	3.885×10^{6}
10.0	2.40×10^{-8}	7.917×10^{6}

Source from Hind, C. W., Aerosol Technology

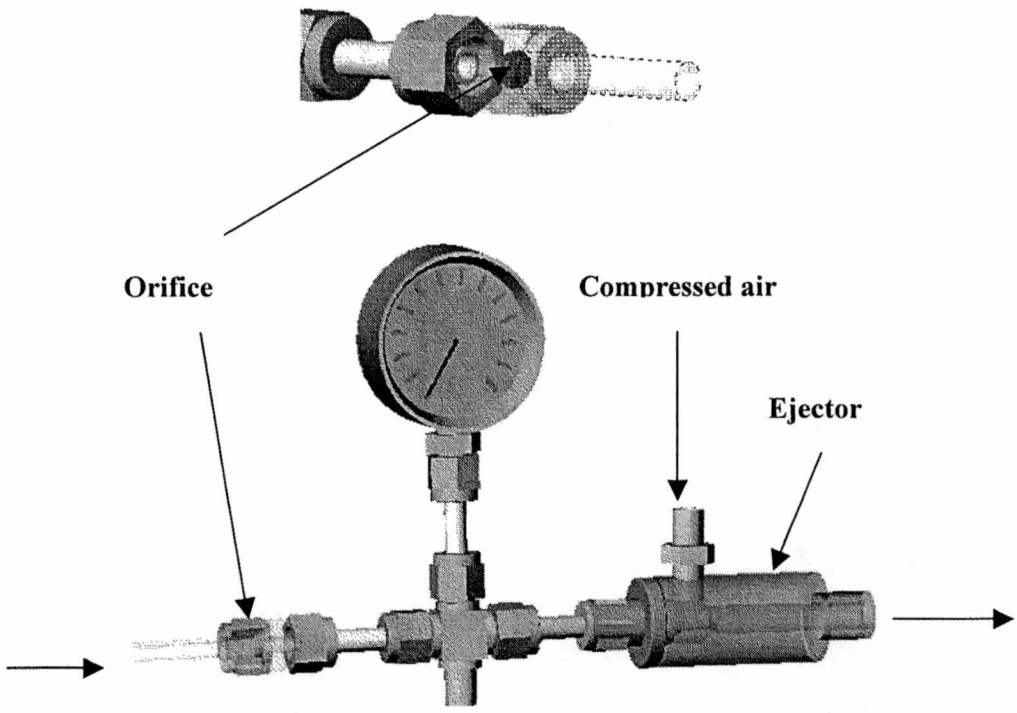


Figure 1.5 Above figure is orifice inserted in sampling line and below figure is ejector and main sampling line setup.

1.3 GAS TO PARTICLE CONVERSION AND GROWTH

In this section, nanoparticle characteristics, thermodynamic equilibrium properties of small particles, and the formation of new particles from a continuos phase referred to as nucleation will be discussed. Hot exhaust gas is a complex mixture of solid carbon, ash particles, nitrogen, oxygen, nitric oxide, carbon dioxide, and volatile species which consist of condensable water vapor, hydrocarbons, and sulfate. During dilution and cooling of hot exhaust, the volatile gas phase material has the potential to nucleate into new particles by adsorbing, or condensing on existing solid particles. Particles can also form from the coagulation of smaller particles. Therefore, it is important to understand the development of gas to particle conversion and growth due to nucleation, condensation, and coagulation.

1.3.1 Nanoparticle Characteristics

Nanoparticle emissions in diesel engines are formed in complex processes. They form in the combustion process, the exhaust process, and the dilution process. Nanoparticle concentrations can be expressed in terms of number, surface, or volume. Particulate matter size and number are the most important focus of this project. Particulate matter size distributions typically follow log-normal bimodal distributions or a lognormal, trimodal distributions (**Figures 1.5** and **1.6**). There are three typical modes of particles: nuclei mode particles, accumulation mode particles and coarse mode particles.

Nuclei-mode particles consist of combustion particles released directly into the atmosphere from exhaust system and formed in the atmosphere by gas-to-particle conversion. The particle range is from 0.005 - 50 nm in diameter size. In this range, the basic building blocks of solids are established, where the first level of organization of atoms and molecules into "defect free" coherent structures such as crystalline grains, and clusters at nanoscale. This scale is between a single atom and bulk behavior.[7] The nuclei mode typically contains $1-20$ % of the particle mass and more than 90 % of the particle number. Engine operating conditions also produce a distinct nuclei mode in the diameter range below about 20 nm and extending down through the lower size limit of the Scanning Mobility Particle Sizer (SMPS), about 7nm. The composition of the particles in the nuclei mode is uncertain. The fact that they exist in a separate, much smaller and

narrower diameter size range from the carbonaceous agglomerates in the accumulation mode suggests that they are formed later, and by a different mechanism. Other work in Germany and Switzerland suggest particles formed in the nuclei mode are volatile. Baumgard[29] suggests that the nuclei mode may be composed of mainly sulfuric acid-water solution. On the other hand, Bagley *et al.*[30] suggested that it may consist of primary carbonaceous nuclei. Earlier work at UMN by Abdul-Khalek and Kittleson [31] with an engine that had a high the soluble organic fraction (SOF) showed that much of the material in the nuclei mode range was volatile, rather than solid, and mainly SOF. They attempted to determine the volatile fraction of the nuclei mode range during some of the tests conducted at UMN using a catalytic stripper developed for this purpose. However, the test failed and they suggested that a significant fraction of the particles in the nuclei range from this engine are solid. They suspected that many of these particles may be metallic ash formed from oil and fuel additives.

The accumulation mode ranges in size from 50 - 300 nm. This mode typically consists of agglomerates formed by coagulation during the expansion stroke of primary carbonaceous nuclei generated early in the combustion process. This mode may also contain adsorbed volatile matter associated partially burnt fuel and lube oil (SOF). Most of the material in the SOF is in the gas phase in the tailpipe and does not undergo gas to particle conversion until the exhaust is cooled and diluted. This process may produce new particles (contributing to the nuclei mode) by homogeneous nucleation or cause growth of existing particles (contributing to the accumulation mode) by heterogeneous nucleation (adsorption and condensation). Most of the mass is primarily of carbonaceous agglomerates and adsorbed materials.

The coarse mode of particulate size distribution consists of particles larger than 1 μm and contains 5-20% of the measured diesel particulate mass. The large particles are formed by reentrainment of particulate matter deposited on the cylinder and the exhaust system wall's surfaces. [31] As shown in Figure 1.6 and 1.7, most of the particle numbers are in the nuclei mode and most of their mass is in accumulation and coarse mode. Figure 1.8 shows the difference between the spherule A in accumulation mode and the spherule B in nuclei mode.

According to Kodas *et al.*,[32] the lower size limit of a cluster or particle (<100 nm in diameter) can be considered as an aerosol. Therefore, an aerosol is a gas containing particles (typically, the particle volume fraction does not exceed 0.01%) that can be either solid or liquid (or both).

Cluster refers to particles smaller than 10 nm that have an appreciable fraction (> 10%) of surface atoms or molecules. A cluster may consist of atoms or molecules and may be either a solid or a liquid. "*Cluster is also applied to particles which are both stable and unstable with respect to evaporation, sublimation, or other processes that result in the removal of atoms from a surface.*"[32] **Table 1.2** above defines some common aerosol technical terms.

The condensation process may be the most important factor in the formation and growth of particles. It requires a supersaturated vapor on small particles (nuclei) or self-nuclei from ions for mass transfer process between gas phase and particulate phase. Partial pressure, P_p and saturation vapor pressures, P_s are needed to understand their basic concept. The saturation ratio, S_r is the ratio of vapor partial pressure on saturation vapor pressure of compound at a given temperature.

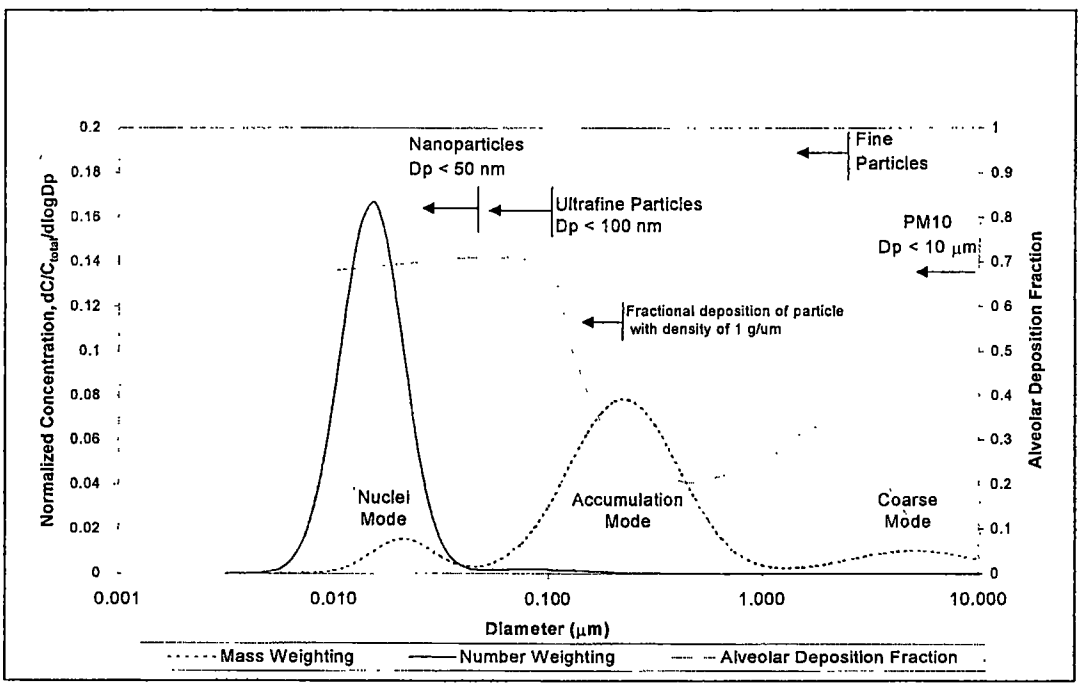


Figure1.6 Typical engine exhaust sizes distribution both mass and number weightings are shown (Kittelson).[31]

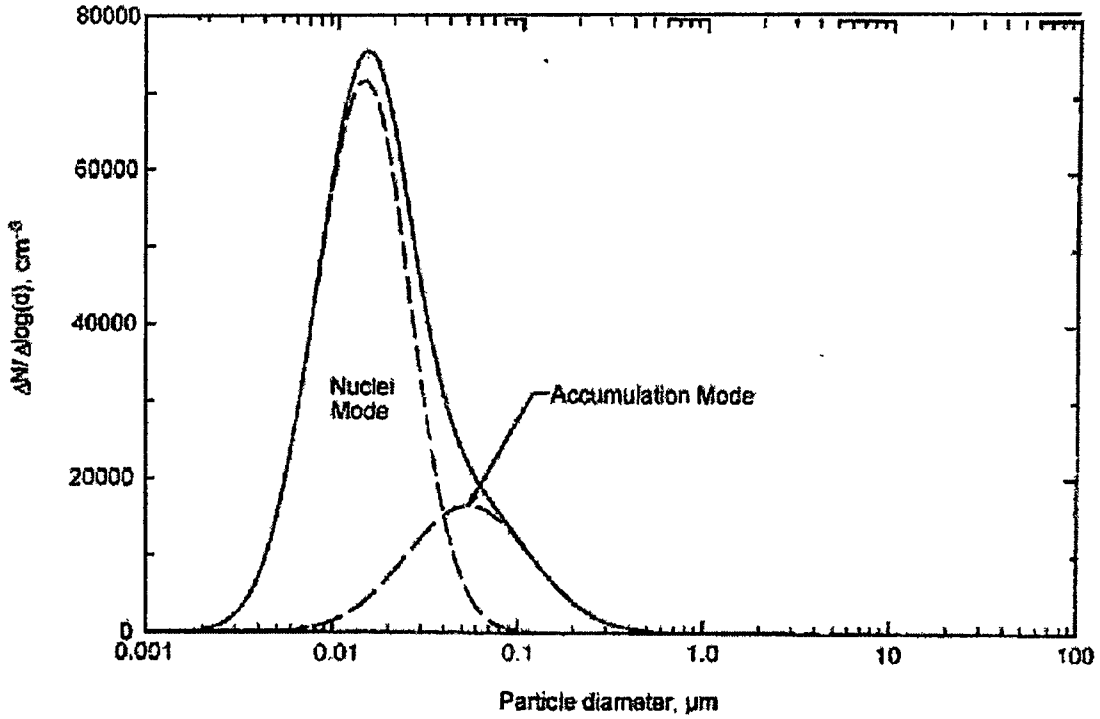


Figure 1.7 Typical engine exhaust sizes distribution both mass and number weightings are shown [33]

Table 1.2. Definitions of some technical terms [17]

Term	Definition
Aerosol	Small particles (solid or liquid)
Mist	Cloud of droplets (atomization of a liquid)
Droplet	Liquid particle
Smoke	Aerosol with residual materials from combustion process or condensation process
Fume	Solid aerosol from the condensation of vapors at high temperature
Haze	Aerosols with high atmospheric temperature and degration of visibility
Fog	Visible mist and is used to describe natural atmospheric aerosols
Smog	Aerosols in urban areas caused by airborne pollutants

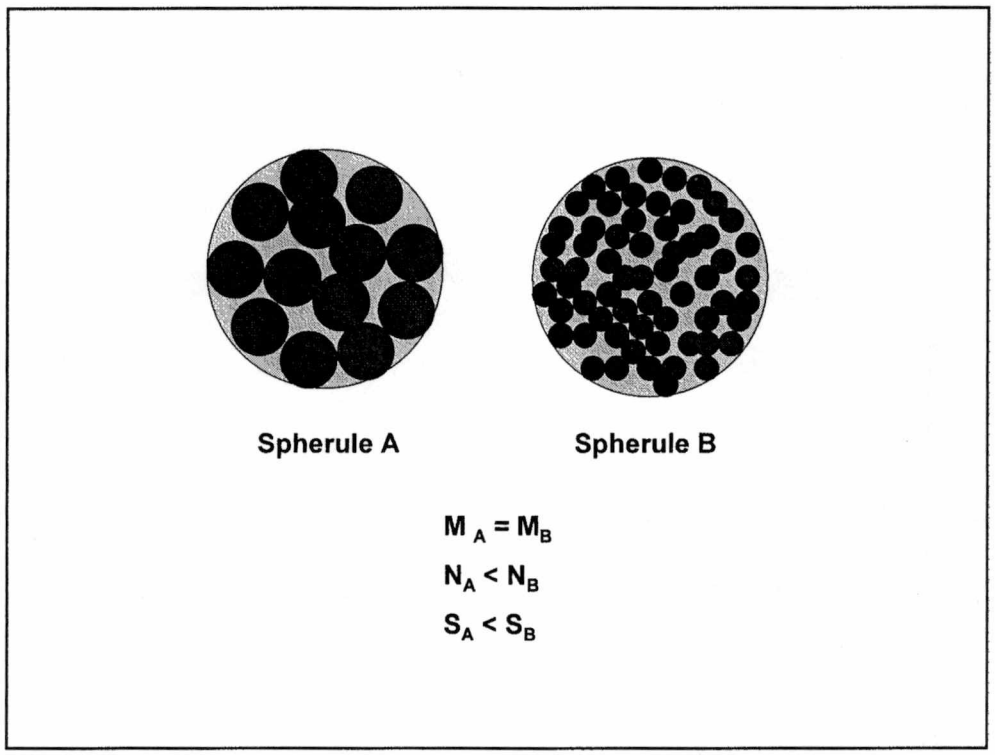


Figure 1.8 Even though mass of spherule A is the same as mass of spherule B, but number of size concentration and surface area of spherule A is less than spherule B.

$$S_r = \frac{P_p}{P_s} \tag{1.19}$$

where S_r: saturation ratio

P_p: partial pressure of compound

P_s: saturation vapor pressure of compound

Condensation occurs when the gas-vapor mixture reaches supersaturation, a saturation ratio greater than unity. There is no condensation when a saturation ratio is less than unity (unsaturated) or equal unity (saturated). Saturation vapor pressure is in equilibrium with partial pressure for a plane (flat) liquid surface at a given temperature. As a result, there are two conditions in which condensation could occur: 1) partial pressure of vapor is increasing or decreasing due to chemical reactions in the process; 2) saturation vapor pressure is increasing or decreasing due to temperature changing in the process. Therefore, the saturation ratio of some exhaust species may be higher than unity in cooling process in exhaust process. **Figure 1.9** shows

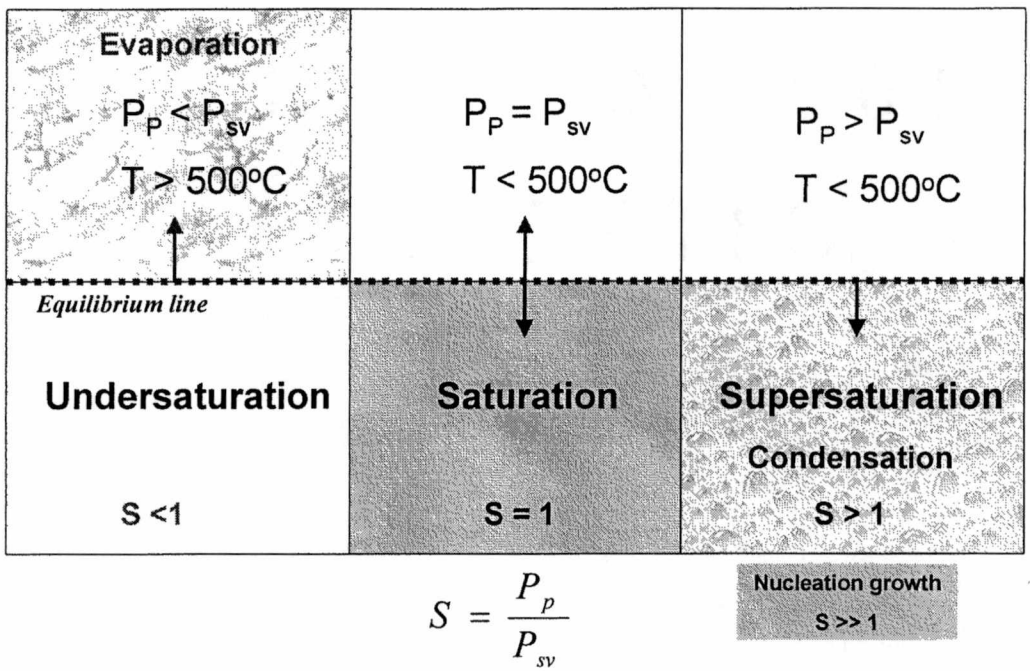


Figure 1.9 The differences between supersaturation and condensation which affect formation of particles (Adapted from Hinds)

three conditions of saturation ratio that affect the formation of condensation. The condensation process is dependent on the temperature and the partial pressures of the single components which are affected by the dilution of the exhaust gas.[17]

1.3.2 Nucleation

"Nucleation plays a fundamental role whenever condensation, precipitation, crystallization, sublimation, boiling, or freezing occur". [34] Nucleation can occur in the absence or presence of foreign material. While homogeneous nucleation is the formation of particles from supersaturated vapor molecules without the assistance of any nuclei or ions, heterogenerous nucleation is the nucleation on a foreign substance or surface, such as an ion or a solid particle. Homogeneous nucleation usually requires saturation ratios of 2-10 while heterogeneous nucleation requires

saturation ratios of few percent. In addition, nucleation processes can be homomolecular or heteromolecular. Homogeneous-homomolecular is the self nucleation of a single species (no foreign nuclei or surfaces involved). Homogenous-heteromolecular is the self nucleation of two or more species. Heterogenerous-homomolecular is nucleation of a single species on a foreign substance. Finally, heterogenerous-heteromolecular is nucleation of two or more species on a foreign substance. Homogeneous nucleation occurs in a supersaturated vapor phase.

Nanoparticles in internal combustion engines could be formed from homogeneous nucleation and heterogeneous nucleation since the exhaust gas consists of various hydrocarbon species, sulfate, water vapor, and solid particles in cooling process. Park *et al.* [35], Mirabel *et al.* [36], Hamill [37] and Doyle [38] predicted that homogenous nucleation between sulfuric acid and water may occur in the atmosphere. These experiments were based on the partial pressure of H_2SO_4 of 10^{-9} Torr, relative humidity 50%, and temperature 32°C.

1.3.3 Growth by Condensation

The rate of growth depends on the saturation ratio, particle size, and gas mean free path. The pathway of condensation and growth may occur on existing solid carbon particles during and after dilution. Condensation and growth of nucleated particles also occur in same way during the dilution process. The mass transfer depends on the Knudsen number (Kn) which is defined as:[34]

$$Kn = \frac{2\lambda}{D_p} = \frac{\lambda}{R_p} \tag{1.20}$$

$$\lambda = \frac{\bar{c}}{n_z} \tag{1.21}$$

where λ is the mean free path of the gas (average distance traveled by a molecule between collisions with other molecules)

D_p is the diameter of a particle

R_p is the radius of a particle

$\bar{c}$ is the average number of collisions a particular molecule

n_z is the average distance that a particle travels in one second.

In the case of Kn >> 1, called the free molecule or kinetic regime vapor, vapor interacts with the particles. However, Kn << 1, called the continuum regime, vapor transferred to particles. The particle size range between these two extremes (0.01 to 0.2 m) is called the transition regime.[34] Engine particles typically have Kn ≈1 to 100. Solid exhaust particle number size distributions emitted from a diesel engine typically has a geometric number mean diameter of about 40 nm (Kn ≈ 3).[7] During dilution and cooling of the exhaust, volatile materials such as sulfuric acid and hydrocarbon species may diffuse to the solid particle surface. The change of particle volume per unit time as a result of molecules diffusing to a particle surface in the transition regime, can be expressed as:

$$\frac{dV_P}{dt} = \frac{F(Kn)2\pi D_p v_l D_v P(t)}{kT} \tag{1.22}$$

where D_p is the particle diameter

v_l is the molecular volume

D_v is the diffusion coefficient of vapor

P(t) is the partial pressure of vapor

P_v is the vapor pressure (negligible for soot growth)

k is the Boltzmann's constant

T is the absolute temperature

F(Kn) is a correction factor for the transition region.

The rate of molecular vapor consumption or the reduction in vapor pressure, assuming the ideal gas law, as a result of molecular depletion by solid particles can be described as:

$$\frac{dC(t)}{dt} = \frac{dP(t)}{kTdt} = -N\frac{\frac{dV_P}{dt}}{v_l} \tag{1.23}$$

$$\frac{dP(t)}{dt} = -NF(Kn)2\pi D_p D_v P(t) \qquad (1.24)$$

where $C(t)$ is the molecular density

N is the solid particle density.

The expression given in equation 1.24 gives the reduction in the partial pressure of the vapor phase as a result of condensing on existing particles.[34]

For nuclei smaller than the mean free path of the gas, nucleated sulfuric acid particles are typically on the other order of 1 nm (Kn ~ 100). Growth of those particles may depend on the free molecular regime theory. Friedlander described the volume change per unit time for a particle growing as [21]:

$$\frac{dv}{dt} = \frac{\pi d_p v_m (p_l - p_d)}{(2\pi mkT)^{1/2}} \qquad (1.25)$$

$$\frac{dP(t)}{dt} = -NkT\frac{\frac{dV_p}{dt}}{vl} = -NkT\frac{\pi D_p^2 (P(t) - Pv)}{\sqrt{2\pi m_m kT}} = -ND_p^2\sqrt{\frac{\pi kT}{2m_m}}(P(t) - Pv) \qquad (1.26)$$

Depend on the square of particle diameter, the smallest particles are unlikely to last long in the atmosphere.

1.3.4 Growth by Coagulation

"*Growth by coagulation is the process in which aerosol particles collide with one another, due to a relative motion between them and adhere to form larger particles*".[17] Brownian motion, called thermal coagulation, is the relative motion between the particles. It may be important in particle sampling during the dilution process under the condition where homogenous nucleation is very strong. The general equation for continuously changing aerosol size distribution with time due to coagulation can be written as: [34]

$$\frac{\partial n(v,t)}{\partial t} = \frac{1}{2}\int_{v_0}^{v-v_0} K(v-q,q)n(v-q,t)n(q,t)dq - n(v,t)\int_{v_0}^{\infty} K(q,v)n(q,t)dq \qquad (1.27)$$

where $v = kv_1$ is the particle volume

v_1 the volume of the monomer

K is the coagulation coefficient

n(v, t) is the particle size distribution function at time t

q represents any particle volume less than v.

While the first term in (1.27) represents to the production of particles by coagulation of small particles, the second term corresponds to their loss by collisions with available particles. Finally, the properties of coagulation, condensation, and nucleation processes that affect number concentration and volume concentration are summarized in **Table 1.3**.

Table 1.3 Properties of Coagulation, Condensation, and Nucleation[34]

Process	Number Concentration	Volume Concentration
Coagulation	Decreases	No change
Condensation	No change	Increases
Nucleation	Increases	Increases
Coagulation and condensation	Decreases	Increases

CHAPTER 2 MICRO-DILUTION DEVICE

This chapter describes the design of the dilution tunnel. The micro-dilution device is used for particulate emissions measurement. The data should be representative of particles emitted from engines to the atmosphere. The dilution and sampling system used in these experiments were designed to give very fast dilution of the exhaust with dry air. The dilution process in a conventional dilution tunnel is much slower resulting in more time available for nucleation and growth to occur. The dilutor itself may lead to inconsistencies and variability in particle measurements. As a result, particle measurement in the laboratory might not be representative of real exhaust particles emitted to the atmosphere. The working principal of each component and some important specifications will be discussed in this chapter.

Most particle detection instruments used for exhaust particle measurements operate at ambient temperature and pressure and require dilution and cooling of hot exhaust. The condensation particle counter (CPC) can detect aerosol concentration of 10^3 to 10^9 particles/cm^3. However, the aerosol number concentrations in diesel exhaust are in the range of 10^{12} to 10^{14} particles/cm^3, therefore, it is necessary to dilute the aerosol concentration before sampling. Dilution and cooling of hot exhaust have been done with a macro dilution system and micro dilution device.

In a recent survey submitted to EPA on diesel particulate matter sampling methods, Kittelson[39,40,41] described the most popular dilution systems in use at laboratories and automotive companies in detail. There are two dilution tunnel systems with different dimensions, residence time and flows from University of Minnesota (UMN) and Perkins Technology Limited (PTL). The UMN system has a longer residence between the primary and secondary, and much longer residence time between the secondary and particle measurement instruments. Dilution ratio is also different between PTL and UMN. The primary dilution used in PTL was varied from 4-85:1 while the secondary dilution ratio was kept constant at about 18:1. On the other hand, the primary dilution used in UMN was about 18:1 and the secondary dilution was about 60:1. This gives an overall dilution ratio of about 1000:1. **Figure 2.1** shows the schematic of mini-dilution device built in UMN.

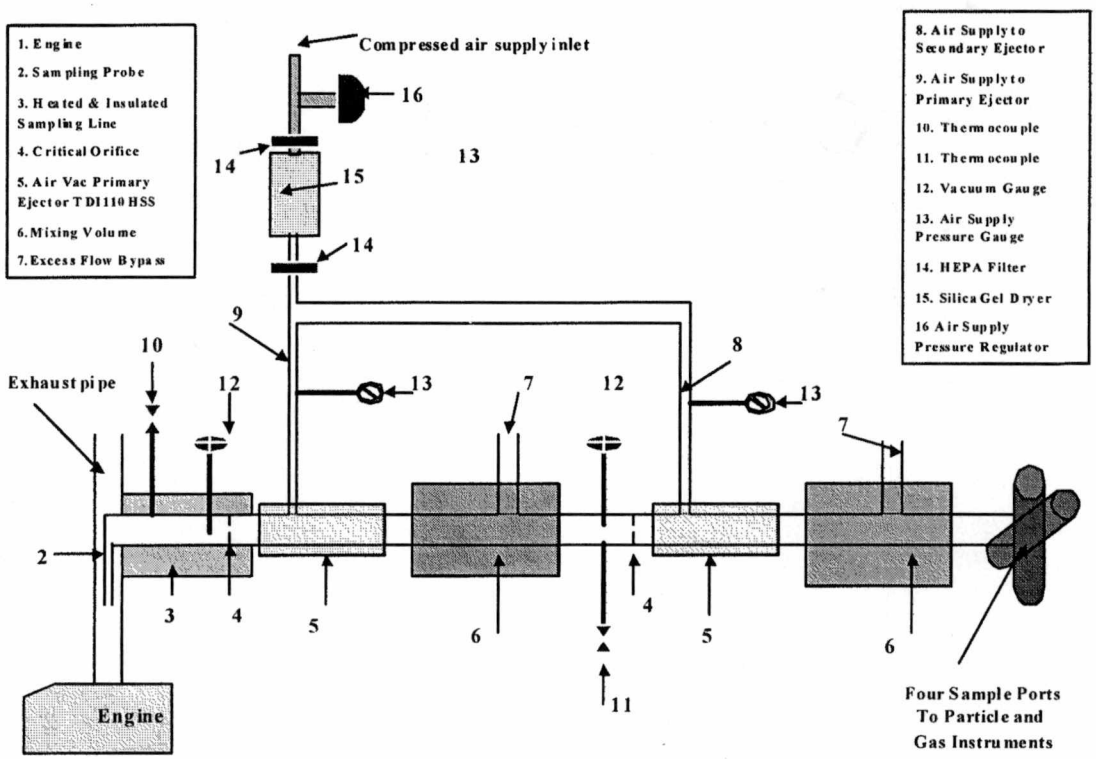


Figure 2.1 Schematic of Mini Dilution device constructed by Abdul-Khalek *et al.* (Redrawn from SAE980525)

2.1 MICRO DILUTION DEVICE

Dilutors, initially based on SAE 980525 [16], were designed and built. Because of several testing purposes, two different types of dilutors were built: Dilutor I with two chambers which allow for long residence times, and Dilutor II with one chamber which is used for short residence time. Dilutor I is capable of diluting the exhaust gas from 1:1 to 10,000:1 in a few seconds. The flow rate is from 0.5 to 2.05 standard cubic feet per minute (SCFM). The temperature range is from 20 ^{0}C to 52 ^{0}C. The residence time is from 10 ms to 2000 ms. Dilutor II is capable of diluting the exhaust gas from 1:1 to 200:1 in a few seconds. The flow rate is from 0.5 to 2.05 standard cubic feet per minute (SCFM). The temperature range is from 20^{0}C to 52^{0}C. The residence time is from 50 to 100 ms. Dry, particle free air is used in both dilutors. Heat and insulation are also used to

prevent cold spots on the walls. Turbulence flow is applied to have a good mixing. Orifices are used to control flow rate.

The dilutor is a dilution tunnel that dilutes the engine exhaust in one step. Particle free compressed air is used as diluting air. There are several sampling positions for sampling diluted engine exhaust. The whole tunnel and an exhaust transfer line are insulated, therefore, heat transfer between the tunnel and ambient air can be ignored. **Figure 2.2** is a schematic of one stage dilution device. The pressure in this tunnel is almost the same as ambient air pressure. The main function of this section of the tunnel is to mix exhaust with dilution air uniformly, and let flow develop and expand to the ambient air pressure. To avoid corrosion, the materials of the tunnel and accessory parts are made of stainless steel. The micro dilution device is low cost, portable and allows simulation of different environment conditions. In this tunnel, diesel exhaust can be diluted by a factor of 1000 in a second. The specifications of the one-stage micro dilution device are summarized in **Table 2.1**. The main dilution tunnel is separated into three sections. The purpose of doing this is to make the dilutor more portable and to easily adjust the position of transfer line probe and sampling probes. **Table 2.2** shows the specification 2.0-in-ID and 1.255-in-ID tubes used in the two dilutors.

A sampling probe, transfer probe, heating tape, and thermocouples are installed in the 2.0-in-ID stainless tube. The mixing of air and exhaust is completed in the main dilution tunnel and the diluted exhaust is sampled in this section. Changing sampling positions allows the sampling of the diluted exhaust with different residence time and distance. Back pressure in the dilutor is controlled by extra holes on the other end of the chamber.

2.1.1 Two-Staged Micro Dilution Device, Dilutor I

The total length of this tunnel is about 34 inches for the main chamber and 20 inches for the second chamber. The diameter of the main tunnel is about 2.5 inches (**Figure 2.3**). The Dilutor I is capable to dilute the exhaust gas from 1:1 to 10,000:1 in a few seconds. The flow rate is from 0.5 to 2.05 standard cubic feet per minute (SCFM). The temperature is from 20^0C to 52^0C. The residence time is from 50 to 100 ms. The advances of this dilutor are its tremendous flexibility for

Table 2.1 Specifications of one-stage micro dilution device

Dilution ratio	5:1 to 1000:1 (in few seconds)
Dilution rate	50 – 5000 s-1
Flow rate	20 – 30 SCFM
Temperature	32 – 52 ^{0}C
Residence time	0.4 – 2.0 second
Relative humidity	Free

Table 2.2 Specification of ID 2.5" and ID 2" tubes

Inside diameter (ID)	2.00"	1.25"
Wall thickness	0.065"	0.120"
Material	ss304	ss316
Total length, ft	2	2

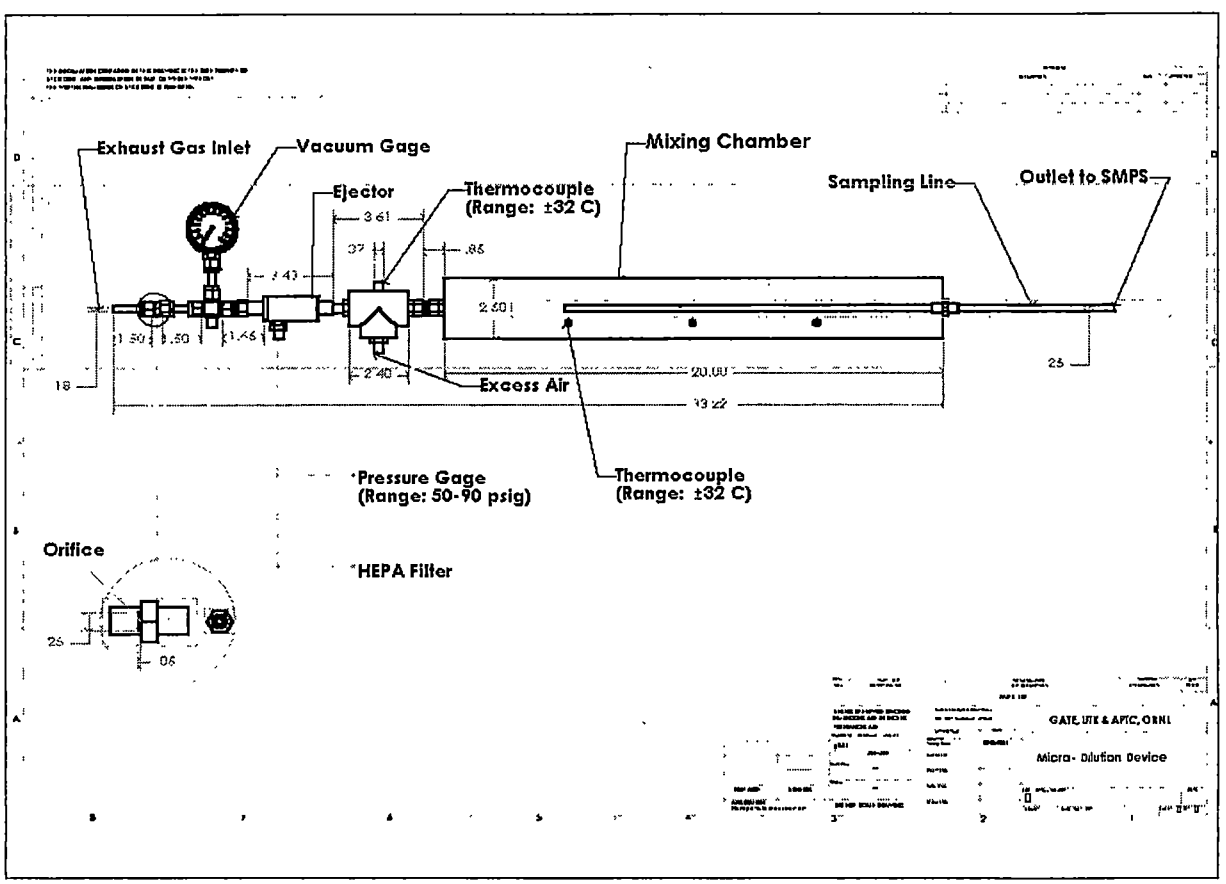


Figure 2.2 A schematic of one stage dilution device.

sampling particles at a variety of dilution ratios and residence times. Dilutor I is used for most of the studies described in this thesis.

2.1.2 One-Staged Micro Dilution Device, Dilutor II

The total length of this tunnel is about 24 inches, and the diameter of the main tunnel is about 1 inch (**Figure 2.4**). The Dilutor II is capable to dilute the exhaust gas from 1:1 to 500:1 in a few seconds. The flow rate is from 0.5 to 2.05 standard cubic feet per minute (SCFM). The temperature is from 20^0C to 52^0C. The residence time is from 50 ms to 200 ms. The compact size allows Dilutor II to be installed very near the sampling port which minimizes particle losses. The unit is also self contained. Heater controllers, regulators, and filters are all mounted to the unit. The ORNL-APTC engineers have used this system to collect filter samples of PM.

The details of main components of the dilution tunnel are described in the following sections.

2.2 TRANSFER AND PROBES

The short exhaust transfer line and probes to minimize the particle losses are constructed of 316 stainless steel tube. Heating the transfer line in order to maintain its temperature the same as the engine exhaust temperature minimizes particle losses by temperature gradient. Heat transfer between the transfer line and ambient air is minimized by insulating the transfer line and probes. The transfer line and probe characteristics are summarized in **Table 2.3**. **Figure 2.5** is picture of the sampling line and probe in the Dilutor I and II. For nanoparticles, the main mechanism of particle losses in the transfer tube is diffusion losses as described in section 1.2.

Due to the small size of the particulate matter and large ID of the tube, the transfer line has high penetration for the whole range of particle size. Since the size of the particles is small, the particle losses due to impacting at the bending could be ignored. The main mechanism to cause particle losses is the diffusion deposition. Losses due to laminar diffusion seem to play a role in two regions of the dilution systems. Referring to the schematic of the dilution system in Figures 2.1,

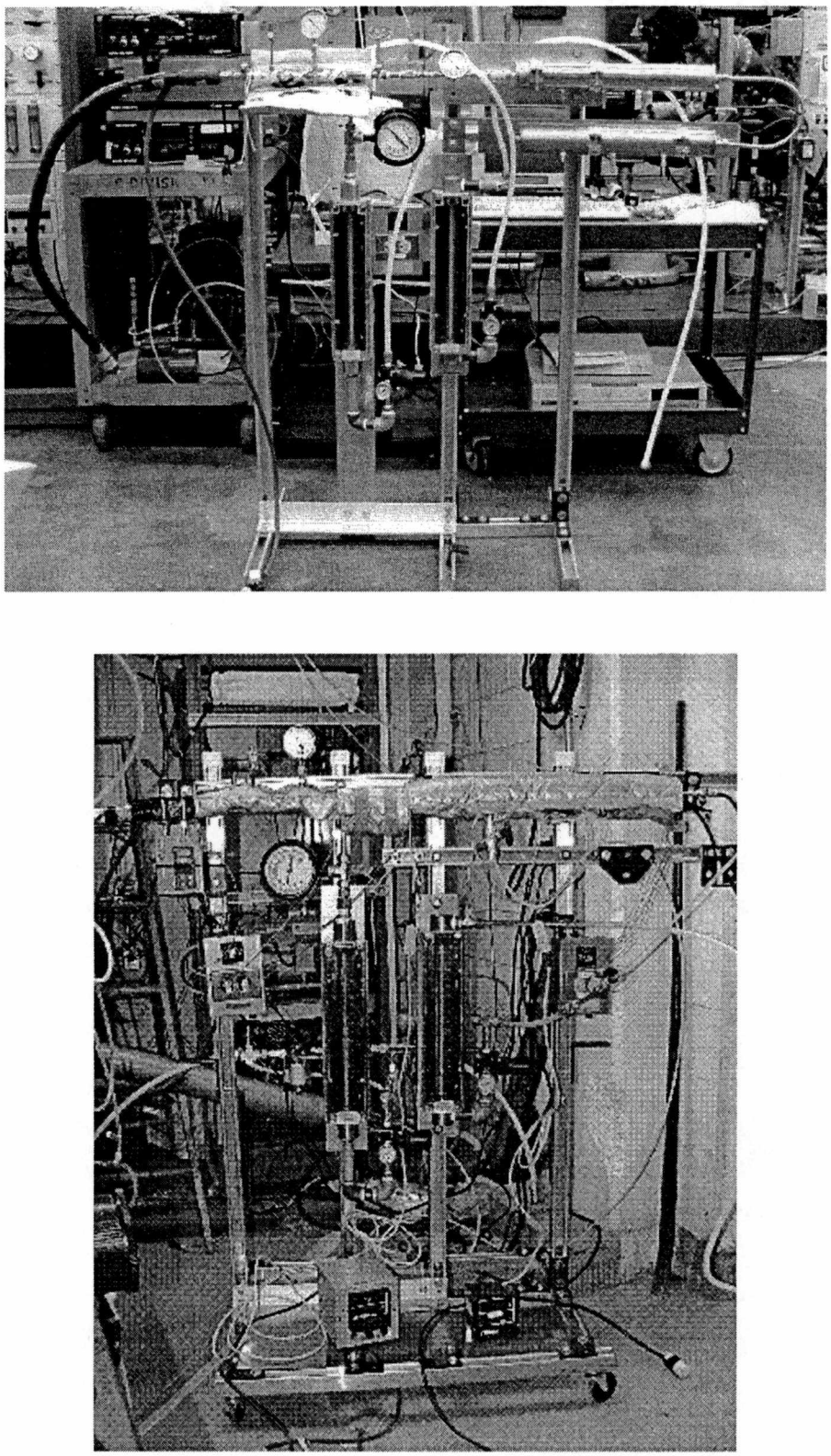
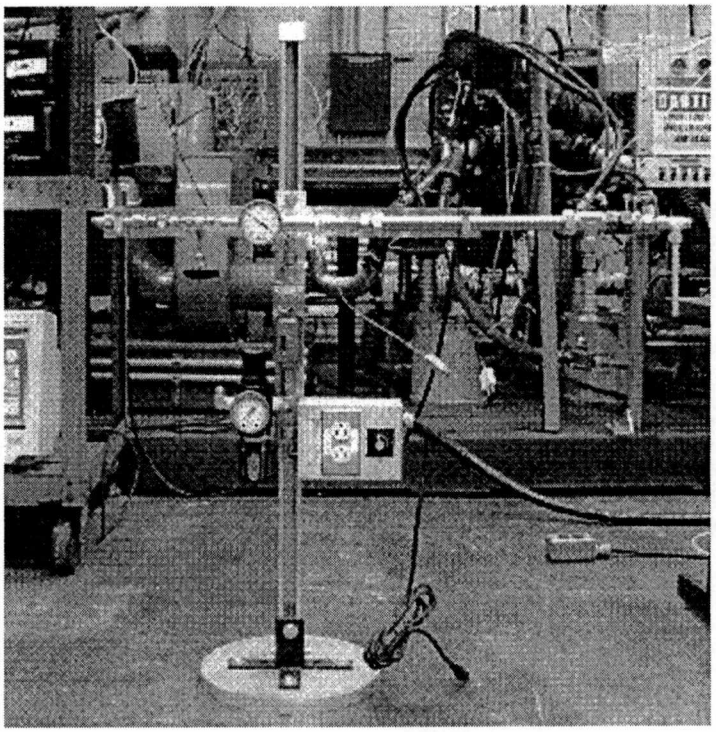


Figure 2.3 Dilutor I is two staged micro dilution device



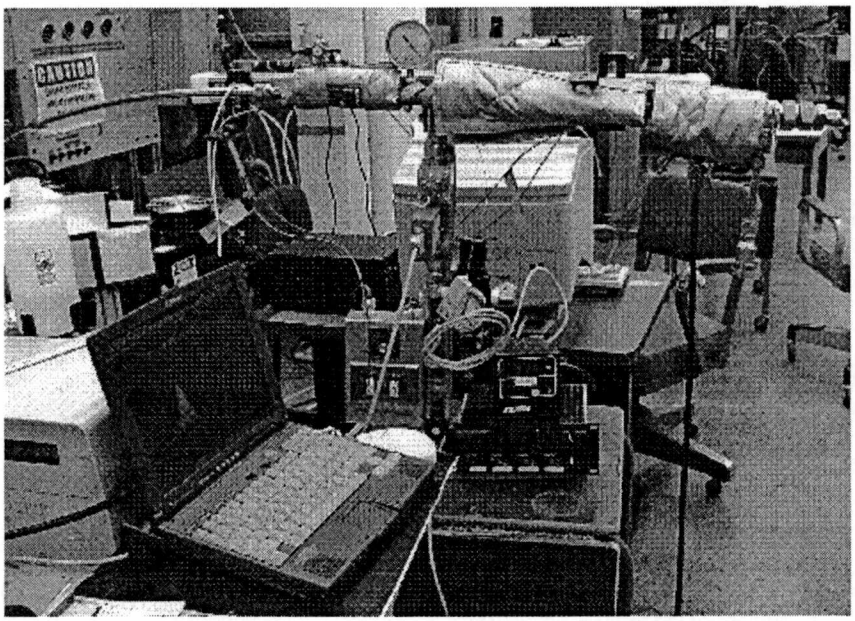


Figure 2.4 Dilutor I is one staged micro dilution device

Table 2.3 Transfer line and probe characteristics

Temperature of exhaust	200 °C
Pressure of the Exhaust Flow	760 mmHg
Flow rate of the exhaust	0.7 LPM
Length of the transfer line, inches	6
ID of the transfer line, inches	1/4
Viscosity of Exhaust @ 200 °C	Viscosity of air @ 200 °C

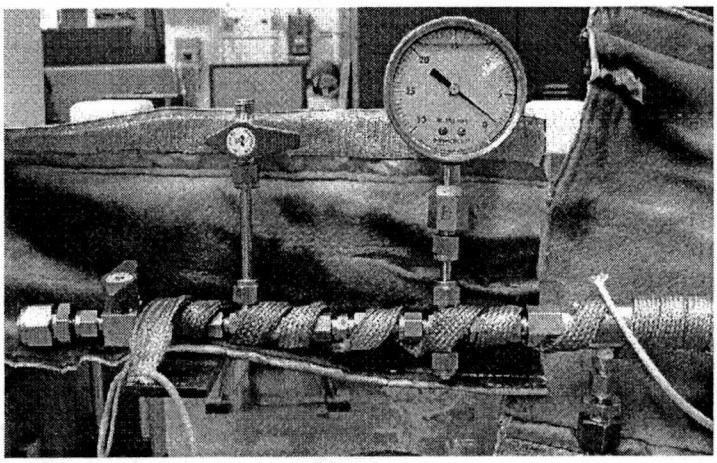


Figure 2.5 Sampling line and probe in Dilutor I and II

the first region is inside the retractable sampling tube, and the second region is inside the line between the secondary dilution system and the SMPS.

2.3 EJECTOR

A compressed air ejector type micro-dilution system is used to rapidly dilute and cool the exhaust. It is responsible for mixing compressed air with a stream of hot or ambient temperature exhaust. Ejector, a very simple device, consists of only two parts (**Figure 2.6**). Since there is no moving part, ejector is maintenance free. High-pressure air is introduced into the side of the ejector and is forced through a small annular orifice to increase its velocity. It is allowed to rapidly expand into an exit section with a resulting decrease in pressure. This decrease creates a vacuum, and vacuum flow into the vacuum chamber. **Table 2.4** shows the specification of ejector

TD110HSS. Air Vac Engineering Company Inc. of Seymour, Connecticut manufactures the ejector.

NaCl and DOP aerosol were used to test the difference in the geometric characteristics of mean diameter and standard deviation of particles before and after passing through the orifice and ejector. The results of these experiments are described in Chapter 4.

2.4 HEATING SYSTEM

The heating system is used to heat the surface of the micro-dilution device in order to maintain constant mixing air temperature in the dilution device and to keep the transfer line temperature the same as the engine exhaust temperature. It consists of a heated line (**Figure 2.7**), heating tapes, thermocouples, insulators (**Figure 2.8**), and temperature controllers. The thermocouples are used to measure the temperature which needs to be in the range between 32 to 52°C. When the required temperature is higher than or lower than the desired temperature, the temperature controller activates the heating tapes.

In order to prevent condensation of the hot engine exhaust, the transfer line is heated to 200 °C. A thermocouple is attached to the wall of the transfer line and the other is attached on the wall of the main chamber. Insulation is used to cover the surface of the transfer line and the chamber. It minimize the heat transfer between the inside mixing air and ambient. As the result, the dilutor reduces particle losses due to the temperature gradient, and prevents condensation of the water vapor in the transfer line. **Table 2.5** shows the specifications of the heating system.

2.5 MIXING PROFILES

In the region of low and high dilution ratio, aerosol concentration is high in the center area. Concentration of gas molecules is uniform over the cross section. Therefore, a retractable line is designed to extract the exhaust gas in the center area.

In turbulent flow, turbulent convection is the main mixing mechanism in the dilution tunnel. Diffusion is still one mixing mechanism except the turbulent convection. Total diffusion

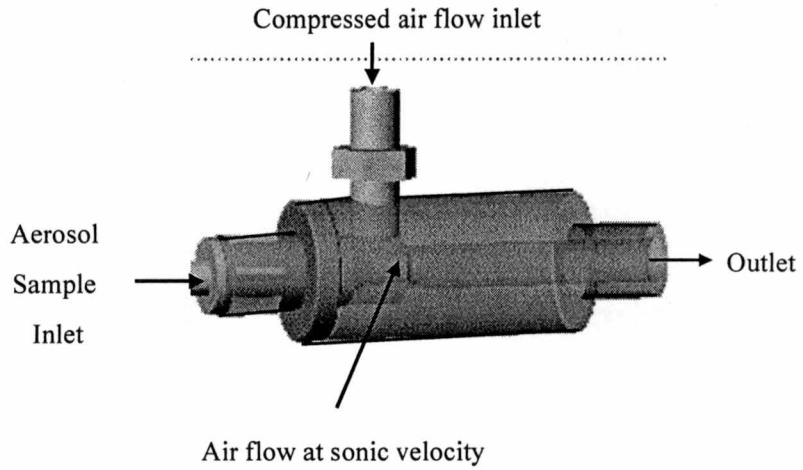


Figure 2.6 Basic structure of ejector.

Table 2.4 Configuration of ejector TD110HSS manufactured by Air Vac Engineering Company Inc.

"A" Diameter	9/64"
Vacuum Level, "Hg	24.8
Vacuum Flow, scfm	2.3
Air Consumption, scfm	4.2
Weight, oz.	9
Material	316 SS

Table 2.5 Specifications of the heating system:

Temperature Controller	
Model	Omega
Temperature range	0 – 1000 F
Heating Tape	
Manufacture	Brewster
Model	
Voltage	110
Thermocouple	
Manufacture	Omega Inc.
Model	Type K

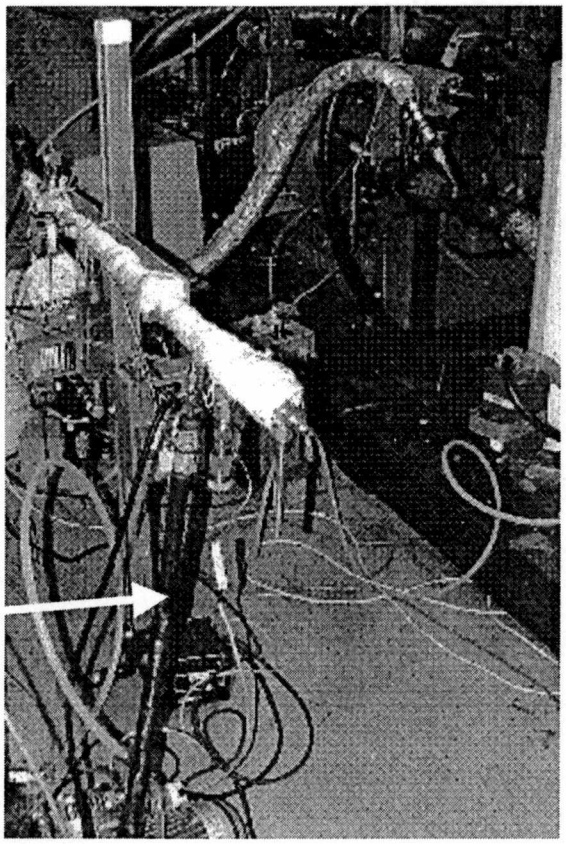


Figure 2.7 Photograph of heated line which is used to connect from the dilutor to exhaust gas system.

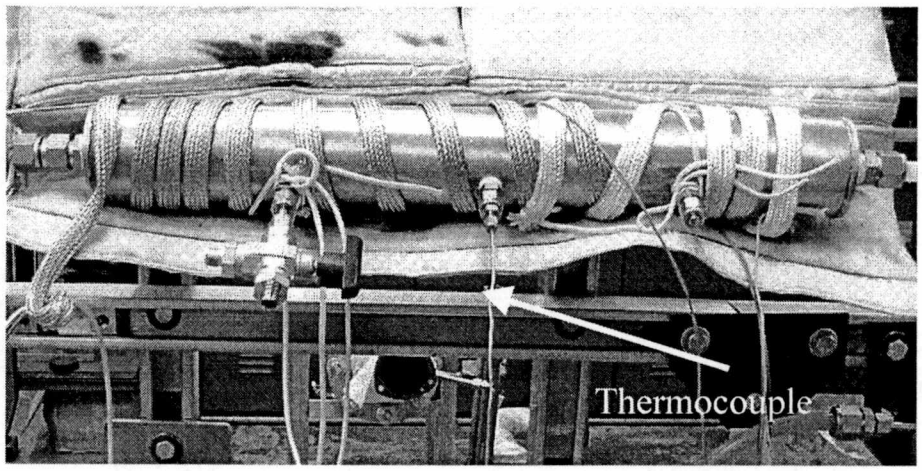


Figure 2.8 Photograph of heating tapes, thermocouple, and mixing chamber.

coefficient can be evaluated as the combination of turbulent diffusion and laminar diffusion. For gas molecules and small particles, turbulent diffusion coefficients have the same values. In typical turbulent flows, laminar diffusion coefficients are much smaller than turbulent ones and can be ignored. Therefore, gas molecules and particles are assumed to have the same diffusion coefficient. Intensity of turbulence also influences the mixing profile in the dilution tunnel.

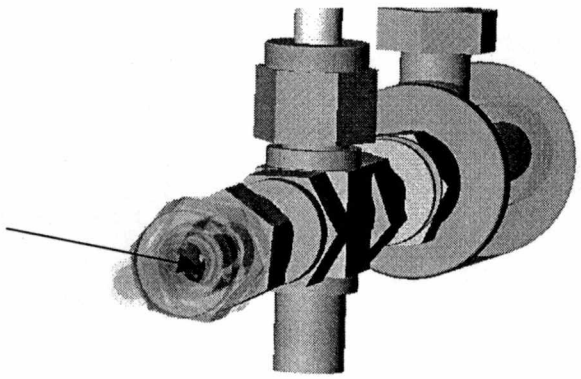
Because the dilution process has a profound effect on the mass concentration and sizes of particles, past experiments were used to determine the optimum dilution characteristics. In the high-flow regime, the measured concentrations varied with flowrate. As the dilution ratio increases, the amount of cooling increases, thereby increasing the tendency for HC vapors to condense on existing particles, and increasing the mass of particles (particularly the smaller ones, since they make up a large fraction of the surface area). However, as the dilution ratio increases, the concentrations of HC vapors decrease, therefore, decrease the rate of condensation. The net effect is an increase in particulate concentrations (corrected for dilution ratio) of up to about a dilution ratio of 15:1 after which the particulate concentration decreases. In the low flow regime, the dilution ratio does not affect the temperature and hence does not affect the tendency for condensation. In this case, as the dilution ratio is increased, the particulate concentration decreases until a dilution ratio of approximately 15:1, after which the condensation appears to be effectively stopped and the concentration remains unaffected. In laminar flow, convection is weak, and diffusion is the main mixing mechanism. Diffusion coefficients are used to characterize the speed of diffusion. Small particles have larger diffusion coefficients than big particles, therefore, small particles mix faster than larger particles in laminar flow. These results were substantiated by theoretical models of diesel exhaust dilution by Amann *et al.*[42]; MacDonald *et al.*[43], and Plee [44] .

Diffusion coefficients for particles and gas molecules are shown in Table 1.1. For gas molecules, diffusion coefficients are much larger for small particles. Therefore, gas molecules mix much faster than particles in laminar flow. For a polydisperse aerosol mixing with dilution air in laminar flow, dilution ratios vary with the size of particles. Measuring the dilution ratio for a gas to obtain the dilution ratio for particles is not suitable for an aerosol diluted in laminar flow.[7]

2.6 ORIFICE

The orifices used in Dilutor I and II were a simple disk with sharp transition hole. More detail about orifice is available in Appendix C.

Orifice

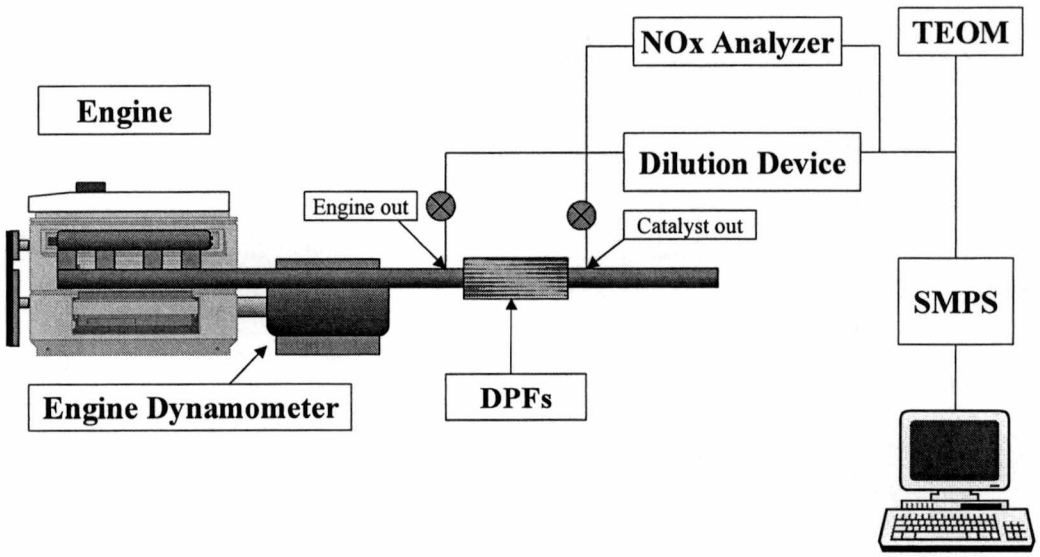


CHAPTER 3 RESEARCH METHOD

This chapter describes the experimental apparatus and procedures used for measuring particle size distributions and number concentrations from the exhaust of diesel engines and gasoline engine. First, it includes a brief description of the devices used such as: particle and gas measurement instruments, dilution systems, engines, and fuels. The summaries of four series test will be described such as: 1) NaCl and Dioctyl-Phthalate (DOP) aerosol tests were used to investigate the artifact formation in dilution tunnels (see Appendix C), 2) one series test with heavy-duty diesel engine, different sulfur fuels, and the Dilutor I, 3) one series test with light duty diesel engine, 150 ppm sulfur fuel, and the Dilutor II, and 4) one series test with gasoline engine, indoline fuel and the Dilutor II.

3.1 APPARATUS

The apparatus in the experiments includes a scanning mobility particle sizer (SMPS), a dilutor, a particulate filter, a NO_x analyzer, and a tapered element oscillating microbalance detector (TEOM), a dynamometer, and an engine. **Figure 3.1** shows the overall schematic of the experiment appartus.



SMPS: Scanning Mobility Particulate Sizer
TEOM: Tapered Element Oscillating Microbalance Detector
NOx Analyzer
DPFs: diesel particulate filter

Figure 3.1 Schematic of experimental apparatus.

The following sections are brief descriptions of each device.

3.1.1 Scanning Mobility Particle Sizer (SMPS)

The TSI Model 3934 was used to measure particle size distributions in the range of 5 to 1000 nm in diameter and concentrations. The SMPS measures a number weighted size distribution based on the electrical mobility diameter. The SMPS is composed of a neutralizer, a mobility analyzer, a TSI Model 3025 condensation particle counter (CPC), a power supply, a computerized control, and a data acquisition system (**Figure 3.2** and **3.3**). The basic principle of the SMPS is that the velocity of a charged particle in an electric field is directly related to the size of the particle. Sheath air enters the mobility analyzer through the axial pipe at the top of the central rod (**Figure 3.4**). The aerosol enters a Krypton-85 neutralizer and is charged to Boltzmann equilibrium. Then the aerosol flow enters the mobility analyzer and flows downward through the annular mobility. The clean sheath air flows along the central rod and forces the aerosol to move downward. The center rod is supplied a variable DC power. By varying the voltage, the electric field in the annular region can also be varied. [45], After electric field causes charged particles with a certain narrow range electrical mobility, the sample flow enters the CPC. The electric mobility of particles is related to particle size and the number of charges. Particles in the sampling flow are mainly single charged. A scanning time of 2 minutes gives more accurate and repeatable size distribution.

However, Model Series SMPS above is limited in generating aerosol in the range of 7 to 1000 nm in diameter. Therefore, Model 3936 Series SMPS systems was used to measure aerosol in the range of 3 to 1000 nm in diameter. With 162 size channels and up to 64 channels per size decade, this system offers very accurate measurement. They consist of an Electrostatic Classifier to determine particle size and a Condensation Particle Counter (CPC) to determine particle concentration (**Figure 3.5**). More information about Model 3934 is available in the web page: http://www.tsi.com.

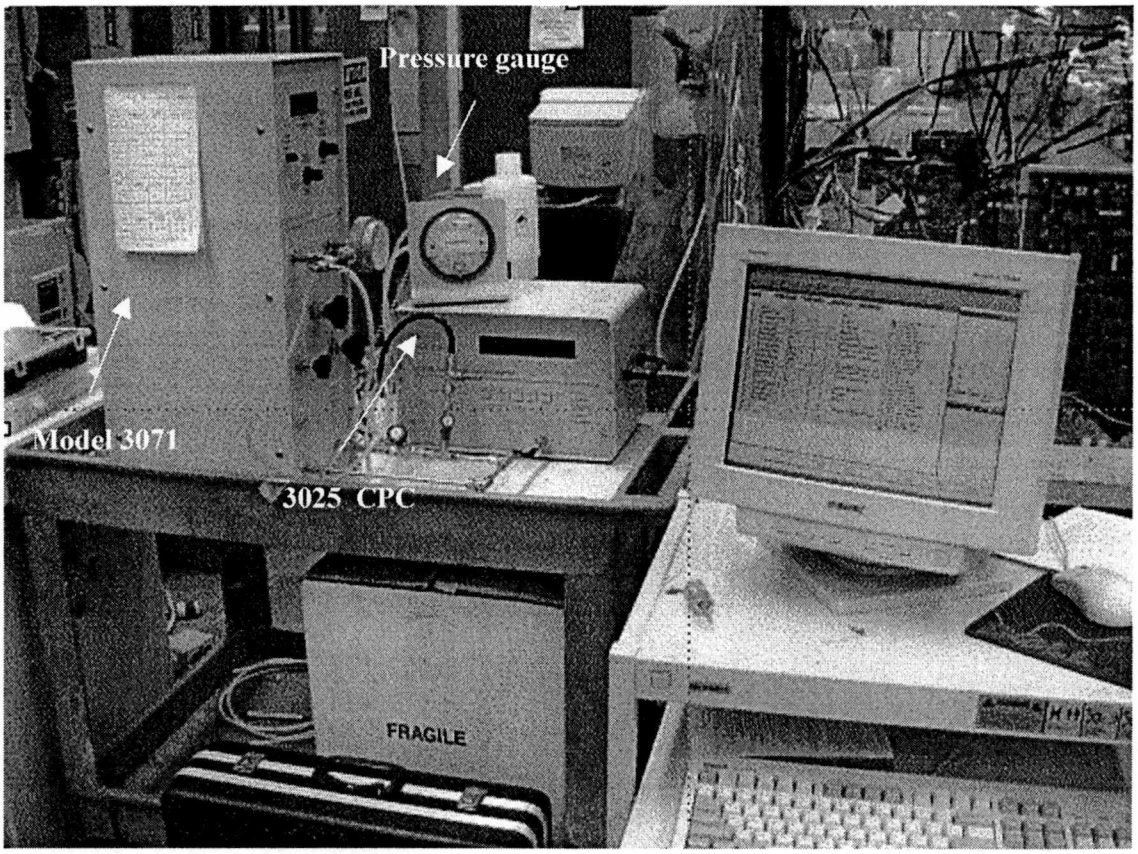


Figure 3.2 TSI Model 3949 SMPS system : 3071 Electrostatic Classifier and 3025 CPC.

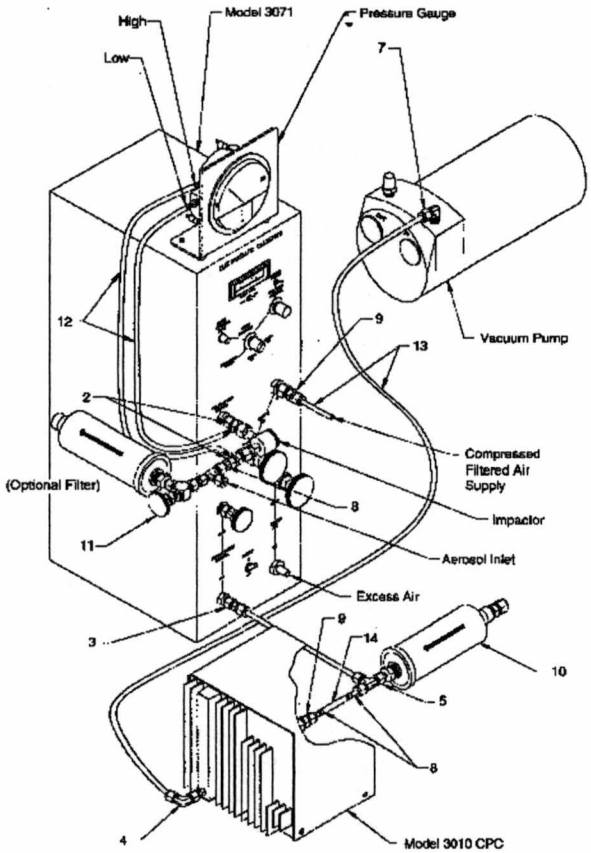


Figure 3.3 Schematic of a TSI Model 3934 SMPS

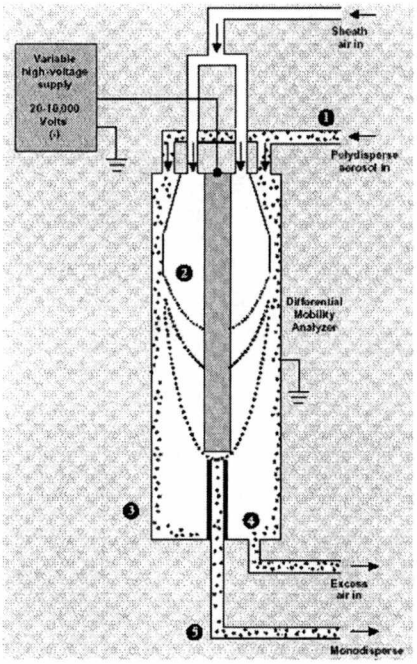


Figure 3.4. A diagram of the central rod

3.1.4 Condensation Nucleus Counter (CNC)

A second particle counter, a TSI 3025 CNC was used to measure total particle number concentration downstream of the SMPS. It consists of a saturator, condenser, particle sensor, flow meter and pump. As an aerosol enters the CNC, it is saturated with alcohol vapor while it passes over a heated pool of alcohol. The aerosol flow is first saturated with alcohol and then cooled in the condenser tube. The cooling process causes a supersaturation condition; therefore, the alcohol condenses onto the particles. The particles are counted in a particle-sensing region with a laser light source. A photodetector measures the particles by light scattering techniques. All particle sizes grow equal, the light scattered is correlated to particle number concentration of size independently (**Figure 3.6**). More information about TSI 3025 CNC is available in the web page: http://www.tsi.com.

3.1.4 Electrospray Aerosol Generator (EAG)

The TSI Model 3488 Electrospray Aerosol Generator is used to generate ultrafine and nanoparticles from 2 to 100 nm in diameter and in concentrations up to 1×10^7 particles per cubic centimeter. A charged liquid solution is sucked up through a capillary tube and exposed to an electric field on the liquid at the tip of the capillary. Then, the electrical field pulls the liquid from the capillary tube and form droplets. The forming droplets are mixed with clean air and CO_2. The liquid evaporates while an ionizer neutralizes the charge. The result is a formation of a neutralized monodisperse aerosol (**Figure 3.7**). This aerosol was used to study the artifact that may happen with the orifice and ejector in the dilution device. More information about Model 3480 is available in the web page: http://www.tsi.com.



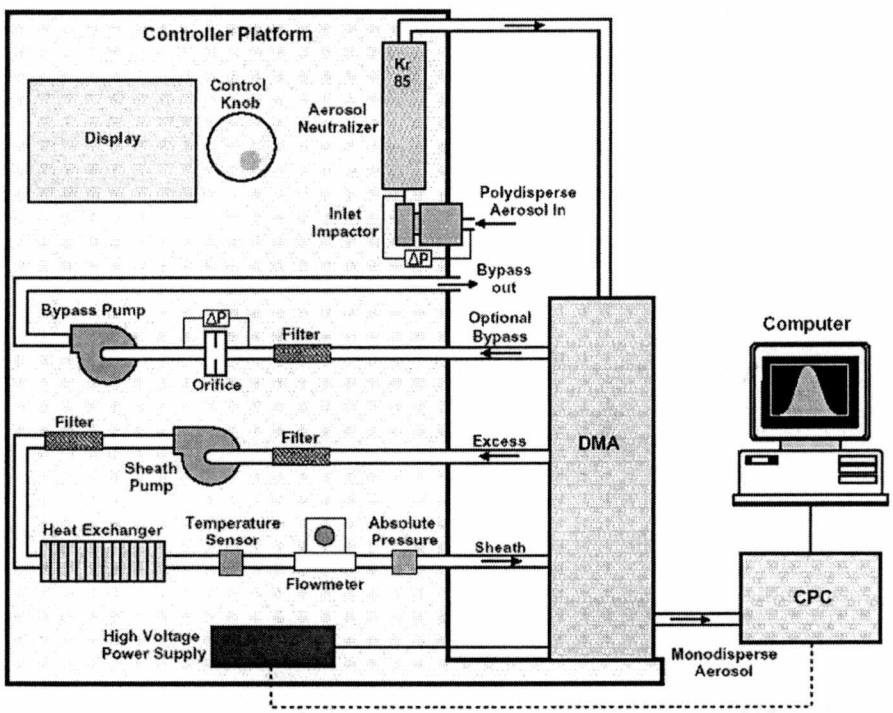


Figure 3.5 The above picture is TSI Model 3936 SMPS and the bottom picture is the schematic of 3936 SMPS.

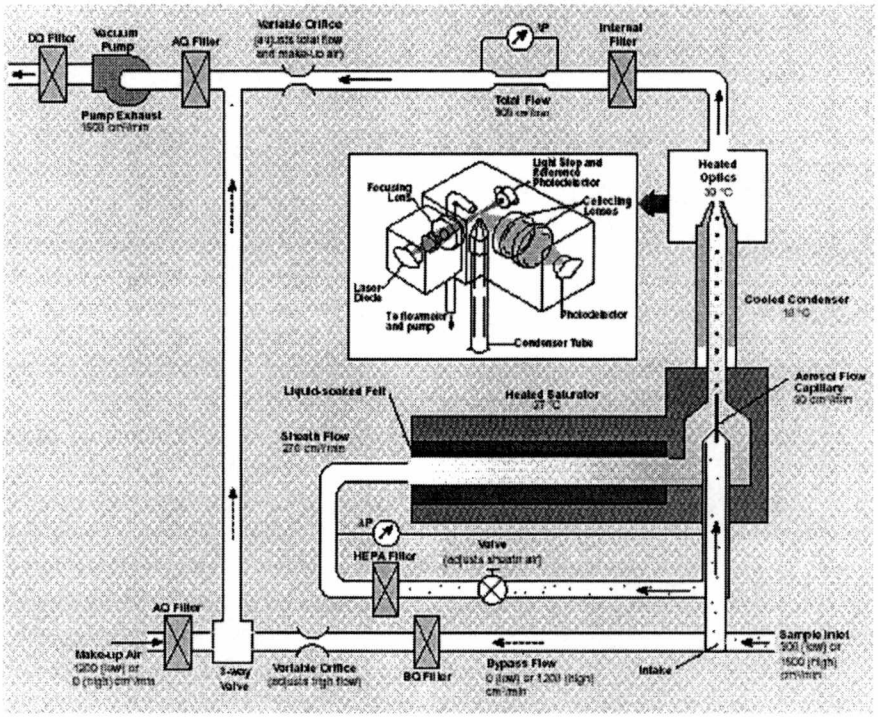


Figure 3.6 Schematic of TSI Model 3025 CNC.

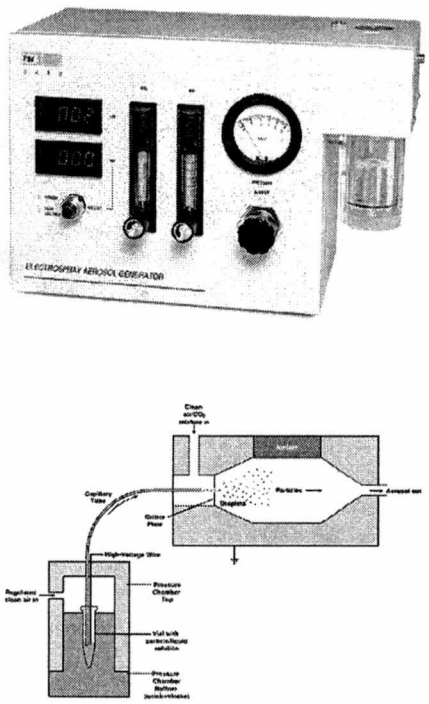


Figure 3.7 The above picture is Model 3480 Electrospray Aerosol Generator. The below picture shows the process in which a neutralized monodisperse aerosol is formed.

3.1.5 Nitrogen Oxides Analyzer

A California Analytical Instruments NOx analyzer is used to measure NOx in the diluted aerosol. (**Figure 3.8**). This analyzer consists of a chopper, two photomultiplier tubes (PMT), and two reaction cells with integral ISOFLO rate controls. Its operation is based on the chemiluminescense of an activated NO_2 species produced by the chemical reaction between ozone and NO. A cylinder of 250 ppm NO_2 in N_2 is used as the span gas to calibrate the instrument. The concentration of the span gas is beyond the range of the instrument. Since the NOx concentration in the diluted aerosol is about 1.0 ppm, the instrument is also calibrated at that concentration to obtain the correct measurement.

3.1.6 Tapered Element Oscillating Micro-balance (TEOM) Detector

The TEOM Series 1105 Monitor is a real-time device for measuring the mass concentration of particulate smaller than 10 microns diameter in outdoor and indoor ambient air (**Figure 3.9**). The TEOM instrument is the only filter-based mass monitor that measures the mass of particulate suspended in gas stream in real time. It measure particulate concentration in the range from 5 x 10^{-6} g/m^3 to several mg/m^3. The United States Environmental Protection Agency (U.S. EPA) has decided to use this instrument as a method for the determination of 24-hour average PM-10 concentrations in ambient air.

3.1.7 Flow System

The flow system is used to control dilution ratio and extract the exhaust gas for measurements. It consists of high efficiency particulate air (HEPA) filters, gas regulators, and flowmeter (**Figure 3.10**). HEPA filter is used to remove dirty airborne particles and mists in the compressed air. Gas regulator is used to control the flow rate of mixing gases. Two gas regulators were used: one system with Hastings Instruments Model HFM-201 Mass Flowmeter and Mass Flow Controller HFC-203 (**Figure 3.11**) used in the Dilutor II and Dilutor III (the other one-staged micro-dilution device), the other with rotameter and regulator system. Dilution ratio in micro dilution device was controlled by two inlet sources. The measured real flow rates are corrected to the standard condition.

3.1.10 Dilutor Cleaner (DC)

A cleaning system was designed to clean sampling lines and the dilutor (**Figure 3.12**). After shutting off engines, particles will deposit on the wall surfaces of the sampling lines and the dilutor. Resulting in particle reentrainment through next experiment. The vacuum pressure of the ejector pump is used to aspirate cleaning solution through the transfer lines and hoses. The turbulence of the system ensures good penetration of the cleaners onto the wall of the dilutor.



Figure 3.8 Photograph of NOx and HC analyzers

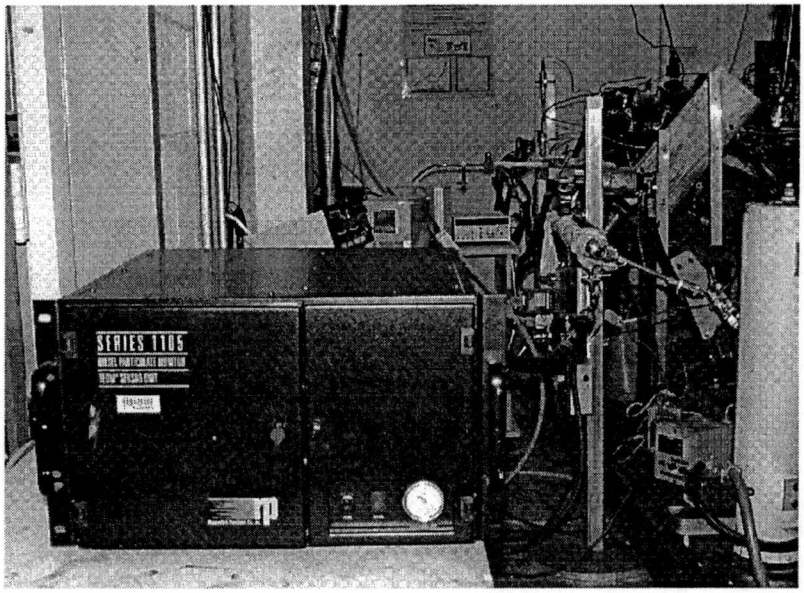


Figure 3.9 TEOM measurement

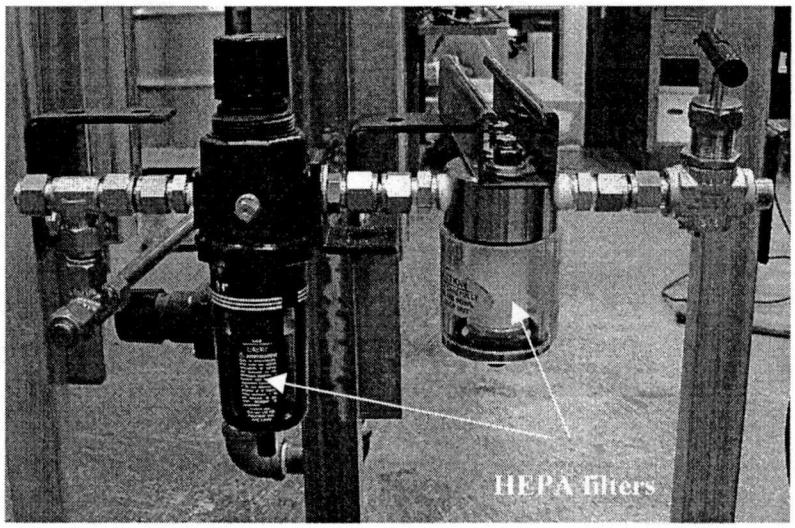


Figure 3.10 Two different HEPA filters and one regulator were installed on the Dilutor I.

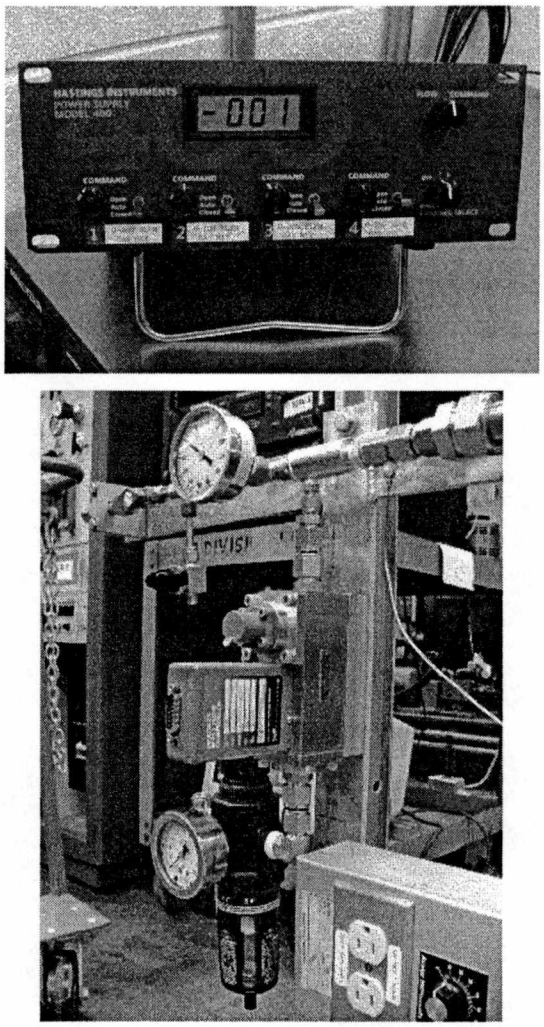


Figure 3.11 Mass Flow system consists of a HEPA filter, a Mass Flow Controller HFC-230 (above picture) and a Mass Flowmeter HFM-201 (bottom picture)

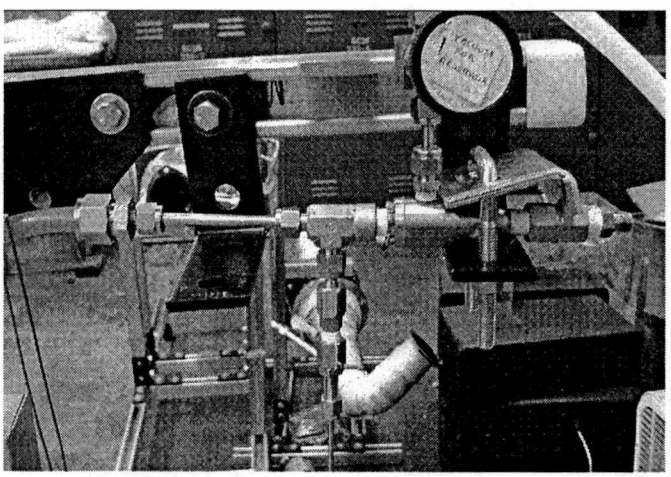


Figure 3.12 Photograph of dilutor cleaner.

3.2 EXPERIMENTAL PROCEDURES

Initially, the micro-diluter was characterized with model aerosol particles. The first series of engine experiments were performed with heavy-duty diesel engine using different sulfur fuels, and the Dilutor I a variable long residence time dilution system to study particle size distributions from engine out and DPF out. A limited number of engine stabilization tests were also conducted during experiment 1. The second series of experiments were run with light duty diesel engine using 150 ppm sulfur fuel, and the Dilutor II a variable short residence time dilution system to study the influence of dilution conditions on particle size distribution and concentration measurements. Parameters such as dilution ratio, dilution air temperature, and residence time were studied in detail. Some selective experiments were also performed with ultra low sulfur diesel fuel (3 ppm sulfur). Finally, the third series of experiments were run with gasoline engine using indoline fuel and the Dilutor II to study the influence of dilution condition, exhaust gas temperature on particle size distribution and concentration measurements.

3.2.1 Dilution Calibration with NaCl and DOP Aerosols

The purpose of this investigation was to determine whether turbulence mixing created by the orifice, the ejector pump and the diverging converging tubing would have an effect on particle size distribution. The 98 ± 6 nm Polystyrene Latex (PSL) particle size distribution was generated by using TSI Model 3076 constant-output non-recycling nebulizer (**Figure 3.13**). The two major peaks 96 and 103 nm were recorded repeatedly by SMPS within the certified range. The PSL aerosols were used to check the dilutor if it works well without any artifact. The dry solid particles were generated from a solution of 0.5% sodium chloride (NaCl) in water. The oil particles were generated from 0.03% dioctyl-phthalate (DOP) in 2-propanol. Sodium chloride and dioctyl-phthalate aerosol experiments were used to test the difference in the geometric characteristics of mean diameter and standard deviation of particles passing through the orifice and ejector. This dilutor calibration was conducted at the Aerosol Laboratory at ORNL.

The other tests were also performed in Advanced Propulsion Technology Center (APTC) to determine the magnitude of (a) particle losses due to particles depositing to the dilution tunnel walls and (b) particle mass gain due to condensation/absorption of HC vapors. Sampling the

diluted exhaust at different points along the dilution tunnel, and comparing the measured concentrations, both on a number and on a mass concentration basis was also undertaken.

The statistical analysis was used in the comparison of particle size distributions before and after the distributor.

3.2.2 Experiments on Engine Dynamometer Tests and Dilutors

The tests were conducted on three different engines (**Table 3.1**) operated on different dynamometers. The dilutor was used to simulate atmospheric dilution processes while the engine was running. A NOx analyzer was used to check dilution ratio. A Tapered Element Oscillating Microbalance (TEOM) was used to measure particulate mass. Engine dynamometer tests were conducted at different engine speed and torque. The test conditions were focused on the effect of dilution ratios, temperatures, residence times, fuels, and catalysts on nanoparticle size distribution.

The engines was warmed up and stabilized at 700 rpm for 30 minutes before running the entire series of experiments (**Table 3.2**). It was necessary to stabilize the engine for 5 to 10 minutes until the temperatures of engine exhaust, cooling water, intake air, fuel, and oil were in a stable reading. All experiments were run under steady state condition and three different modes (**Table 3.3**). Exhaust particulate measurements with the SMPS and CNC require about 20 minutes for each condition. One or two scans of the SMPS were taken at each dilution condition. Each scan was set for 2 minutes. The particle diameter range was set up from 7 nm to 400 nm for Model 3934 SMPS and from 3 nm to 100 nm for Model 3936 SMPS. The dilution condition parameters varied during experiments were dilution ratio and residence time. Engine exhaust NOx and diluted NOx concentrations were used to check dilution ratio. Experiments were run with ultra low sulfur diesel fuel (3 ppm), low sulfur diesel fuel (40 ppm), 150 ppm sulfur fuel, and gasoline fuel (**Table 3.4**).

Table 3.1 Specifications of the engines used in this project

	Detroit	**Volkwagen**	**Mitsubishi**
Engine	Heavy duty diesel	Light duty diesel	Light duty gasoline
Displacement, liter	5.3	1.9	1.6
Injection device	Electronic unit injector	Direct Injection	Direct Injection
Aspiration	Turbochaged	Turbocharged	Turbocharged
Compression ratio	15:1		10:1
Number of cylinder	4	4	4
Year	1999	1999	1997

Table 3.2 Experiment Conditions

	Detroit	**Volkwagen**	**Mitsubishi**
Dilution Ratio	5-1000	5-500	5-20
Residence Time, ms	50 – 7000	100	100
Mixing Temperature. ^{0}C	32 - 45	32 - 45	32 - 45
PDF out	CDPF**, CR-DPF	MRPF*, CDPF	No
Torque, lbs./ft	0 – full load	0 – full load	0 – full load
Fuel	Diesel (low sulfur)	Diesel (low sulfur)	Isooctane
Engine Speed, rpm	700 - 2100	700 - 2500	700 - 4500

** MRPF: Microwave Regenerated Particulate Filter*
*** CDF: Catalyzed Diesel Particulate Filter*
**** CR-DPF: Continuously Regenerating-Diesel Particulate Filter*

Table 3.3 Summary of three different modes

N, RPM	**Torque, lbf/ft**	**Throttle**
2100	100	37 %
	373	48 %
	755	100 %
1950	550	80 %
	105	
700	1	5 %

Table 3.4 Composition of Fuels

Fuel Type	Diesel	Low Sulfur	Ultra Low Sulfur
	% weight	% weight	% weight
Carbon	87.81	87	86.59
Hydrogen	12.75	13	13.97
Sulfur	0.04	0.0030	0.0010

3.2.2 Diesel Particulate Filter

Three different kinds of catalytic converters were used in this project: Continuosly Regeneting-Diesel Particulate Filter (CR-DPF), Catalyzed Diesel Particulate Filter (CDPF) (**Figure 3.14**), and Microwave Regeneration Particulate Filter (MRPF) (**Figure 3.15**). The MRPF contains special carbide fibers that convert microwave energy to thermal energy which is used to burn and remove 90 % of collected diesel particulate matter from the exhaust stream. Previous traps have used catalyzed coatings, fuel additives, and electrical heating to assist trap regeneration. Failure to consistently regenerate the trap can lead to plugging, excessive exhaust back-pressure, and eventually overheating and permanent damage to the trap. Inconsistent regeneration due to the high frequency of fairly low exhaust temperatures has been a particular problem in using PM traps to some lightly loaded diesel applications.

3.2.3 Heavy-Duty Diesel

The heavy-duty diesel engine 8.3 liters was displaced and used to run with and without DPF with different sulfur fuels (**Figure 3.16**). The test conditions are listed in **Table 3.5** .

3.2.4 Light-Duty Diesel

Volkswagen light duty diesel engine with a capacity of 1.9 liters was used to run with and without MRPF with 150 ppm sulfur fuel to ultra low sulfur diesel fuel at 3 ppm (**Figure 3.17**). The test conditions are listed in **Table 3.6** .

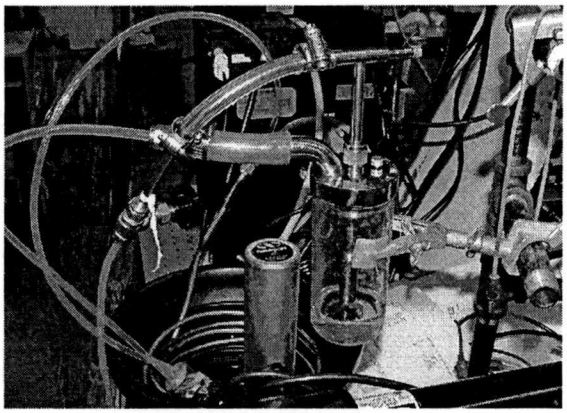


Figure 3.13 TSI Model 3076 Constant-output non-recycling Nebulizer

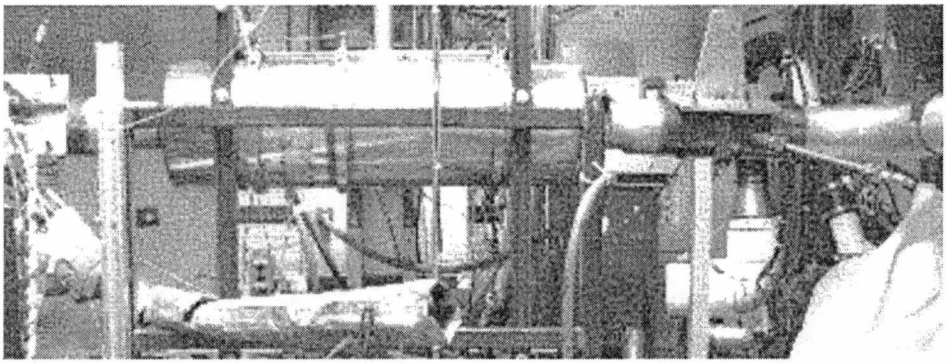
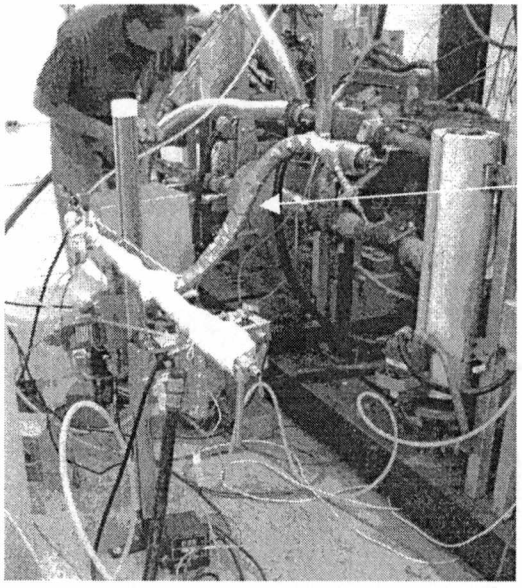


Figure 3.14 Diesel particulate filter



MRPF

Figure 3.15 Microwave regenerated particulate filter

3.2.5 Spark-Ignited Direct Injection Gasoline Engine

The primary objectives of this study was to determine the number and size distributions from SI engines operating at steady state conditions as a function of fuel type, operating conditions, and emission sampling measurement. Mitsubishi 4G9 Series 1.9 liters was used to determine number concentration of nanoparticles in gasoline engine (**Figure 3.18**). The indolene fuel was used in this test. In the past, only a small number of tests have been done to quantify the total mass and chemical composition of PM emitted by representative SI automobiles and fleets from (Rogge *et al.*[46]; Greenwood *et al.*[47], Hildemann *et al.*[48], and Hochgreb *et al.* [49]). The formation of particulate matter in spark-ignited engines revealed some of the basic trends in PM emission with respect to engine type and age, steady state engine operating conditions, and fuel/lubricant composition.

Table 3.5 Summary of test conditions on heavy duty diesel

Catalyst	Sulfur Fuel ppm	DR	Speed rpm	Load
DPFs	3, 40	10 - 100	idle	0
DPFs	3, 40	10 - 100	2100	37 %
DPFs	3, 40	10 - 100	2100	100 %

Table 3.6 Summary of test conditions on light duty diesel

Catalyst	Sulfur Fuel, ppm	DR	Speed rpm	Load
MRPF	3, 150	10 - 20	idle	0
MRPF	3, 150	10 - 20	1500	37 %
MRPF	3, 150	10 - 20	1800	100 %

Table 3.7 Summary of test conditions on light duty gasoline

DR	Speed rpm	Load
10 - 20	idle	0
10 - 20	1400	10 %
10 - 20	1950	37 %
10 - 20	2100	100 %
100	idle	0
100	1950	37 %
100	2000	80 %

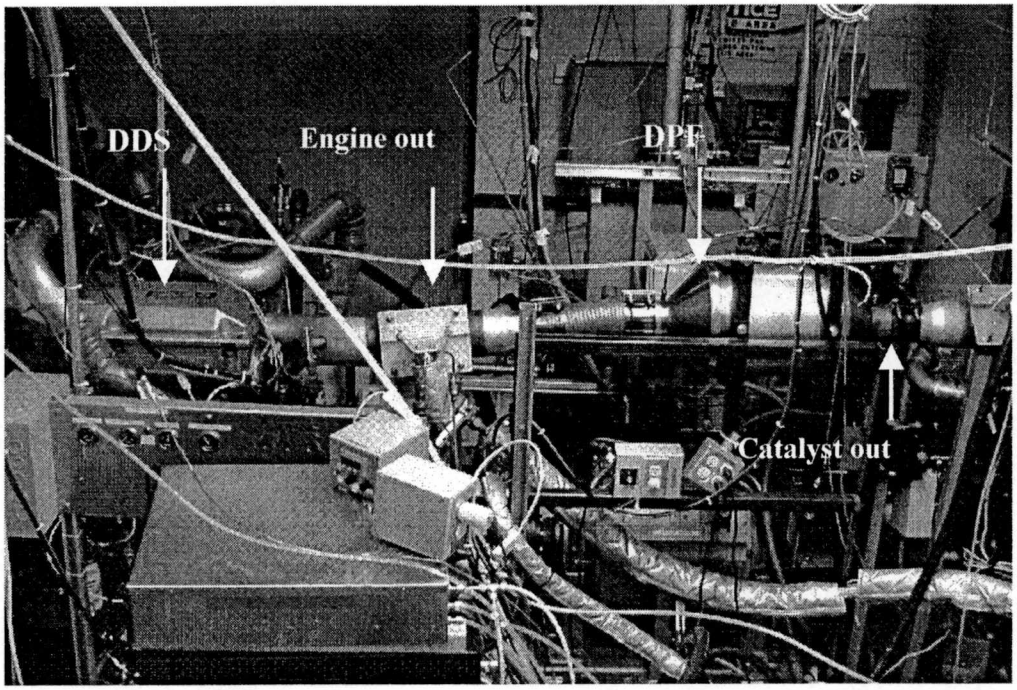


Figure 3.16 Heavy duty Diesel Detroit Series (DDS) 50 engine

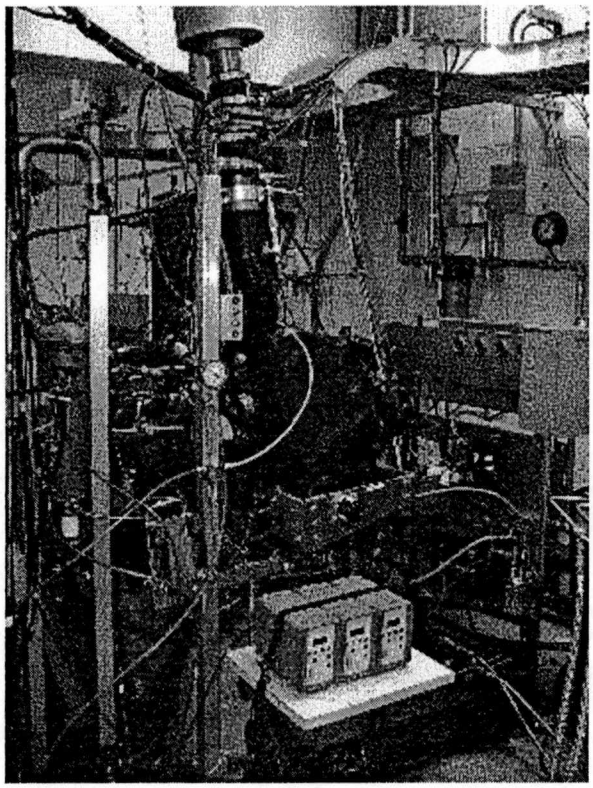


Figure 3.17 Volkswagen 1.9 liter engine

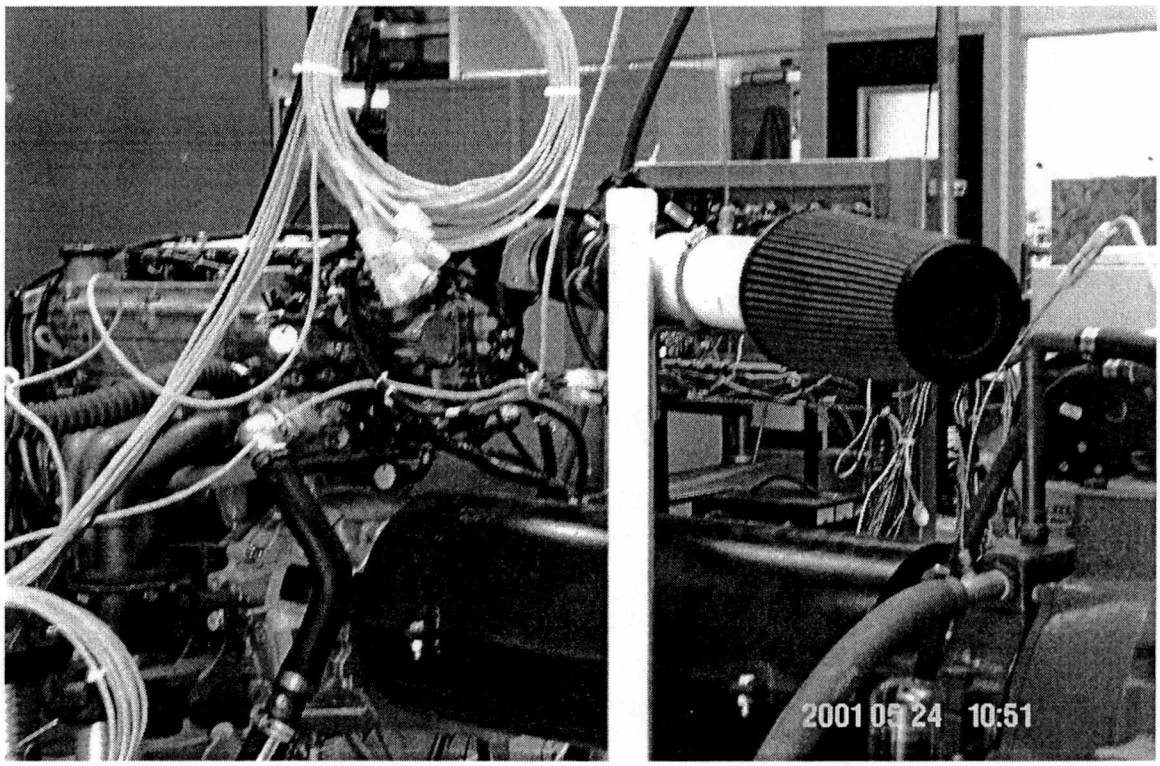


Figure 3.18 Mitsubishi 4G9 Series 1.9 liters

CHAPTER 4 EXPERIMENT RESULTS AND ANALYSIS

This chapter presents the effect of a number of parameters on the number concentration of the particulate. These parameters include dilution ratio, residence time, and engine parameters such as diesel particulate filters, fuel sulfur and exhaust gas temperature. The results from the calibration of the dilutors are presented first. All the data was obtained from the experiments performed for two years at ORNL-APTC.

4.1 DILUTION DEVICE CALIBRATION

As discussed in Chapter 2, it is important to calibrate the dilutors to make sure artifacts are not created. Cheng *et al.* [50] reported the experiments and results of dilution device calibration in detail. The 0.5% (w/v) sodium chloride (NaCl) in water results showed no difference in particle distribution at pre and post dilution device. There were no shift in the center as well as the spread of the particle size distributions (**Figure 4.1A**). Both distributions were symmetrical and centered at 77 nm. The coefficient of variation (CV) for the pre and post dilutor data in **Figure 4.1B** showed that the CV was less than 10% for the central region and more than 20% for the tail ends where the particle concentration was high and low, respectively. The skewness values in these NaCl experiments were all positive and the ranges overlap each other for the pre- and post-ejector data indicating they were the same (**Figure 4.1C**). However, the both distributions were fairly symmetrical in DOP data. (**Figures 4.2A**). The CV for each particle size range was greatest for the size ranges with low concentrations by particle size (**Figure 4.2B**). The skewness values in these DOP experiments were almost positive except for the right tail end (**Figure 4.2C**). The dilutor might have an effect on the variability of the post dilutor aerosol. But an increasing scan time might limit the uncertainty of the distributions. The results showed the dilutor is fine to use in this project.

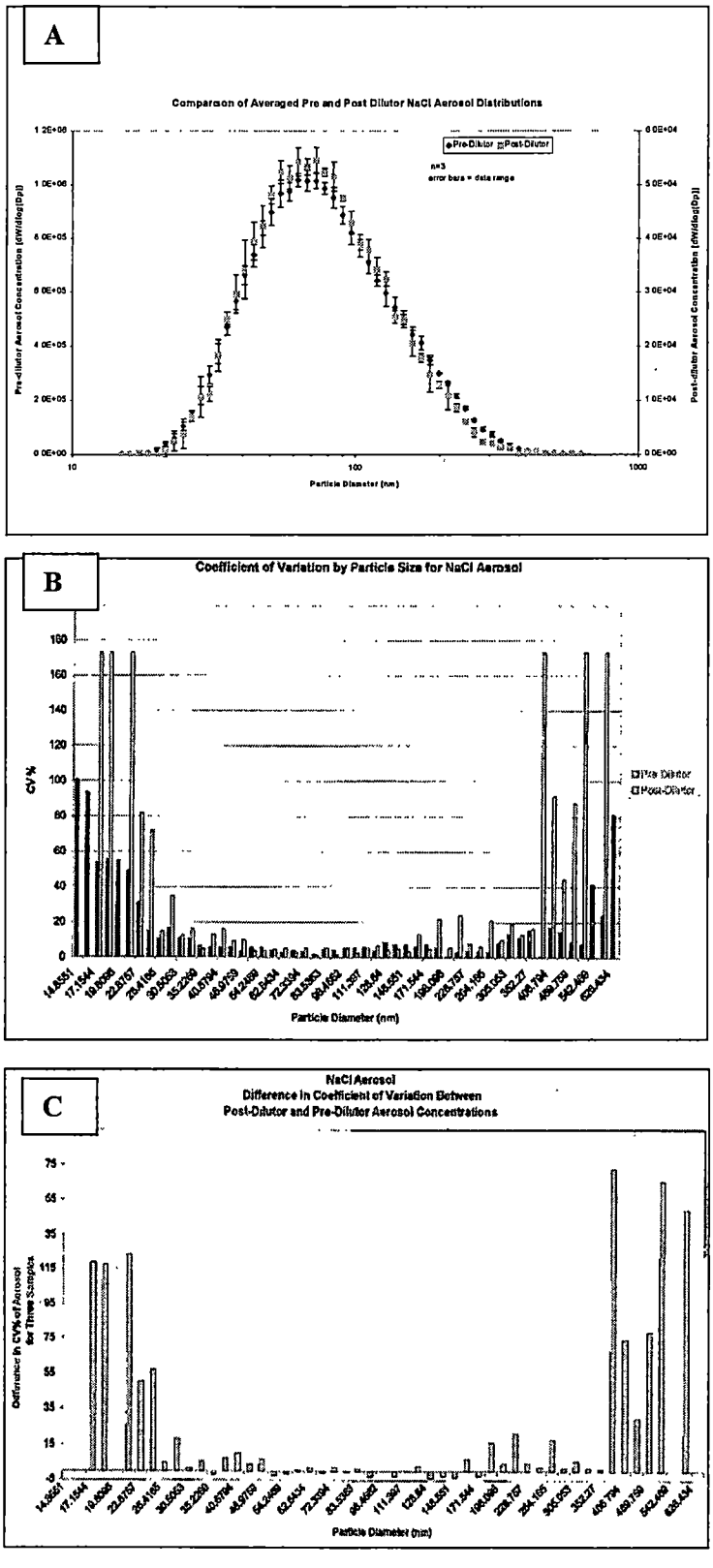


Figure 4.1 NaCl aerosol distribution (A), coefficient of variation by particle size (B), and coefficient of skewness (C) before and after dilutor. (source from Cheng *et al.*[50])

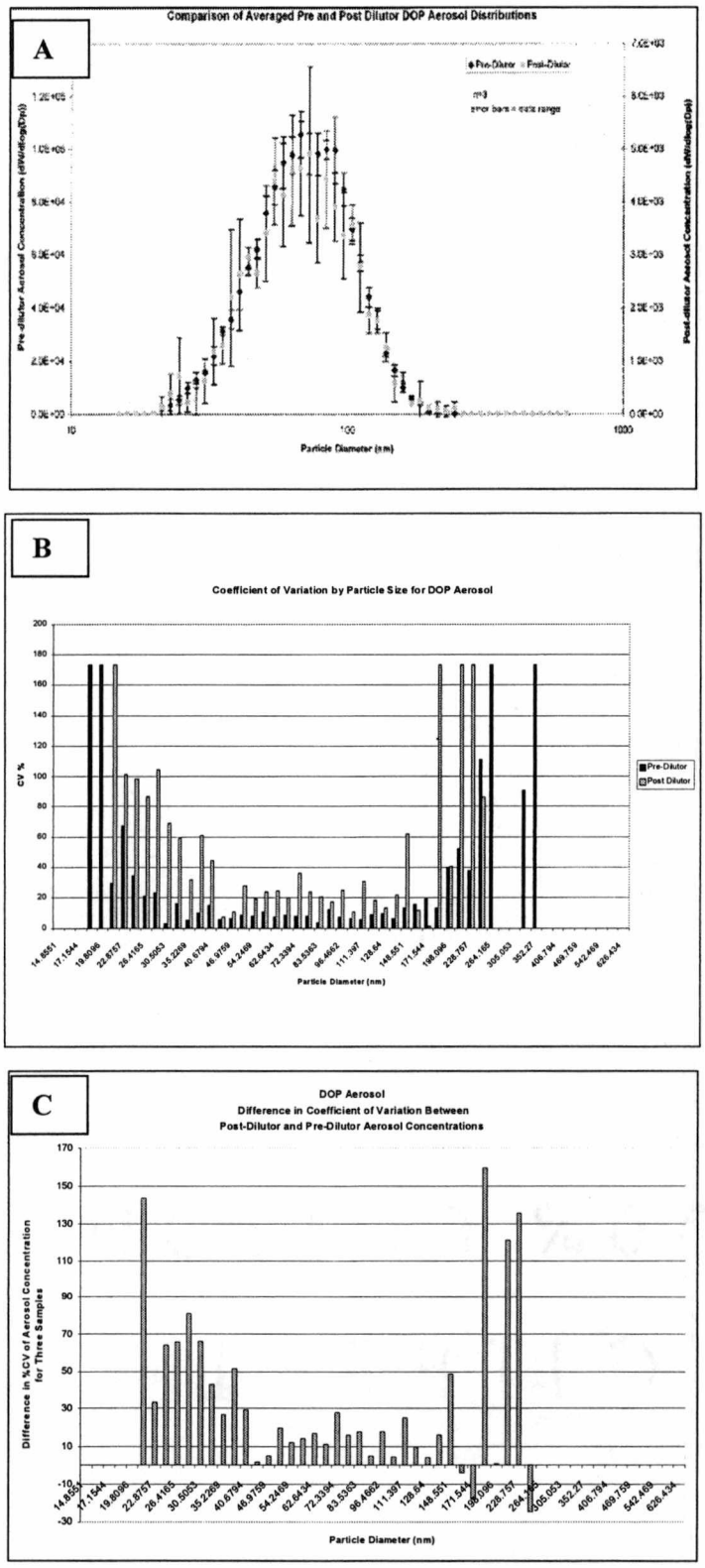


Figure 4.2 DOP aerosol distribution (A), coefficient of variation by particle size (B), and coefficient of skewness (C) for DOP aerosol comparison before and after dilutor. (source from Cheng *et al.*[50])

4.2 INFLUENCE OF DILUTION RATIO

It was shown that the residence time influences particle concentrations and size distributions upstream and downstream of trap during the test. In this section, results will be reported on a series of experiments that were designed to study the influence of dilution condition on filter out and engine out particle measurements. High dilution ratio will prevent the formation of nucleation growth. At high dilution ratios particles has a longer residence time to collide and coagulate. At low dilution ratio and low temperature, the influence of the residence time is the strongest, and the concentration in the nanoparticle size range is the highest (**Figure 4.3**).

4.3 INFLUENCE OF RESIDENCE TIME

The influence of residence time on nanoparticle formation was conducted on engine out condition. Four residence times of 50, 700, 2000, and 5000 ms and two dilution ratios of 10 and 125:1 were applied (**Table 4.1**). The temperature and dilution ratio in the primary dilution section were 35 ^{0}C, and 10, respectively.

Figure 4.4 shows the size distribution and number concentrations at each of the residence time in engine out, speed 1950 rpm, 37% load, and 40 ppm sulfur fuel. All distributions are bimodal and lognormal shape. For a residence time of 50 ms the nuclei mode peaks at 12 nm. At 700 ms the number in the mode increases and peak shifts to about 10 nm. At 700 ms the number concentration is highest and the peak occurs at about 7 nm which is the lower size detection limit of the instrument (Figure 4.4A). Figure 4.4B and C shows the influence of residence time on particle number size distributions at different dilution ratios of 10 and 125.

Particles in the accumulation mode above 50 nm diameter should not be affected by the changes in residence time. The size distributions of the nuclei mode could be influenced by the residence time. At low dilution ratio, the influence of the residence time is the strongest, and the number of concentrations in the nanoparticle size range is the highest.

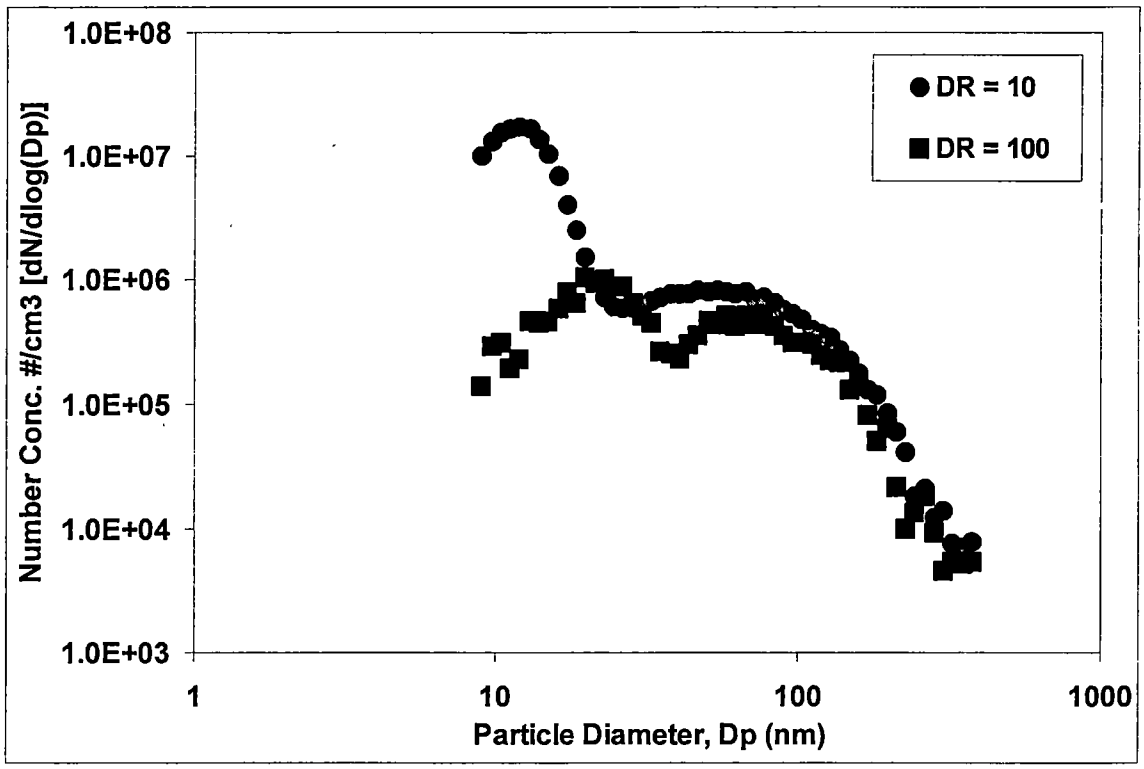


Figure 4.3 Number concentration difference for different dilution ratio (DDS engine, 1950 rpm, 37% load, 3ppm S fuel, engine out).

Table 4.1 Testing Conditions

DR	RT, ms	N, rpm	Load
10	50, 700	1950	37 %
10	2000, 5000	1950	37 %
125	50, 5000	1950	37 %

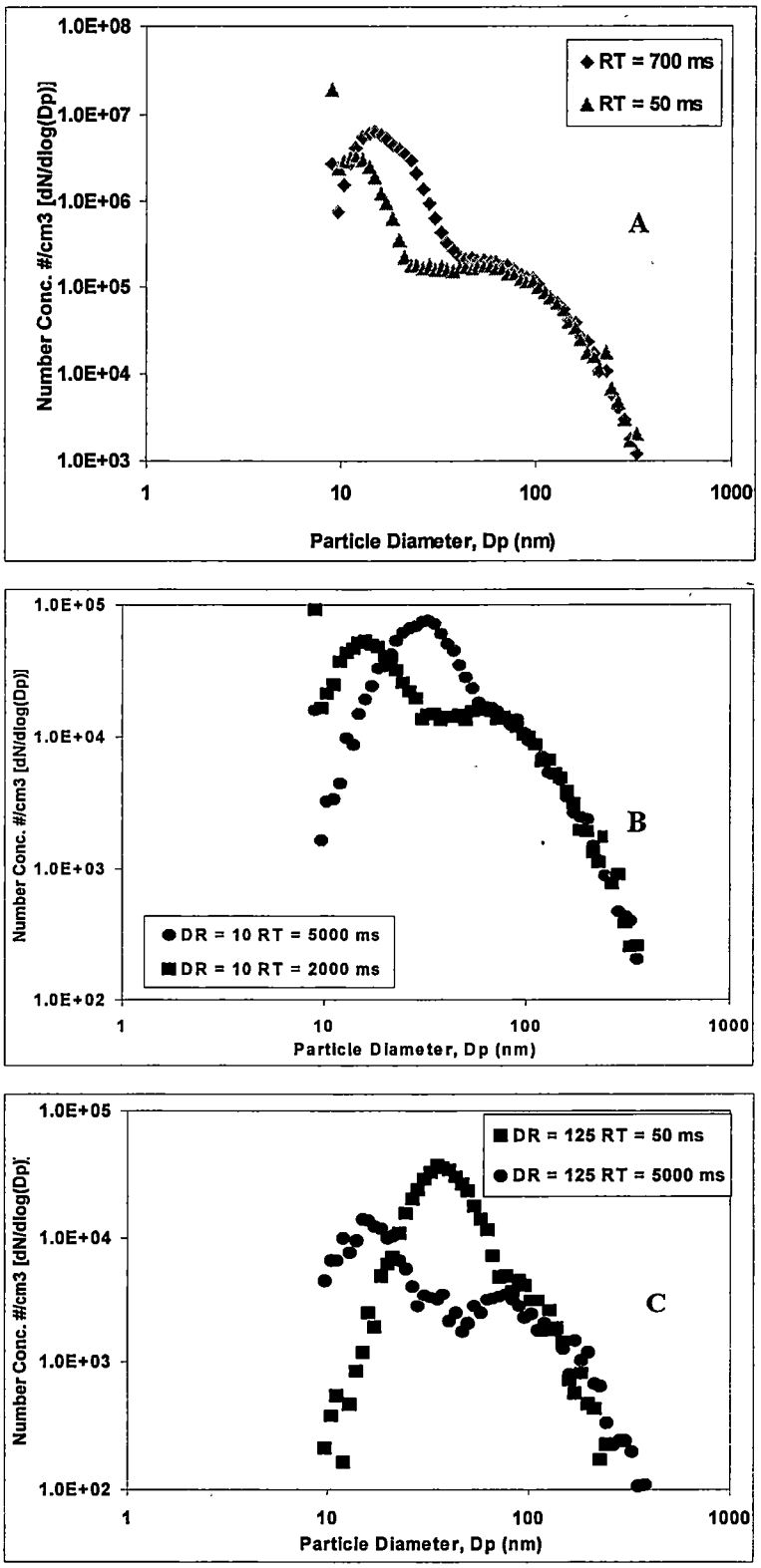


Figure 4.4 Number concentration distributions for different residence times . The volume in the nuclei mode grows considerably with residence time (DDS engine, 1950 rpm, 37% load, 40ppm S fuel, engine out).

4.4 INFLUENCE OF DIESEL PARTICULATE FILTERS

Diesel particulate filters have been designed to remove particulate matter from the exhaust by collection on a filter element. They are considered a possible means of meeting future emission regulations. Various studies have shown that filters reduce particulate mass emission very effectively. However, some researchers reported that filters increase emissions of nanoparticles under certain engine operating conditions while others report significant reductions. Therefore, the influences of the exhaust filters on number concentrations were examined. This included particle size distributions, concentrations, and residence time. The diesel particulate filters used in this project were a Catalyzed Diesel Particulate ilter (CDPF), a Continuously Regenerating Diesel Particulate filter (CR-DPF), and Microwave Regenerable Particulate filter (MRPF).

Figure 4.5 shows the total exhaust number concentrations engine out and catalyst out of the filter at dilution ratio of 10:1 and residence time of 700 ms. SMPS was scanned two times with each for two minutes. The size distribution of engine out shows a bimodal structure: nuclei mode (Dp < 50 nm) and accumulation mode (Dp > 50 nm). This structure is typical for diesel particles. Particles in the accumulation mode consist of carbonaceous agglomerates formed during the combustion process. They are most of the particulate mass. In Figure 4.5, the DPF clearly removes a high percentage of the particles. **Figure 4.6** shows particle number concentration difference on CR-DPF and CDF. They were operated with 40 ppm fuel in idle condition. The number concentration from CR-DPF was 1 x 10^5 part./cm^3 compared to CDPF at about 1 x 10^4 part./cm^3. Even though exhaust temperature was too low to burn the particles, the CDPF does a better job removing small particles.

The results on MRPF also showed that MRPF reduced number concentration of nanometer size. Regeneration of the MRPF may lead to nucleation and growth. **Figure 4.7** shows an increasing in the concentration of nanometer sized particles (o) measured downstream of the filter occurs early in the regeneration process. As regeneration continues the concentration of nanoparticles decreases (□) while the concentration of what as presumably carbonaceous agglomerates in the diameter range above about 30 nm increases. The results could be the reaction between sulfur trioxide a water molecules in catalyst. It also could be from high temperature and clogged particles in the trap. In addition, the emission of nanoparticles downstream of the trap was also influenced by the residence time. Solid particles act to suppress nucleation of volatile exhaust

species during dilution and cooling of hot exhaust. High nanoparticle emission downstream of the trap is due to nucleation and growth that is improved by the removal of solid particles. The concentration of nanoparticles also lowered one order of magnitude between engine out and catalyst out.

Even thought DPFs clean mass concentration from the filter with 95% to 100% efficiency, it could be concluded that DPFs might cost some problem in nanoparticle formation. DPFs and MWPF may not significantly help in reducing number concentration of nanoparticles.

4.5 INFLUENCE OF SULFUR FUEL

Influence of sulfur fuel is clearly effecting on nucleation growth due to sulfuric acid aerosol formation. **Figure 4.8** shows the influence of ultra low sulfur fuel (sulfur mass concentrations of about 3 ppm) and low sulfur fuel (40 ppm) on particle number size distributions at a primary dilution ratio of 15, dilution temperature of 48°C, residence times of 150 ms, and low load condition. The number concentration distribution decreased from 1 x 10^4 part./cm^3 to 1 x 10^3 part./cm^3; that was one order of magnitude reduction. Sulfur in the exhaust could be oxidized over these filters with different catalyst materials, forming sulfates that were measured as PM because filters may convert SO_2 in the exhaust gas to SO_3. SO_3 will combine with water to become sulfuric acid aerosols. The impact of sulfur might affect the filter's regeneration capability. PM emissions during the high torque (high exhaust temperature) steady state tests showed a fuel sulfur influence.

4.6 INFLUENCE OF ENGINE TECHNOLOGY

As discussed in section 1.2, nucleation growth happens with absence of carbonaceous material in the process. In light duty gasoline engine as SIDI Mitsubishi in this project, EGR recirculate an amount of exhaust gas particles back to the chamber. These particles prevented the nucleation growth. **Figure 4.9** shows the influence of advanced EGR in reducing number concentration of particles, a increasing in load only affects the range of diameter size larger than 50 nm but not

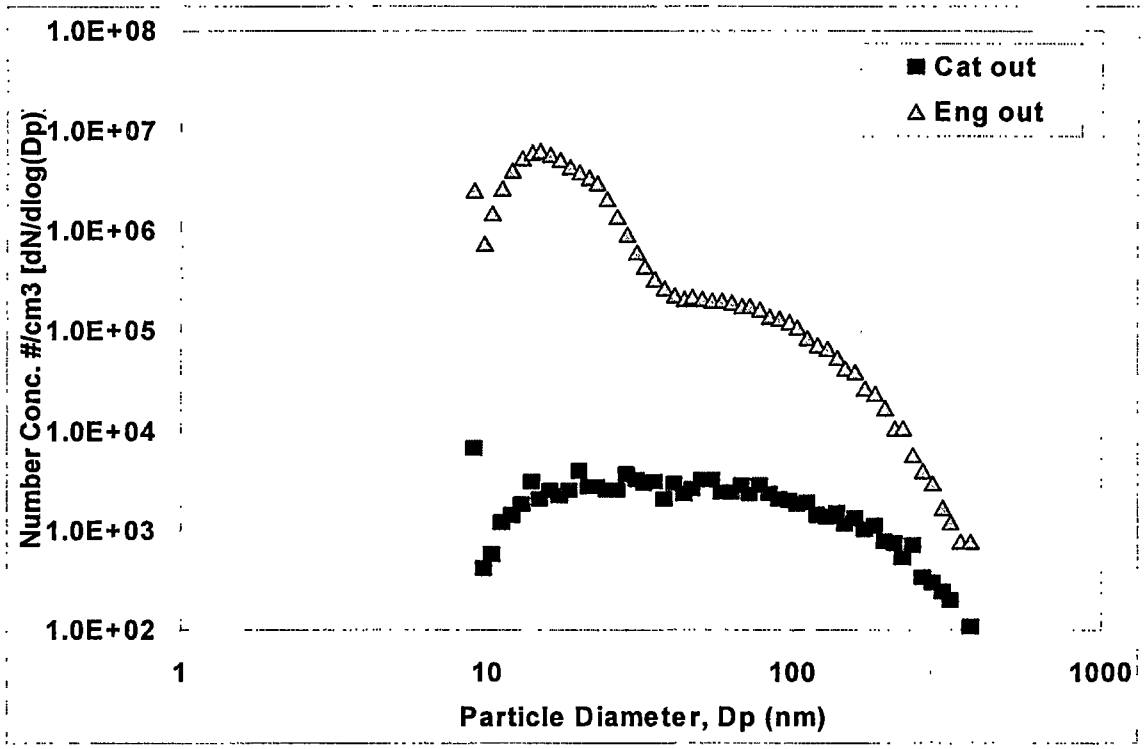


Figure 4.5 Influence of catalyzed diesel particulate filter exhaust in engine out and catalyst out in DR = 10 and RT = 700 ms (DDS engine, 1950 rpm, 37% load, 40ppm S fuel).

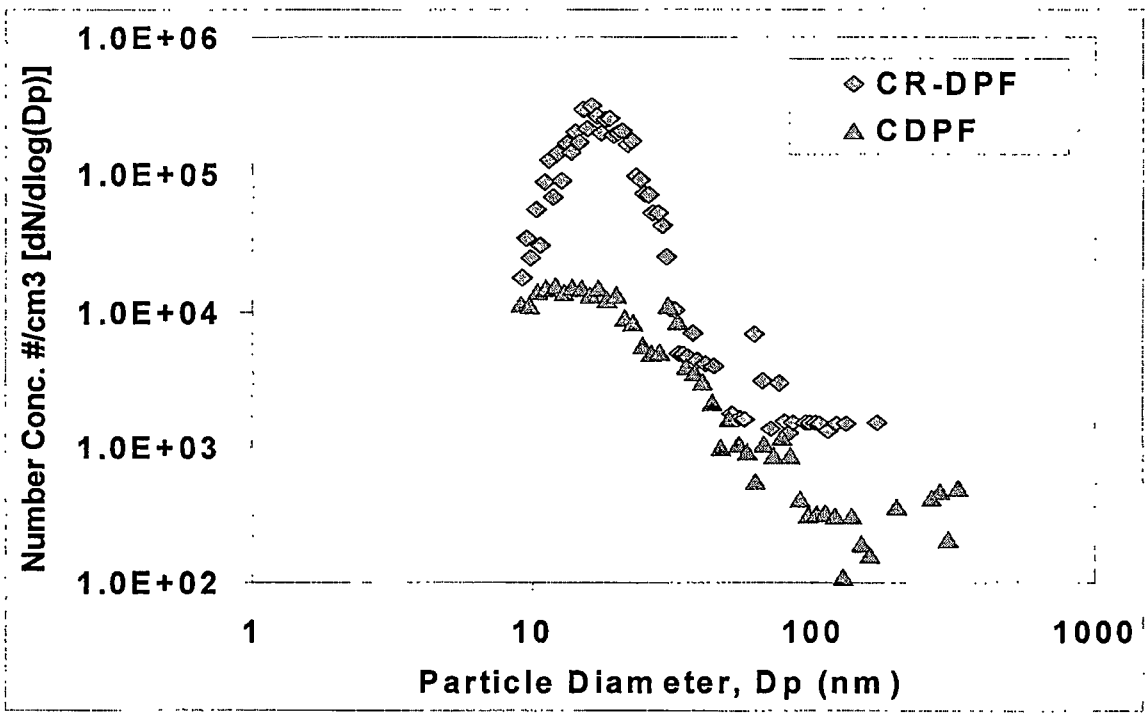


Figure 4.6 Comparison between CR-DPF and CDPF in effect on number concentrations (DDS engine, idle, 40ppm S fuel).

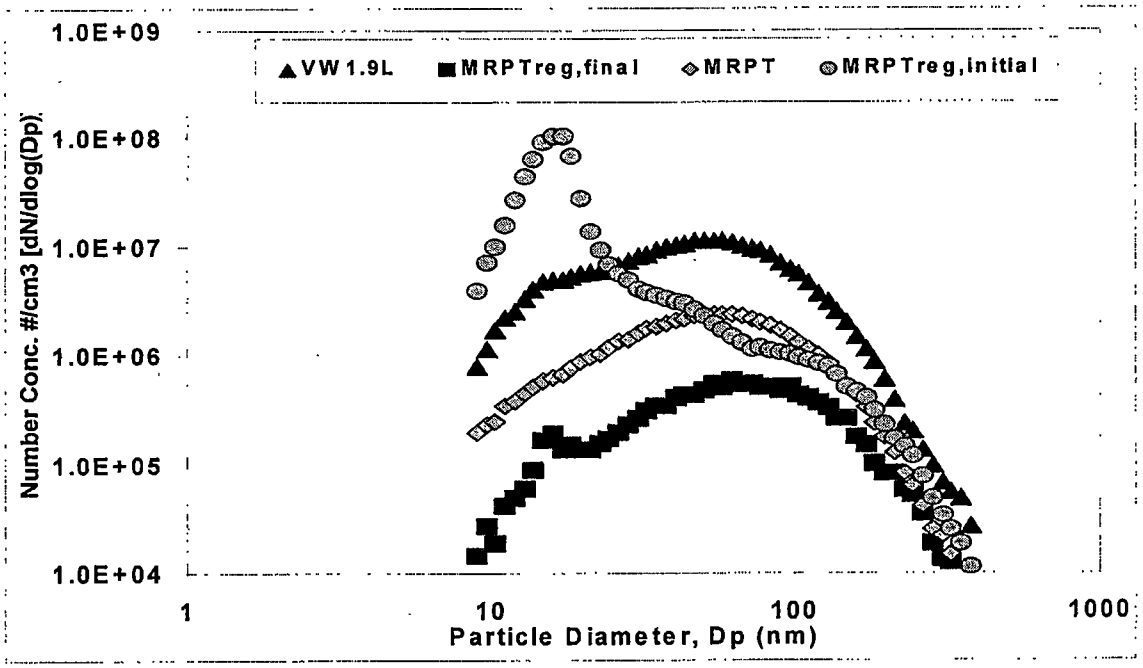


Figure 4.7 Number concentration difference between regeneration process (o), engine out (Δ), and MRPF out (□) (VW 1.9 L engine, 1491 rpm, 150ppm S fuel).

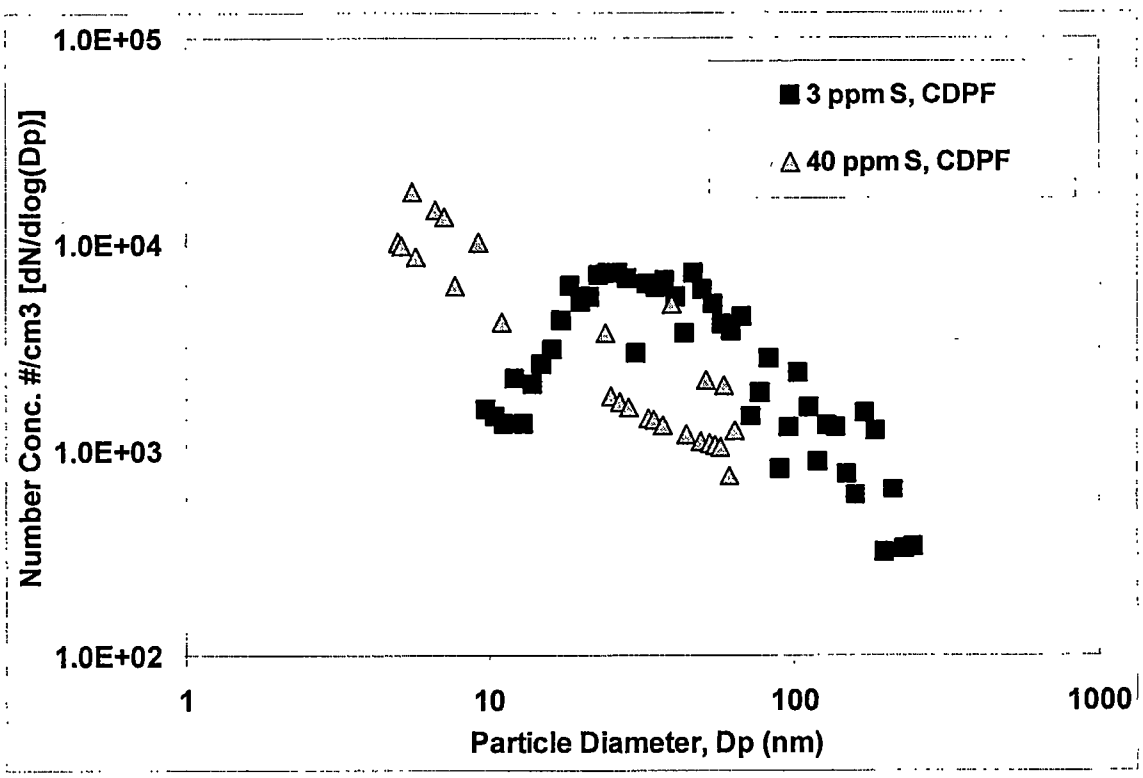


Figure 4.8 Comparison between two different sulfur fuels: 3 ppm and 40 ppm operated in DDS engine and DPF from Engelhard (DDS engine, 2100 rpm, full load).

nanoparticle size. Indolene fuel was used to run the engine and the test was carried out without a filter.

In advanced internal combustion engines, the highest number concentration appeared in heavy-duty diesel engine but not in light duty diesel engine and light duty gasoline engine. **Figures 4.10-12** show the results of size distribution and number concentration from three different internal combustion engine from this project. Even though engine test condition was different which is summarized in **Table 4.2**. In heavy-duty diesel engine, new nanoparticle number concentration increased and particulate mass decreased. On the other hand, these happened oppositely in light duty diesel and gasoline engines. Both the light-duty diesel and the SIDI engines were equipped with EGR. Nucleation by the ash particles is favored by the relatively low soot emissions from this engine. Nucleation of SOF and sulfuric acid during dilution and sampling might have contributed additional volatile material to the nuclei mode.

4.6 INFLUENCE OF EXHAUST GAS TEMPERATURE

Temperature has a very important of effect on vapor pressure. As temperature increases, saturation ratio decreases. As discussed in section 1.2, nucleation growth and condensation happen only when saturation ratio is larger or equal unity. The influence of exhaust gas temperature was checked on SIDI gasoline engine. **Figure 4.13** shows the results of the influence of exhaust temperature in increasing number concentrations. As exhaust gas temperature reduce from 830 °C to 533 °C number concentration increase at nuclei mode.

Table 4.2 Summary of the three engine test conditions.

Engine	DR	RT	Speed, N	Fuel
Heavy Diesel Engine	10	100 ms	1950 rpm	40 ppm S
Light Diesel Engine	10	100 ms	1950 rpm	150 ppm S
Light Gasoline Engine	10	100 ms	1950 rpm	Indolene

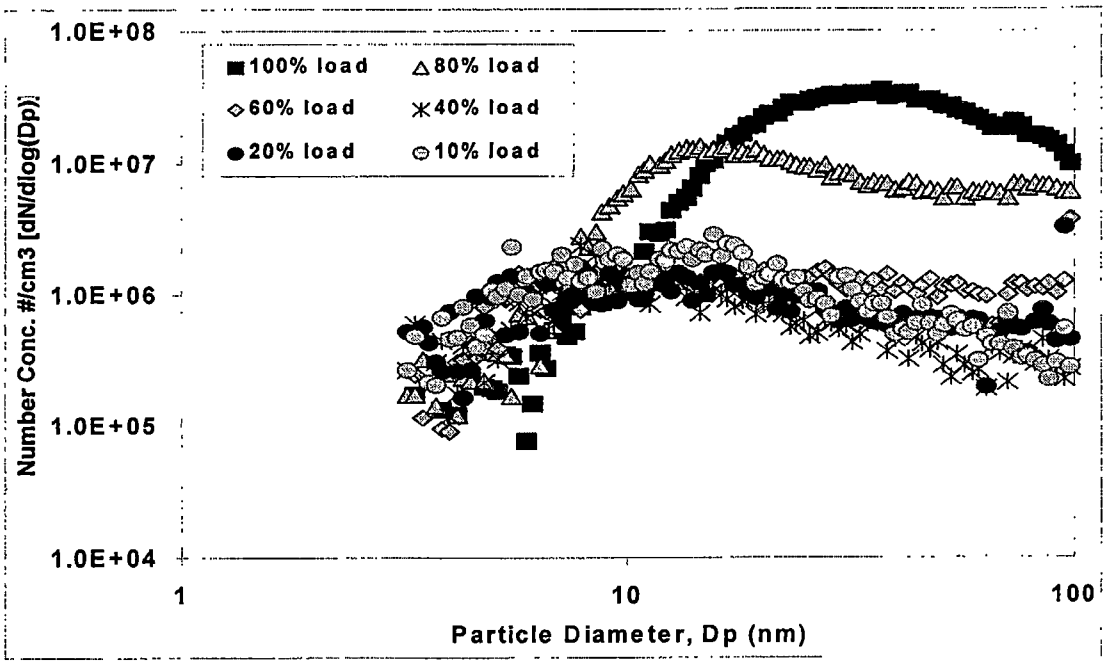


Figure 4.9 Influence of EGR in engine technology, a increasing in load only effect the range of diameter size larger than 50 nm. The nuclei mode did not happen.

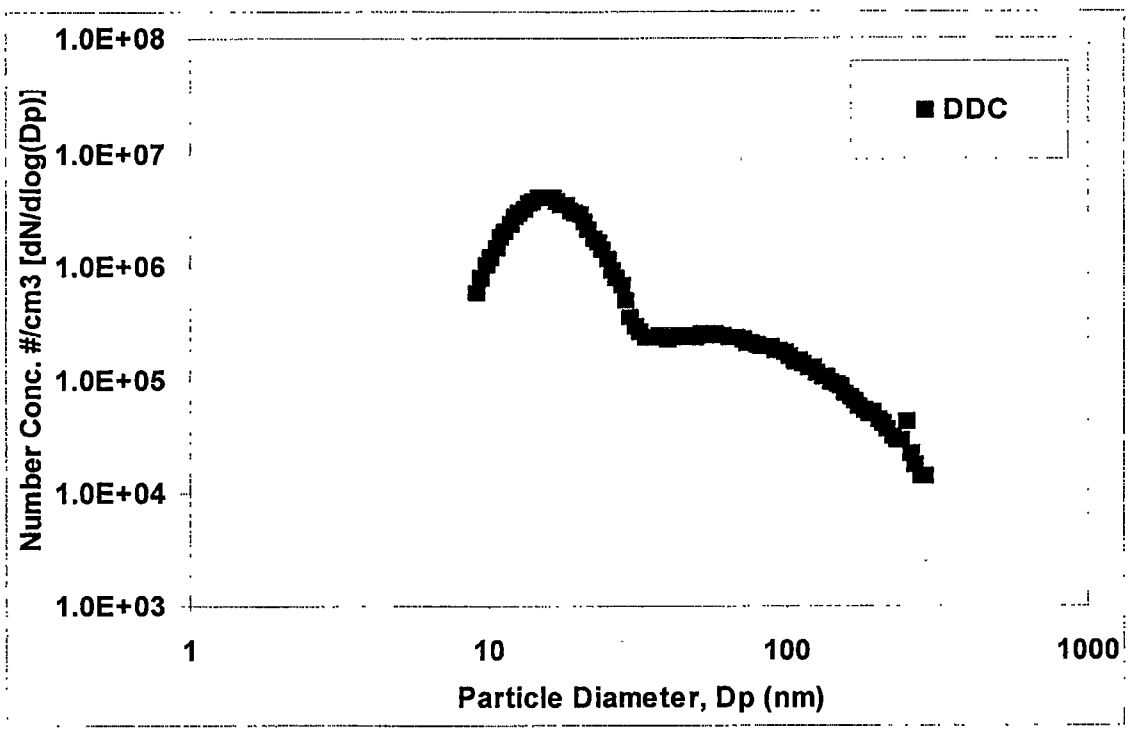


Figure 4.10 Size distribution and number concentration in heavy duty Detroit diesel engine . (2100 rpm, 37% load, 3ppm S fuel, engine out).

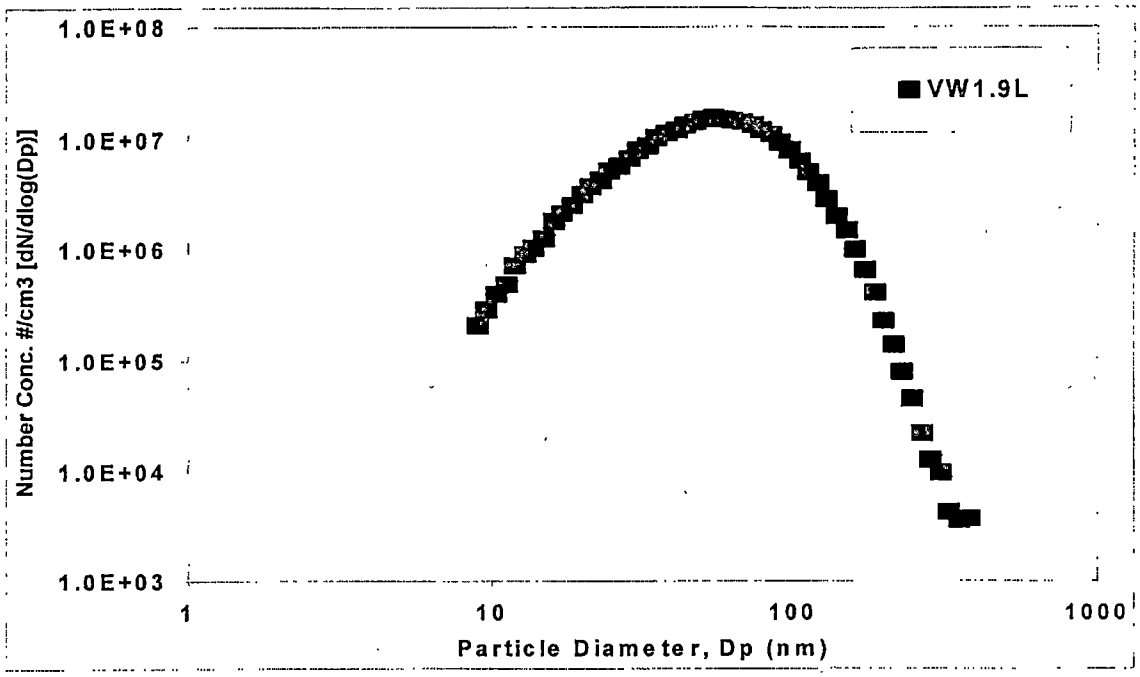


Figure 4.11 Size distribution and number concentration in light duty Volkswagen 1.9 L diesel engine (1991 rpm, 150ppm S fuel, engine out).

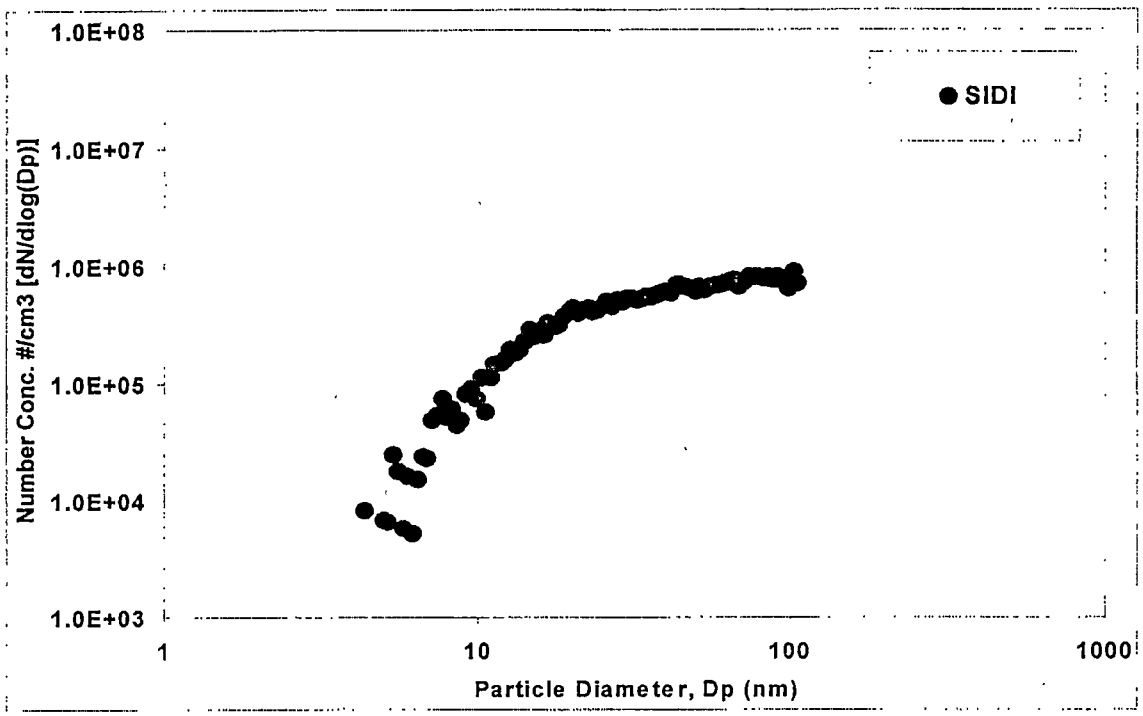


Figure 4.12 Size distribution and number concentration in light duty Mitsubishi SIDI gasoline engine (1950 rpm, 40% load, indolene fuel, engine out).

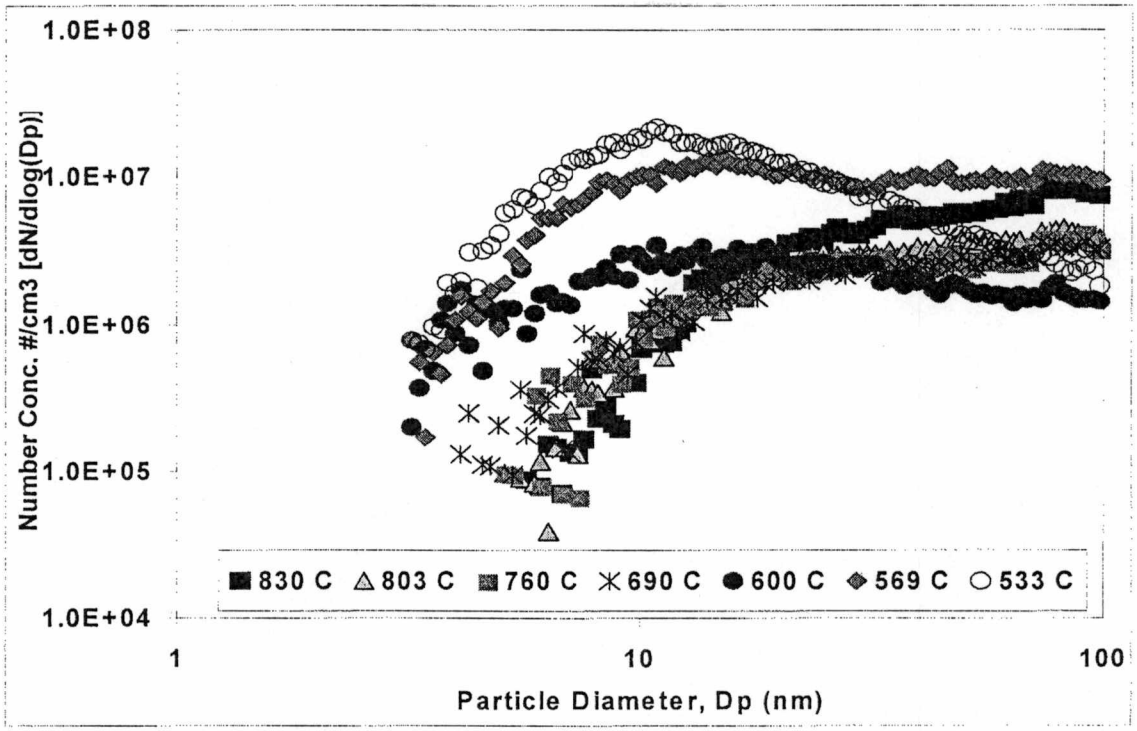


Figure 4.13 Shows the trend of increasing the number concentration at low exhaust temperature (SIDI engine, 3400 rpm, Indolene fuel, engine out).

CHAPTER 5 SUMMARY AND CONCLUSION

A micro-dilution device was designed and built based on the micro-dilution device used at UMN. The influence of dilution parameters on particle size and number emissions was investigated at different dilution ratios, residence times, diesel particulate filters, engine technology, fuel sulfur content and exhaust gas temperature. Some studies were performed upstream and downstream of a diesel particulate filter.

Number concentration ranged from $1x10^4$ to $7.5x10^7$ particles/cm^3 over the tests. The number size distributions were bimodal and log-normal with a nuclei mode in the 7-15 nm diameter range and an accumulation mode in the 30-80 nm range.

Dilution ratio changes the number size distribution due to coagulation process. The dilution ratio seems to have a significant influence on the number concentrations and size distributions of particles. Increasing the primary dilution ratio from 10-125 results in significant decreases in number and volume concentrations, with number concentrations influenced the most.

Residence time changes number size distribution due to nucleation growth.

Diesel particulate filters and Microwave Regenerable Particulate trap are effective in removing particulate matter mass and number. Nanoparticle distribution did not change very much with CDPF. The CR-DPF may increase nanoparticle number concentration. CDPF may be better than CR-DPF filter in PM treatment under some engine conditions.

Ultra low sulfur fuel (3 ppm sulfur in fuel) leads to a reduction in nanoparticles when compared with 40 ppm sulfur in fuel.

Decreasing exhaust gas temperature may lead to an increase in nanoparticles. The exhaust gas temperature is also an important variable in formation of nucleation growth because supersaturation ratio happens only at low temperature. However, the number concentration was

low at idle (low temperature). The high number concentrations were observed at 0 % load at both rated speed and maximum torque speed in SIDI engine.

In conclusion, nanoparticle number concentration could be affected by dilution ratio, residence time, particulate filter, engine technology, sulfur fuel, and exhaust gas temperature. The large number concentrations emitted by some modern low emission diesel engines are formed by a similar mechanism, nucleation of SOF and sulfuric acid that results from low solid carbon particle concentrations in the accumulation to adsorb/condense volatile matter and thus suppress nucleation. Therefore, the reduction of soot and volatile matter should help to minimize the formation of new nuclei mode particles during dilution and cooling.

5.1 RECOMMENDATION FOR FUTURE RESEARCH

Several interesting and important future research projects are highlighted as a result of this work:

1. Develop of a technique to measure the chemical composition of nanoparticles.
2. Use the dilution tunnel to dilute engine exhaust with different dilution air temperature and humidity. Find out how these parameters could influence the formation of small particles in the dilution process.
3. Compare the performance of the one-staged dilution tunnel with two-staged dilution tunnel.
4. Find a method to simulate the dilution process in the laboratory. Study nucleation during exhaust dilution. Compare results from the measurement with the numerical model.
5. Control temperature better to avoid thermophoresis.
6. Dilution tunnel should be cleaned before using.

REFERENCES

[1] Hodgson, W. Jefferey, Irick, K. David, and Fussell, M. Lori, *Automotive Engines and Vehicles*, Meyers, A. Robert ed., Encyclopedia of Environmental Analysis and Remediation, John Wiley & Sons, Inc., New York, pp.552-553, 1998.

[2] Masters, M. Gilbert, *Introduction to Environmental Engineering and Science*, Prentice Hall, New Jersey, pp. 292, 1991.

[3] Ferin, G.O., D. P. Penney, "Pulmonary Retention of Ultrafine and Fine Particles in Rats", *Am. J. Respir. Cell Mol. Biol*, Vol. 6, pp. 534-542, 1992

[4] Donaldson, K., P. H. Beswich, and P.S. Gilmour, Free Radical Activity Associated with the Surface of Particles: A unifying factor in determining Biological Activity, *Toxicology Letters*, Elsevier, pp. 293-298, 1966.

[5] Storey, J., Cheng, M. D. and Malone, B., Response of Human Lung Cells to Nanoparticles, Presented at the 2001 *Diesel Engine Emissions Reduction Workshop*, Portsmouth, VA, July, 2001.

[6] Annette, P., Dockery, W. Douglas, Muller, E. James, and Mittleman, A. Murray, Increased Particulate Air Pollution and the Triggering of Myocardial Infarction, *Journal Circulation*, Vol. 103, pp. 2810-2815, 2001

[7] Khalek, S. A. I., Kittelson, B. D., Graskow, A. B., Wei, Q., and Bear, F, Diesel Trap Performance: Particle Size Measurements and Trends, *SAE982599*, 1998.

[8] Heywood, B. John, *Internal Combustion Engine Fundamentals*, McGraw-Hill, New York, pp. 626-648, 1988.

[9] Amann, A. C. and Siegla, C. D., Diesel Particulates-What They Are and Why, *Aerosol Science and Technology*, Vol. 1, pp. 73-101, 1982.

[10] Spurny, R. Kvetoslav and Hocrainer Dieter, *Aerosol Chemical Processes in the Environmental*, Lewis Publishers, New York, pp. 457-523, 2000.

[11] Storey, John, Exhaust Emission Control Effects on Diesel Particulate Matter Characteristics, *Proceedings of the 1999 Diesel Engine Emissions Reduction Workshop*, Maine, Vol. 3, pp. 41-54, 1999.

[12] Bagley, S. T., K.J. Baumgard, L.D. Gratz, J.H. Johnson, and D.G. Leddy, Characterization of Fuel and Aftertreatment Device Effects on Diesel Emissions, *Health Effects Institute Research*, Report No. 76, pp. 88, 1996.

[13] Kato, S., Takayama, Y., Sato, T. G., and Tanabe, H., Investigation of Particulate Formation of DI Diesel Engine with Direct Sampling from Combustion Chamber, *SAE972969*, 1997.

[14] Lipkea, H. W. and Johnson, H. J., The Physical and Chemical Character of Diesel Particulate Emissions-Measurement Techniques and Fundamental Considerations, *SAE780108*, 1978.

[15] Sher, E, Handbook of Air Pollution from Internal Combustion Engines, Academic Press, San Diego, pp. 297-301, 1998.

[16] Kittelson, D. B., Characterization of Diesel Particles in the Atmosphere, *Coordinating Research*, Council AP-2 Project Group Final Report, 1988

[17] Hinds, C. William, *Aerosol Technology-Properties, Behavior, and Measurement of Airborne Particles*, 2nd Edition, John Wiley & Sons, New York, 1999.

[18] Gormley, P. G., and Kennedy, M., Diffusion from a Stream Flowing Through a Cylinder Tube, *Proc. Royal Irish acad. Sci.*, Vol. 52, pp 163-169, 1949

[19] Fuchs, N. A., The Mechanics of Aerosols, Pergamon Press, 1964.

[20] Davis, C. N., The Entry of Aerosols into Sampling Tubes and Heads, *Journal of Apply Physics*, Vol. 1, 1968.

[21] Friedlander, S. K., *Smoke Dust and Haze*, Willey and Sons, 1977

[22] Malet, J., Allout, L., Michielsen, N., Boulaud, D., Renoux, A., Deposition of Nanosized Particulates in Cylindtrical tubes under Laminar and Turbulent Flow Conditions, *Journal of Aerosol Science*, Vol. 31, pp. 335-348, 2000.

[23] He, C. and Ahmadi, G., Particle Deposition with Thermophoresis in Laminar and Turbulent Duct Flows, *Aerosol Science and Technology*, Vol. 29, pp. 525-546, 1998.

[24] Talbot, L., Cheng, K. R., Shefer, W. R. and Willis, R. D., Journal of Fluid Mechanics, Vol. 101(4), pp.737-758, 1980.

[25] Agarwal, J. K., B. Y. H. Liu, A Criterion for Accurate aerosol sampling in Calm air, *American Industry Hygiene Association Journal*, 1980.

[26] Cheng, Y. S., and Wang, S. C., Motion of Particles in Bends of Circular Pipes, *Atmospheric Environment*, Vol. 15, pp. 301-306, 1981.

[27] Pui, Y. H., Rmay-Novas, F., and Liu, Y. H. B., Experimental Study of Particle Deposition in Bends of Circular Cross Section, *Aerosol Science Technology*, pp. 301-305, 1987.

[28] Yan, Y., and Pui, H. Y., Particle Deposition in a Tube with an Abrupt Contraction, *Journal of Aerosol Science*, Vol. 21, No. 1, pp 29-40, 1991.

[29] Baumgard, K. J. and Kittelson, B. D., The Influence of a Ceramic Particle Trap on the Size Distribution of Diesel Particles, *SAE850009*, 1985.

[30] Bagley, S. T., Characterization of Fuel and Aftertreatment Device Effect on Diesel Emissions, *Health Effect Research*, Report No. 76, 1996.

[31] Abdul-Khalek, S., Kittelson, B. Davis, Graskow, R. B., Brear, F., Diesel Exhaust Particle Size: Measurement Issues and Trends, *SAE980525*, 1998.

[32] Kodas, T. Toivo, Hampden-Smith, J. Mark, *Aerosol Processing of Materials*, Wiley-VCH, 1999.

[34] Seinfeld, H. J.,and Pandis, N. S., *Atmospheric Chemistry and Physics*, John Wiley & Sons, Inc., 11998.

[35] Park, H. S., Lee, W. K., Shimada, M., and Okuyama, K., Alternative Analysis Solution to Condensational Growth of Polydisperse Aerosols in the Continuum Regime, *Journal of Aerosol Science*, Vol. 32, pp. 187-197, 2001.

[36] Mirabel, P., and Kalz, L. J., Binary Homogeneous Nucleation as a Mechanism for the Formation of Aerosols, *Journal of Chemical Physics*, Vol. 60, No. 3, pp. 1138-1144, 1974.

[37] Harmill, P., The Nucleation of H2SO4-H2O Solution Particles in the Stratosphere, *Journal of Atmospheric Sciences*, 1976.

[38] Doyle, G. J., Self-Nucleation in the Sulfuric Acid-Water System, *Journal of Chemical Physics*, Vol. 35, pp. 795-799, 1961.

[39] David B. Kittelson, Winthrop F. Watts, Jr., Megan Review of Diesel Particulate Matter Sampling Methods: Report I, *University of Minnesota*, 1998.

[40] David B. Kittelson, Winthrop F. Watts, Jr., Megan Review of Diesel Particulate Matter Sampling Methods: Report II, *University of Minnesota*, 1998.

[41] David B. Kittelson, Winthrop F. Watts, Jr., Megan Review of Diesel Particulate Matter Sampling Methods: Final Report, *University of Minnesota*, 1999.

[42] Amann, C. A., Stivender, D. L., Plee, S. L., MacDonald, J. S., Some Rudiments of Diesel Particulate Emissions, *SAE Paper 800251*, 1980.

[43] MacDonald, J. S., Plee, S. L., D'Arcy, J. B., Schreck, R. M., Experimental Measurements of the Independent Effects of Dilution Ratio and Filter Temperature on Diesel Exhaust Particulate Samples, *SAE Paper 800185* , 1980.

[44] Plee, S. L., MacDonald, J. S., Some Mechanisms Affecting the Mass of Diesel Exhaust Particulate Collected Following a Dilution Process, *SAE Paper 800186* , 1980.

[45] Knutson, E. O., and Whitby, K. T., Aerosol Classification by Electric Mobility: Apparatus, Theory, and Applications, *Journal of Aerosol Science*, Vol. 6, pp. 443-451, 1975.

[46] Rogge, W. F., Hildemann, L. M., Mazurek, M. A., Cass, G. R., "Sources of Fine Organic Aerosol. 2. Noncatalyst and Catalyst-Equipped Automobiles and Heavy-Duty Diesel Trucks," *Environ. Sci. Technol.*, 27: 636-651, 1993.

[47] Greenwood, S. J., Coxon, J. E., Biddulph, T., Bennett, J., "An Investigation to Determine the Exhaust Particulate Size Distributions for Diesel, Petrol, and Compressed Natural Gas Fueled Vehicles," *SAE Paper 961085* , 1996.

[48] Greenwood, S. J., Coxon, J. E., Biddulph, T., Bennett, J., "An Investigation to Determine the Exhaust Particulate Size Distributions for Diesel, Petrol, and Compressed Natural Gas Fueled Vehicles," *SAE Paper 961085* , 1996.

[49] Hochgreb, S, and Lafleur, A., Investigation of the Formation of Particulate Matter in Spark-Ignited Engines, *Massachusetts Institute of Technology*, 1999.

[50] Cheng, D., M., Storey, J., Waiman, T., and Dam, T., On the Use of Ejector for Dilution-Impacts on the Size Distributions of NaCl and DOP Aerosols, *Oak Ridge National Laboratory*, 2001.

APPENDICES

A AEROSOL CALCULATIONS

Table A.1 Calculated properties on the size of 0.01-nm particles at 293 K*

Temperature	293.15	Kelvin		
Pressure	101.3	kPa		
Particle diameter	0.01	µm		
Particle velocity	101	cm/s		
Tube diameter	0.46	cm		
Inlet length	9.27	cm		
m. f. p. (ref)	0.0674	µm		
Sutherland constant (S)	110.4	Kelvin		= 28.96 for air
Molecular weight	28.96	g/mole		
Particle density	1.2	g/cm^3		
Sampling angle (theta)	45	degrees		keep between 0 to 90°
Air velocity in Inlet (U)	102	cm/s		
Velocity ratio (R=U0/U)	1	R is 1 for isokinetic, > 1 for subisokinetic, < 1 for superisokinetic		
Air density =	0.001205	g/cm^3		
Air viscosity =	0.000181	poise		
Reynolds number (Re) =	0.000673			If Re < 0.1 then flow is laminar
Air density =	0.001205	g/cm^3		
Air viscosity =	0.000181	poise		If Re < 2000 then flow is laminar
Reynolds number (Re) =	309.7451			If Re > 4000 then flow is turbulent
Molecular mean free path =	6.65E-06	cm		
	6.65E-08	m		
Knudsen number (Kn) =	13.30647			
Slip correction factor =	22.44762			
Diffusion coefficient =	0.000242	cm^2/s		molecular range
Diffusion coefficient =	0.000533	cm^2/s		particle range
Mechanical mobility =	1.32E+10	cm/(dyne*s)		
Mean thermal velocity =	404.9157	cm/s		
Settling velocity =	8.12E-06	cm/s		
Stokes number =	1.84E-06			
Gravitational dep. parameter =	1.61E-06			
K(theta) =	3.43E-07			
Fraction penetrating =	0.999933			
□ =	0.000291			
□ < 0.009				
Penetration =	0.98		98	%
□ >= 0.009				
Penetration =	0.91		91	%
Stopping distance =	8.45E-07	cm		
Relaxation time =	8.28E-09	s		
Drag coefficient =	4.43E+11			

*: *Based on Aerosol Calculations by Paul Baron-email: pab2@cdc.gov*

B PARTICLE MEASUREMENT SYSTEMS

The following table is mini-dilution system's parameters used at UMN and PTL

Mini-Dilution System Parameters

		Length		Inside Diameter		Flow rate		Residence Time		
		mm	in	mm	in	SLPM	SI3PM	ms	ins	
Sampling Probe	PTL	100	3.94	4.5	0.1773	9	549.2133	11	0.4334	1/8"
	UMN	55	2.17	4.5	0.1773	9	549.2133	6	0.2364	
Sampling Line	PTL	1500	59.10	4.5	0.1773	9	549.2133	159	6.2646	
	UMN	1500	59.10	4.5	0.1773	9	549.2133	159	6.2646	

		Length		Inside Diameter			Flow Rate			
		mm	in		mm	in			SLPM	SI3PM
Ejector Diluter	Overall	500	19.70	Overall	20	0.788	Air flow		157	9580.7209
	Sample Inlet	30	1.18	Vacuum Inlet	4	0.1576	Sample Flow	Primary	9	549.2133
Ejector Diluter	Air Inlet	flush mounted		Air Inlet	4	0.1576		Secondary	2	122.0474
	Outlet	10	0.39	Outlet	4	0.1576				
Ejector Diluter	Resisdence Time	9	0.3546	PTL						
		9	0.3546	UMN						

	PTL		UMN	
	ms	ins	ms	ins
Residence time between Primary and Secondary:	14	0.5516	594	23.4036
Residence time between Secondary and Particle Instruments:	474	18.6756	1500	59.1

UMN: University of Minnesota
PTL:Perkins Technology Limited

Conversion Factor

mm	in
1	0.0394

liter	m3	in3
1	0.001	61.0237

C DILUTION RATIO

The dilution device is used to provide a dilution ratio. Exhaust enters a sampling probe in the exhaust flow, and then passes through a short section of stainless steel tubing that is insulated and maintained at the exhaust temperature (300°F). An ejector pump with a critical flow orifice provides a constant flow rate. Compressed air is used to drive the ejector pump, which draws an exhaust sample flow through the critical orifice.

According to Kittelson *et al.*[40] and Heywood[8], typical dilution ratios are from 5:1 to 50:1 **Figure C1** shows the relation of dilution ratio and the resulting saturation ratio for two condensable hydrocarbons of a diesel exhaust. These two condensable hydrocarbons have different boiling points and are shown at different exhaust temperatures. The saturation ratio has the highest values for dilution ratios of about 5 to 50 for both.

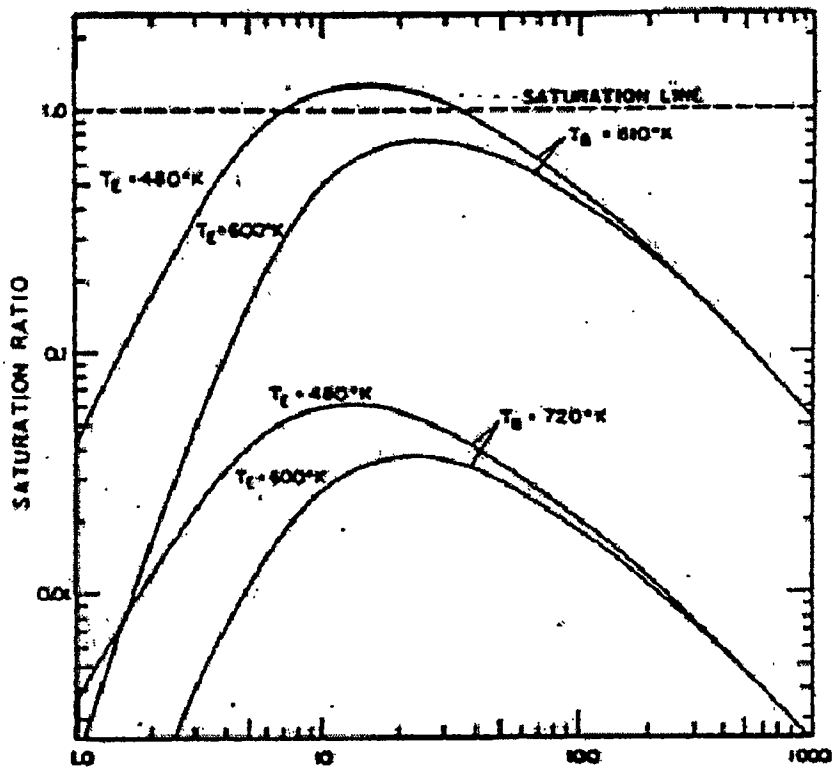


Figure C1 Effect of saturation ratio for two condensable species at two exhaust temperatures (Kittelson and Dolan, 1980)

The dilution ratio based on mass flow is defined as:

$$DR = \frac{m_{air} + m_{aerosol}}{m_{aerosol}}$$

where m_{air} is the mass flow rate of dilution air, and $m_{aerosol}$ is the mass flow rate of sampling aerosol. It is assumed that the aerosol has the same density as the same temperature air. In our experiment, we kept aerosol and dilution air in the same temperature. Therefore, equation is written as:

$$DR = \frac{Q_{air} + Q_{aerosol}}{Q_{aerosol}}$$

where Q_{air} is the volume flow rate of the dilution air, and $Q_{aerosol}$ is the volume flow rate of the sampling aerosol.

The dilution ratio can be defined as:

$$DR = \frac{N_{undiluted} - N_{air}}{N_{diluted} - N_{air}} \qquad DR = \frac{C_{undiluted} - C_{air}}{C_{diluted} - C_{air}}$$

where unit of N is #/cm^3 and unit of C is ppm

Residence time

Residence time may be varied to examine its influence on nanoparticle formation. The residence time is varied from 150 to 6000 ms.

$$RT = \frac{L * A}{Q}$$

where L: distance between the mixing point of exhaust gas and air to sampling outlet; A: cross sectional area; Q: volume flow rate

Dilution rate

Dilution rate is defined as the variability of the dilution ratio in an interval of time. It can be written as:

$$Dilution\ rate = \frac{dDr}{dt}$$

where,, dDr is variance of the dilution ratio in time interval dt.

Constant flow rate (choking)

Conservation of mass:

$$(\frac{dm}{dt})_{syst} = 0 = \frac{d}{dt}\left(\int_{CV} \rho d\vartheta\right) + \int_{CS} \rho(V_r . n) dA$$

Control volume has only a number of one-dimensional inlets and outlets, so it can be

$$\int_{CV} \frac{\partial \rho}{\partial t} d\vartheta + \sum_i (\rho_i A_i V_i)_{out} - \sum_i (\rho_i A_i V_i)_{in} = 0$$

Suppose that the flow within the control volume is steady state, then

$$\sum_i (\rho_i A_i V_i)_{out} - \sum_i (\rho_i A_i V_i)_{in} = 0$$

The maximum possible mass flow passes through a duct when its throat is at the critical or sonic condition. The duct is then said to be choked and can carry no additional mass flow unless the throat is widened.

Energy equation

$$h_1 + \frac{1}{2}V_1^2 + gz_1 = h_2 + \frac{1}{2}V_2^2 + gz_2$$

Critical values at the sonic point

$$\frac{\rho^*}{\rho_o} = \left(\frac{2}{k+1}\right)^{k/(k-1)} = 0.5283 \qquad \frac{T^*}{T_o} = \frac{2}{k+1} = 0.8333$$

where

(*): sonic, critical condition, and March number = 1 @ sonic flow

The local mass-flow function which occurs at the choking condition. It can be modified to predict the actual mass flow at any section where local area A and pressure p are known.

$$Mass - flow\ function = \frac{\dot{m}}{A}\frac{\sqrt{RT_0}}{p_0} = \sqrt{\frac{2k}{k-1}\left(\frac{p}{p_0}\right)^{2/k}\left[1-\left(\frac{p}{p_0}\right)^{(k-1)/k}\right]}$$

The following tables are the summary of dilution ratio and orifice size relationship

Table C1 Relationship between sonic velocity and orifice sizes.

Conversion Units

psi	mmHg	"Hg	Torrs		atm
0.497		1			0.0334
14.7	760		760		

Vacuum					Air Supply		
Flow Rate		Vacuum Level		Pvac*	Pressure	Consumption[1]	
slpm	scfm	"Hg	psia	psia	psig	scfm	slpm
65.1	2.3000	0.0	0.000	14.700	-1.813	0.072	2.0
56.6	2.0000	1.5	0.737	13.964	2.807	0.516	14.6
51.5	1.8200	3.0	1.473	13.227	7.426	0.940	26.6
39.9	1.4100	6.0	2.946	11.754	16.666	1.723	48.8
32.8	1.1600	9.0	4.419	10.281	25.905	2.421	68.5
23.2	0.8200	12.0	5.892	8.808	35.144	3.033	85.9
14.2	0.5000	15.0	7.365	7.335	44.383	3.560	100.8
9.6	0.3400	18.0	8.838	5.862	53.623	4.002	113.3
9.0	**0.3176**	**18.4**	**9.044**	**5.656**	**54.916**	**4.057**	**114.9**
5.1	0.1800	21.0	10.311	4.389	62.862	4.358	123.4
2.3	0.0800	24.0	11.784	2.916	72.101	4.629	131.1
2.0	**0.0700**	**24.8**	**12.177**	**2.523**	**74.565**	**4.687**	**132.7**

**: Pvac = 14.7 - Vacuum Level, psi*

*[1] Air Supply Consumption = (-0.0005*F16^2)+(0.0968*F16)+0.2487*

*Vaccum, psia = "Hg*0.491*

Pvac, psia = 14.7 - Vaccum, psia

Inch Hg = 25.4 mmHg

mmHg at 0°C = 1.933*10^{-2} psig

psia = 14.7 + psig

Table 2: Sonic Velocity, Vsonic = 476.3 m/s

$P_{vac}/Po < 0.528 = 7.762/14.7 = 0.528$

P_0	P_{vac}	P_{vac}/Po
14.7	14.700	1.000
14.7	13.964	0.950
14.7	13.227	0.900
14.7	11.754	0.800
14.7	10.281	0.699
14.7	8.808	0.599
14.7	7.335	0.499
14.7	5.862	0.399
14.7	**5.656**	**0.385**
14.7	4.389	0.299
14.7	2.916	0.198
14.7	**2.523**	**0.172**

Therefore, P_{vac} has to be less than 7.762

"Hg	mmHg	psig	psia	Pvac/Po
0.0	0.000	0.000	14.700	1.000
1.5	38.100	-0.736	13.964	0.950
3.0	76.200	-1.473	13.227	0.900
6.0	152.400	-2.946	11.754	0.800
9.0	228.600	-4.419	10.281	0.699
12.0	304.800	-5.892	8.808	0.599
15.0	**381.000**	**-7.365**	**7.335**	**0.499**
18.0	457.200	-8.838	5.862	**0.399**
18.4	467.868	-9.044	5.656	**0.385**
21.0	533.400	-10.311	4.389	**0.299**
24.0	609.600	-11.784	2.916	**0.198**
24.8	629.920	-12.176	2.524	**0.172**

Temp.= 40 °C= 313.15 K Diameter 0.0254 m

Orifice in.	Pair psi	M-air cfm	CF	ActM-air cfm	ActM-air lpm	Pvac in. Hg	M-vac, lpm lpm	TotFlow lpm	DR	ρ kg/m3	μ kg/m.sec	Reynold Number	TotFlow lpm
0.0100	80	1.88	2.538	4.77	135.135	20	0.5312	135.666	**255**	1.225	0.00001781	306926	40
0.0132	80	1.88	2.538	4.77	135.135	20	0.781	135.916	**174**	1.225	0.00001781	307491	50
0.0160	80	1.88	2.538	4.77	135.135	19.8	1.486	136.621	**92**	1.225	0.00001781	309086	60
0.0200	80	1.88	2.538	4.77	135.135	19.6	2.175	137.310	**63**	1.225	0.00001781	310645	70
0.0210	80	1.88	2.538	4.77	135.135	19.5	2.248	137.383	**61**	1.225	0.00001781	310810	80
0.0225	80	1.88	2.538	4.77	135.135	19.5	2.455	137.590	**56**	1.225	0.00001781	311278	90
0.0240	80	1.88	2.538	4.77	135.135	19.4	2.762	137.897	**50**	1.225	0.00001781	311973	100
0.0250	80	1.88	2.538	4.77	135.135	19.4	2.969	138.104	**47**	1.225	0.00001781	312441	110
0.0260	80	1.88	2.538	4.77	135.135	19.4	3.087	138.222	**45**	1.225	0.00001781	312708	120
0.0310	80	1.88	2.538	4.77	135.135	19.2	3.778	138.913	**37**	1.225	0.00001781	314272	130
0.0400	80	1.88	2.538	4.77	135.135	17.5	9.09	144.225	**16**	1.225	0.00001781	326289	140
0.0520	80	1.88	2.538	4.77	135.135	14.4	14.7	149.835	**10**	1.225	0.00001781	338981	150

Table C2 Summary of the orifice sizes and dilution ratios used in the dilutors.

Dilution Ratio at Air Pressure 80 psi

Ori. Dia. inch.	Air Pres. psi	Air Flow scfm	CF1	Act.Air Flow2 scfm	Act.Air Flow2 lpm	Vac. Pressure in Hg. Vac	Vac. Flowrate lpm	Vac. Flowrate scfm	Tot. Flowrate scfm	Tot. Flowrate lpm	DR
0.010	80	2.05	2.54	5.203	147.355	16.10	0.53	0.02	5.22	147.88	279
0.014	80	2.05	2.54	5.203	147.355	17.50	0.77	0.03	5.23	148.12	192
0.016	80	2.05	2.54	5.203	147.355	16.00	1.19	0.04	5.25	148.54	125
0.018	80	2.05	2.54	5.203	147.355	19.70	1.52	0.05	5.26	148.87	98
0.020	80	2.05	2.54	5.203	147.355	16.00	2.16	0.08	5.28	149.51	69
0.031	80	2.05	2.54	5.203	147.355	19.70	5.32	0.19	5.39	152.67	29
0.038	80	2.05	2.54	5.203	147.355	14.60	6.70	0.24	5.44	154.05	23
0.040	80	2.05	2.54	5.203	147.355	14.60	8.60	0.30	5.51	155.95	18
0.047	80	2.05	2.54	5.203	147.355	16.00	12.00	0.42	5.63	159.35	13
0.052	80	2.05	2.54	5.203	147.355	13.00	14.45	0.51	5.71	161.80	11

Dilution Ratio at Air Pressure 60 psi

Ori. Dia. inch.	Air Pres. psi	Air Flow scfm	CF1	Act.Air Flow2 scfm	Act.Air Flow2 lpm	Vac. Pressure in Hg. Vac	Vac. Flowrate lpm	Vac. Flowrate scfm	Tot. Flowrate scfm	Tot. Flowrate lpm	DR
0.010	60	1.80	2.25	4.058	114.913	16.10	0.53	0.02	4.08	115.44	218
0.014	60	1.80	2.25	4.058	114.913	17.50	0.77	0.03	4.08	115.68	150
0.016	60	1.80	2.25	4.058	114.913	16.00	1.19	0.04	4.10	116.10	98
0.018	60	1.80	2.25	4.058	114.913	19.70	1.52	0.05	4.11	116.43	77
0.020	60	1.80	2.25	4.058	114.913	16.00	2.16	0.08	4.13	117.07	54
0.031	60	1.80	2.25	4.058	114.913	19.70	5.32	0.19	4.25	120.23	23
0.038	60	1.80	2.25	4.058	114.913	14.60	6.70	0.24	4.29	121.61	18
0.040	60	1.80	2.25	4.058	114.913	14.60	8.60	0.30	4.36	123.51	14
0.047	60	1.80	2.25	4.058	114.913	16.00	12.00	0.42	4.48	126.91	11
0.052	60	1.80	2.25	4.058	114.913	13.00	14.45	0.51	4.57	129.36	9

Air Pres. psi	Air Flow scfm	CF[1]	Act.Air Flow[2] scfm	Act.Air Flow[2] lpm	Vac. Pressure in Hg. Vac	Vac. Flowrate lpm	Vac. Flowrate scfm	Tot. Flowrate scfm	Tot. Flowrate lpm	DR[3]
80	2.05	2.54	5.20	147.355	19.70	5.43	0.19	5.39	152.78	28
75	1.99	2.47	4.92	139.214	19.00	5.42	0.19	5.11	144.64	27
70	1.95	2.40	4.68	132.560	17.60	5.42	0.19	4.87	137.98	25
65	1.86	2.33	4.33	122.653	16.00	5.41	0.19	4.52	128.07	24
60	1.80	2.25	4.06	114.913	14.20	5.41	0.19	4.25	120.32	22
55	1.74	2.18	3.79	107.300	11.70	5.39	0.19	3.98	112.69	21
50	1.67	2.10	3.50	99.221	11.10	5.35	0.19	3.69	104.57	20
45	1.61	2.02	3.24	91.886	10.10	5.28	0.19	3.43	97.17	18

0.0100

Air Pres. psi	Air Flow scfm	CF[1]	Act.Air Flow[2] scfm	Act.Air Flow[2] lpm	Vac. Pressure in Hg. Vac	Vac. Flowrate lpm	Vac. Flowrate scfm	Tot. Flowrate scfm	Tot. Flowrate lpm	DR[3]
80	2.05	2.54	5.20	147.355	19.70	0.53	0.02	5.22	147.88	279
75	1.99	2.47	4.92	139.214	19.00	0.53	0.02	4.93	139.74	264
70	1.95	2.40	4.68	132.560	17.60	0.53	0.02	4.70	133.09	251
65	1.86	2.33	4.33	122.653	16.00	0.53	0.02	4.35	123.18	232
60	1.80	2.25	4.06	114.913	14.20	0.53	0.02	4.08	115.44	218

0.0135

Air Pres. psi	Air Flow scfm	CF[1]	Act.Air Flow[2] scfm	Act.Air Flow[2] lpm	Vac. Pressure in Hg. Vac	Vac. Flowrate lpm	Vac. Flowrate scfm	Tot. Flowrate scfm	Tot. Flowrate lpm	DR[3]
80	2.05	2.54	5.20	147.355	19.70	0.77	0.03	5.23	148.12	192
75	1.99	2.47	4.92	139.214	19.00	0.77	0.03	4.94	139.98	182
70	1.95	2.40	4.68	132.560	17.60	0.77	0.03	4.71	133.33	173
65	1.86	2.33	4.33	122.653	16.00	0.77	0.03	4.36	123.42	160
60	1.80	2.25	4.06	114.913	14.20	0.77	0.03	4.08	115.68	150

0.016

Air Pres. psi	Air Flow scfm	CF[1]	Act.Air Flow[2] scfm	Act.Air Flow[2] lpm	Vac. Pressure in Hg. Vac	Vac. Flowrate lpm	Vac. Flowrate scfm	Tot. Flowrate scfm	Tot. Flowrate lpm	DR[3]
80	2.05	2.54	5.20	147.355	19.70	1.19	0.04	5.25	148.54	125
75	1.99	2.47	4.92	139.214	19.00	1.19	0.04	4.96	140.40	118
70	1.95	2.40	4.68	132.560	17.60	1.19	0.04	4.72	133.75	112
65	1.86	2.33	4.33	122.653	16.00	1.19	0.04	4.37	123.84	104
60	1.80	2.25	4.06	114.913	14.20	1.19	0.04	4.10	116.10	98

0.018

Air Pres. psi	Air Flow scfm	CF[1]	Act.Air Flow[2] scfm	Act.Air Flow[2] lpm	Vac. Pressure in Hg. Vac	Vac. Flowrate lpm	Vac. Flowrate scfm	Tot. Flowrate scfm	Tot. Flowrate lpm	DR[3]
80	2.05	2.54	5.20	147.355	19.70	1.52	0.05	5.26	148.87	98
75	1.99	2.47	4.92	139.214	19.00	1.52	0.05	4.97	140.73	93
70	1.95	2.40	4.68	132.560	17.60	1.52	0.05	4.73	134.08	88
65	1.86	2.33	4.33	122.653	16.00	1.52	0.05	4.38	124.17	82
60	1.80	2.25	4.06	114.913	14.20	1.52	0.05	4.11	116.43	77

0.020

Air Pres. psi	Air Flow scfm	CF[1]	Act.Air Flow[2] scfm	Act.Air Flow[2] lpm	Vac. Pressure in Hg. Vac	Vac. Flowrate lpm	Vac. Flowrate scfm	Tot. Flowrate scfm	Tot. Flowrate lpm	DR[3]
80	2.05	2.54	5.20	147.355	19.70	2.16	0.08	5.28	149.51	69
75	1.99	2.47	4.92	139.214	19.00	2.16	0.08	4.99	141.37	65
70	1.95	2.40	4.68	132.560	17.60	2.16	0.08	4.76	134.72	62
65	1.86	2.33	4.33	122.653	16.00	2.16	0.08	4.41	124.81	58
60	1.80	2.25	4.06	114.913	14.20	2.16	0.08	4.13	117.07	54

0.031

Air Pres. psi	Air Flow scfm	CF[1]	Act.Air Flow[2] scfm	Act.Air Flow[2] lpm	Vac. Pressure in Hg. Vac	Vac. Flowrate lpm	Vac. Flowrate scfm	Tot. Flowrate scfm	Tot. Flowrate lpm	DR[3]
80	2.05	2.54	5.20	147.355	19.70	5.32	0.19	5.39	152.67	29
75	1.99	2.47	4.92	139.214	19.00	5.32	0.19	5.10	144.53	27
70	1.95	2.40	4.68	132.560	17.60	5.32	0.19	4.87	137.88	26
65	1.86	2.33	4.33	122.653	16.00	5.32	0.19	4.52	127.97	24
60	1.80	2.25	4.06	114.913	14.20	5.32	0.19	4.25	120.23	23

0.038

Air Pres. psi	Air Flow scfm	CF[1]	Act.Air Flow[2] scfm	Act.Air Flow[2] lpm	Vac. Pressure in Hg. Vac	Vac. Flowrate lpm	Vac. Flowrate scfm	Tot. Flowrate scfm	Tot. Flowrate lpm	DR[3]
80	2.05	2.54	5.20	147.355	19.70	6.70	0.24	5.44	154.05	23
75	1.99	2.47	4.92	139.214	19.00	6.70	0.24	5.15	145.91	22
70	1.95	2.40	4.68	132.560	17.60	6.70	0.24	4.92	139.26	21
65	1.86	2.33	4.33	122.653	16.00	6.70	0.24	4.57	129.35	19
60	1.80	2.25	4.06	114.913	14.20	6.70	0.24	4.29	121.61	18

0.040

Air Pres. psi	Air Flow scfm	CF[1]	Act.Air Flow[2] scfm	Act.Air Flow[2] lpm	Vac. Pressure in Hg. Vac	Vac. Flowrate lpm	Vac. Flowrate scfm	Tot. Flowrate scfm	Tot. Flowrate lpm	DR[3]
80	2.05	2.54	5.20	147.355	19.70	8.60	0.30	5.51	155.95	18
75	1.99	2.47	4.92	139.214	19.00	8.60	0.30	5.22	147.81	17
70	1.95	2.40	4.68	132.560	17.60	8.60	0.30	4.98	141.16	16
65	1.86	2.33	4.33	122.653	16.00	8.60	0.30	4.63	131.25	15
60	1.80	2.25	4.06	114.913	14.20	8.60	0.30	4.36	123.51	14

0.0465

Air Pres. psi	Air Flow scfm	CF[1]	Act.Air Flow[2] scfm	Act.Air Flow[2] lpm	Vac. Pressure in Hg. Vac	Vac. Flowrate lpm	Vac. Flowrate scfm	Tot. Flowrate scfm	Tot. Flowrate lpm	DR[3]
80	2.05	2.54	5.20	147.355	19.70	12.00	0.42	5.63	159.35	13
75	1.99	2.47	4.92	139.214	19.00	12.00	0.42	5.34	151.21	13
70	1.95	2.40	4.68	132.560	17.60	12.00	0.42	5.10	144.56	12
65	1.86	2.33	4.33	122.653	16.00	12.00	0.42	4.75	134.65	11
60	1.80	2.25	4.06	114.913	14.20	12.00	0.42	4.48	126.91	11

0.052

Air Pres. psi	Air Flow scfm	CF[1]	Act.Air Flow[2] scfm	Act.Air Flow[2] lpm	Vac. Pressure in Hg. Vac	Vac. Flowrate lpm	Vac. Flowrate scfm	Tot. Flowrate scfm	Tot. Flowrate lpm	DR[3]
80	2.05	2.54	5.20	147.355	19.70	14.45	0.51	5.71	161.80	11
75	1.99	2.47	4.92	139.214	19.00	14.45	0.51	5.43	153.66	11
70	1.95	2.40	4.68	132.560	17.60	14.45	0.51	5.19	147.01	10
65	1.86	2.33	4.33	122.653	16.00	14.45	0.51	4.84	137.10	9
60	1.80	2.25	4.06	114.913	14.20	14.45	0.51	4.57	129.36	9

0.059 (apply for Hasting Controller)

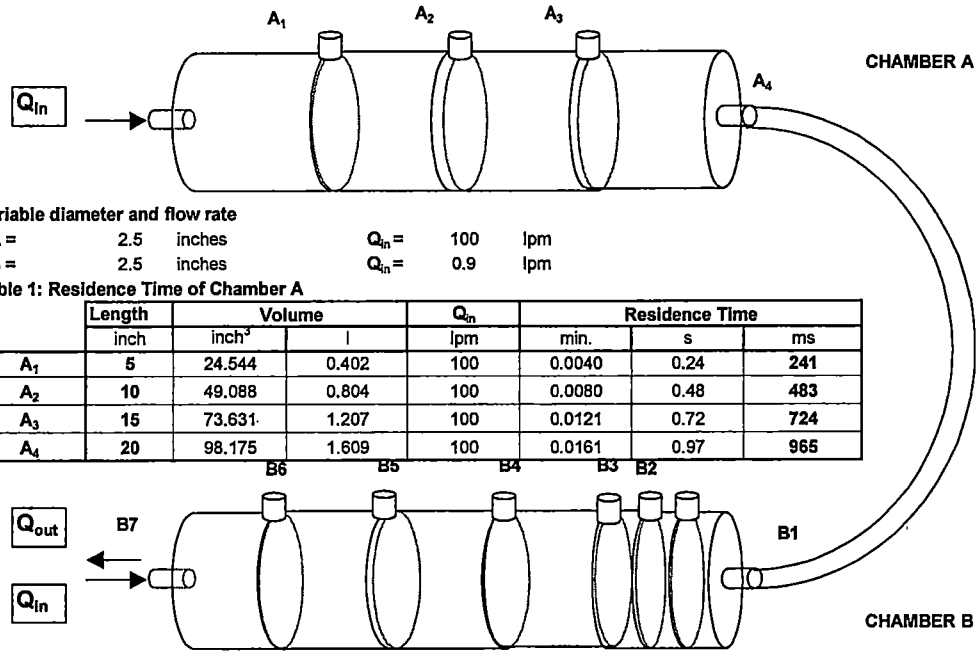
Air Pres. psi	Air Flow lpm	CF[1]	Act.Air Flow[2] scfm	Act.Air Flow[2] lpm	Vac. Pressure in Hg. Vac	Vac. Flowrate lpm	Vac. Flowrate scfm	Tot. Flowrate scfm	Tot. Flowrate lpm	DR[3]
80	158.000		0.00	119.000	14.90	13.30	0.47	0.47	132.30	10
	145.000		0.00	110.000	14.90	13.48	0.48	0.48	123.48	9
	140.000		0.00	105.000	14.70	13.40	0.47	0.47	118.40	9
	135.000		0.00	101.000	14.70	13.35	0.47	0.47	114.35	9
	130.000		0.00	97.500	14.50	13.30	0.47	0.47	110.80	8

0.070 (apply for Hasting Controller)

Air Pres. psi	Air Flow lpm	CF[1]	Act.Air Flow[2] scfm	Act.Air Flow[2] lpm	Vac. Pressure in Hg. Vac	Vac. Flowrate lpm	Vac. Flowrate scfm	Tot. Flowrate scfm	Tot. Flowrate lpm	DR[3]
80	158.000		0.00	119.000	14.50	17.80	0.63	0.63	136.80	8
	145.000		0.00	110.000	14.60	17.80	0.63	0.63	127.80	7
	140.000		0.00	105.000	14.50	17.80	0.63	0.63	122.80	7
	135.000		0.00	101.000	14.50	17.90	0.63	0.63	118.90	7
	130.000		0.00	97.500	14.00	17.90	0.63	0.63	115.40	6

Table C3 Residence time calculation: Dilutor I and II

RESIDENCE TIME CALCULATION: DILUTOR I



Variable diameter and flow rate

DA = 2.5 inches Q_{in} = 100 lpm

DB = 2.5 inches Q_{in} = 0.9 lpm

Table 1: Residence Time of Chamber A

	Length	Volume		Q_{in}	Residence Time		
	inch	$inch^3$	l	lpm	min.	s	ms
A_1	5	24.544	0.402	100	0.0040	0.24	241
A_2	10	49.088	0.804	100	0.0080	0.48	483
A_3	15	73.631	1.207	100	0.0121	0.72	724
A_4	20	98.175	1.609	100	0.0161	0.97	965

Table 2: Residence Time of Chamber B

	Length	Volume		Q_{in}	Residence Time		
	inch	$inch^3$	l	lpm	min.	s	ms
B_1	1	4.909	0.080	0.9	0.0894	5.36	5363
B_2	3	14.726	0.241	0.9	0.2681	16.09	16088
B_3	4	19.635	0.322	0.9	0.3575	21.45	21451
B_4	8	39.270	0.644	0.9	0.7150	42.90	42901
B_5	12	58.905	0.965	0.9	1.0725	64.35	64352
B_6	16	78.540	1.287	0.9	1.4300	85.80	85803
B_7	19	93.266	1.528	0.9	1.6982	101.89	101891

Table 3: Residence time of Chamber A+ Chamber B

	Length	Volume		Q_{in}	Residence Time		
	inch	$inch^3$	l	lpm	min.	s	ms
A_1	5	24.544	0.402	100	0.0040	0.24	241
A_2	10	49.088	0.804	100	0.0080	0.48	483
A_3	15	73.631	1.207	100	0.0121	0.72	724
A_4	20	98.175	1.609	100	0.0161	0.97	965
B_1	24.4	119.774	1.963	100	0.0196	1.18	1178
B_2	28.4	139.409	2.284	100	0.0228	1.37	1371
B_3	32.4	159.044	2.606	100	0.0261	1.56	1564
B_4	36.4	178.679	2.928	100	0.0293	1.76	1757
B_5	37.2	182.606	2.992	100	0.0299	1.80	1795
B_6	38	186.533	3.057	100	0.0306	1.83	1834
B_7	38.8	190.460	3.121	100	0.0312	1.87	1873

Volume = 3.1416*r²*height (cylinder)

liter = 61.0237 in^3

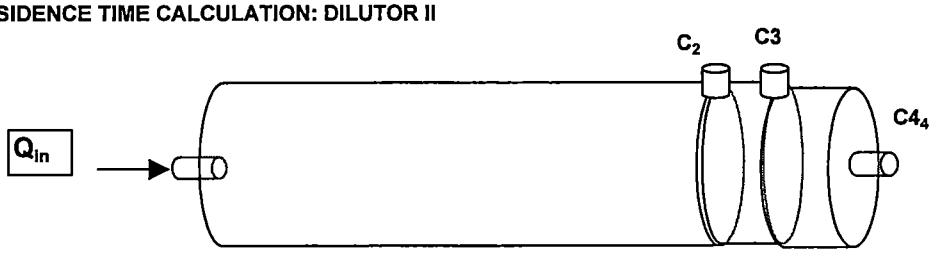
in^3 = 0.16387 liter

Heating Tape: BH Thermal Corp. size: .5X44FT; Type: FG HVY

Table 4: Residence Time for each port versus different flow rates

	Chmaber A			Chamber B							
Flow Rate	A1	A2	A3	A4	B1	B2	B3	B4	B5	B6	B7
lpm	ms	ms	ms	ms	ms	ms	ms	ms	ms	ms	ms
90	268	536	804	1073	1308	1523	1738	1952	1995	2038	2081
92	262	525	787	1049	1280	1490	1700	1910	1952	1994	2035
94	257	513	770	1027	1253	1458	1664	1869	1910	1951	1992
96	251	503	754	1006	1227	1428	1629	1830	1870	1910	1951
98	246	492	739	985	1202	1399	1596	1793	1832	1871	1911
100	241	483	724	965	1178	1371	1564	1757	1795	1834	1873
102	237	473	710	946	1155	1344	1533	1722	1760	1798	1836
104	232	464	696	928	1132	1318	1504	1689	1726	1763	1801
106	228	455	683	911	1111	1293	1475	1657	1694	1730	1767
108	223	447	670	894	1090	1269	1448	1627	1662	1698	1734
110	219	439	658	878	1071	1246	1422	1597	1632	1667	1702
112	215	431	646	862	1051	1224	1396	1569	1603	1638	1672
114	212	423	635	847	1033	1202	1372	1541	1575	1609	1643
116	208	416	624	832	1015	1182	1348	1514	1548	1581	1614
118	205	409	614	818	998	1162	1325	1489	1522	1554	1587
120	201	402	603	804	981	1142	1303	1464	1496	1528	1561
122	198	396	593	791	965	1124	1282	1440	1472	1503	1535
124	195	389	584	778	950	1105	1261	1417	1448	1479	1510
126	192	383	575	766	935	1088	1241	1394	1425	1456	1486
128	189	377	566	754	920	1071	1222	1373	1403	1433	1463
130	186	371	557	743	906	1054	1203	1351	1381	1411	1440
132	183	366	548	731	892	1038	1185	1331	1360	1389	1419
134	180	360	540	720	879	1023	1167	1311	1340	1369	1397
136	177	355	532	710	866	1008	1150	1292	1320	1349	1377
138	175	350	525	699	853	993	1133	1273	1301	1329	1357
140	172	345	517	689	841	979	1117	1255	1282	1310	1338
142	170	340	510	680	829	965	1101	1237	1264	1292	1319
144	168	335	503	670	818	952	1086	1220	1247	1274	1300
146	165	331	496	661	807	939	1071	1203	1230	1256	1283
148	163	326	489	652	796	926	1057	1187	1213	1239	1265
150	161	322	483	644	785	914	1043	1171	1197	1223	1248
152	159	318	476	635	775	902	1029	1156	1181	1207	1232
154	157	313	470	627	765	890	1015	1141	1166	1191	1216
156	155	309	464	619	755	879	1002	1126	1151	1176	1200
158	153	305	458	611	745	868	990	1112	1136	1161	1185
160	151	302	452	603	736	857	977	1098	1122	1146	1170
154	157	313	470	627	765	890	1015	1141	1166	1191	1216
156	155	309	464	619	755	879	1002	1126	1151	1176	1200
158	153	305	458	611	745	868	990	1112	1136	1161	1185
160	151	302	452	603	736	857	977	1098	1122	1146	1170
162	149	298	447	596	727	846	965	1084	1108	1132	1156

RESIDENCE TIME CALCULATION: DILUTOR II



CHAMBER C

Variable diameter and flow rate

DA = 1 inches Q_{in} = 100 lpm

	Length	Volume		Q_{in}	Residence Time		
	inch	$inch^3$	l	lpm	min.	s	ms
C1	5	3.927	0.064	100	0.0006	0.04	39
C2	10	7.854	0.129	100	0.0013	0.08	77
C3	15	11.781	0.193	100	0.0019	0.12	116
C4	20	15.708	0.257	100	0.0026	0.15	154

Table 2: Residence Time for each port versus different flow rates

Flow Rate	C1	C2	C3	C4
lpm	ms	ms	ms	ms
90	43	86	129	172
92	42	84	126	168
94	41	82	123	164
96	40	80	121	161
98	39	79	118	158
100	39	77	116	154
102	38	76	114	151
104	37	74	111	149
106	36	73	109	146
108	36	72	107	143
110	35	70	105	140
112	34	69	103	138
114	34	68	102	135
116	33	67	100	133
118	33	65	98	131
120	32	64	97	129
122	32	63	95	127
124	31	62	93	125
126	31	61	92	123
128	30	60	90	121
130	30	59	89	119
132	29	59	88	117
134	29	58	86	115
136	28	57	85	114
138	28	56	84	112
140	28	55	83	110
142	27	54	82	109
144	27	54	80	107
146	26	53	79	106
148	26	52	78	104
150	26	51	77	103
152	25	51	76	102
154	25	50	75	100
156	25	50	74	99
158	24	49	73	98
160	24	48	72	97

Flow Correction Factor of the Flowmeter.

Metering tube and float combinations have a known maximum capacity which is stated for water and for air at 70°F (21°C) and 14.7 psia. Since water and air at 70°F (21°C) and 14.7 psia are both the basis for all capacity tables, and the most commonly used calibration fluids, the object of the following equations is to determine the flow capacity when using with air at 70°F (21°C).The sizing equation is calculated to determine the scfm air equivalent 70°F (21°C).

The flow equation is calculated to determine the maximum flow of gas at a particular set of operating conditions when using a given tube and float combination with a listed maximum capacity for air at 70°F (21°C).

$$Sizing, CF = \sqrt{\frac{(Gas\ Sp.\ Gr.)\ (Oper.\ Temp.\ in\ ^{o}F + 460^{o})}{((36)\ (Oper.\ Back\ \mathrm{Pr}essure\ in\ PSIG + 14.7))}}$$

$$Flow = \sqrt{\frac{(36)\ (Oper.\ Back\ \mathrm{Pr}essure\ in\ PSIG + 14.7)}{(Gas\ Sp.\ Gr.)\ (Oper.\ Temp.\ in\ ^{o}F + 460^{o})}} = 1/CF$$

Actual flowrate

$$Sizing, CF = \frac{P.Actual}{P.Std.} x \frac{Temp.Std + 460^{o}}{Temp.Actual + 460^{0}} x \sqrt{\frac{(Sp.\ Gr.)\ (Temp. + 460^{o})}{((36)\ (Oper.\ Back\ \mathrm{Pr}essure + 14.7))}}$$

$$Flow,\ FCF = \frac{P.Std}{P.Actual} x \frac{Temp.Actual + 460^{o}}{Temp.Std + 460^{0}} \sqrt{\frac{(36)\ (Oper.\ Back\ \mathrm{Pr}essure + 14.7)}{(Sp.\ Gr.)\ (Temp. + 460^{o})}}$$

Table C4 Relationship between pressure and air flow correction factor of the flowmeter

Pressure, psi		Air Flowrate
Inlet	Outlet	cfpm
88.0	86.0	1.700
86.0	84.5	1.675
83.5	82.0	1.650
81.0	79.5	1.625
78.0	76.5	1.600
75.5	74.5	1.575
73.0	72.0	1.550
71.5	70.0	1.525
68.5	67.0	1.500
66.5	65.5	1.475
63.5	62.0	1.450
61.5	60.0	1.425
58.5	57.5	1.400
56.5	55.5	1.375
54.0	52.5	1.350
51.5	50.5	1.325
50.0	49.0	1.300
47.5	46.0	1.275
45.5	44.5	1.250
43.5	42.0	1.225
41.5	40.0	1.200

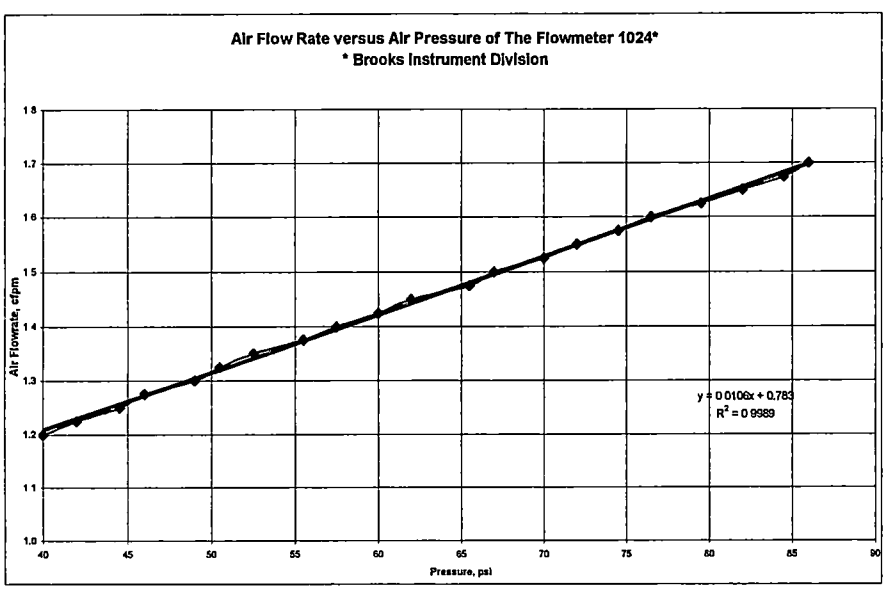


Figure C.2 Air supply and air consumption for the ejector.

Table C5 Relationship between mass air flow correction factor of the Mass Flowmeter (HFM-201) and controller (HFC-203)

$mass_{Act.}$	$mass_{CR}$	$mass_{Hast.}$
0	0.0	0.0
5	2.5	3.8
10	5.0	7.5
15	7.5	11.3
20	10.0	15.0
25	12.5	18.8
30	15.0	22.5
35	17.5	26.3
40	20.0	30.0
45	22.5	33.8
50	25.0	37.5
55	27.5	41.3
60	30.0	45.0
65	32.5	48.8
70	35.0	52.5
75	37.5	56.3
80	40.0	60.0
85	42.5	63.8
90	45.0	67.5
95	47.5	71.3
100	50.0	75.0
105	52.5	78.8
110	55.0	82.5
115	57.5	86.3
120	60.0	90.0
125	62.5	93.8
130	65.0	97.5
135	67.5	101.3
140	70.0	105.0
145	72.5	108.8
150	75.0	112.5
155	77.5	116.3
160	80.0	120.0
165	82.5	123.8
170	85.0	127.5
175	87.5	131.3
180	90.0	135.0
185	92.5	138.8
190	95.0	142.5
195	97.5	146.3
200	100.0	150.0

D HOW TO OPERATE THE DILUTORS

The fundamental design for the two dilutors is the same. The only difference is the residence time. The following is the procedure to operate both of the dilutors.

The first step is checking the ejector condition. There are three bolts used to tighten two main parts of the ejector. These bolts are often loosening after several runs. As a result, the mixing air will often leak under high pressure. Therefore, it is very important to tighten these bolts before running an experiment (see the bolts location in **Figure D1**).

The second step is to prepare the orifice size. Orifice sizes from 0.01 inches to 0.070 inches are used to provide dilution ratio from 279:1 to 6:1, respectively. Depending on desired dilution ratio, an appropriate orifice size is chosen. Table C2 describes the relationship between orifice size, air supply, vacuum pressure, air supply pressure, and dilution ratio. The orifice size is built into an orifice sampler (**Figure D2**). **Figure D3** shows the orifice box with different orifice samplers. For example, an orifice size of 0.040 inches and an air supply of 2.05 cfm (from pressure gauge) should provide a dilution ratio of 18:1.

The third step is to choose a residence time. Dilutor I is provided with the retractable sampling line and the outputs A1, A2 to B7. Depending on air supply flow rate and different sampling locations in the dilutors, residence times are determined. (See residence time calculation for dilutor I and II on pages 86 to 88)

The fourth step is to open the air supply regulator and check the pressure gauge. Normally, the pressure should be at least 60 psi to have choked flow (See Table C1 and C2). Air supply pressure determines air supply flow rate, which affects the residence time and dilution ratio. The fifth step is to check the vacuum gauge. Vacuum pressure should not be less than 14.5 to get choked flow if a gas analyzer is not available for determining dilution ratio. The sixth step is to adjust the mixing temperature in the dilutors. The temperature is maintained in the range of 32 to 52°C.

Lastly, it is advised to clean the inside the dilutors often. The result should be more accurate due to no particle deposition. Their small size makes cleanup easy.

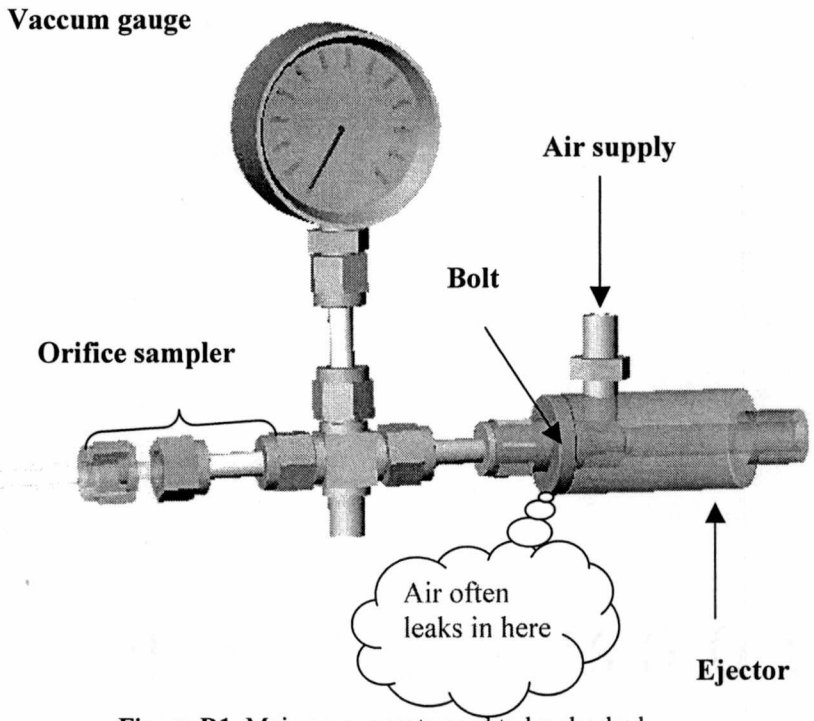


Figure D1 Main components need to be checked.



Figure D2 Orifice sampler

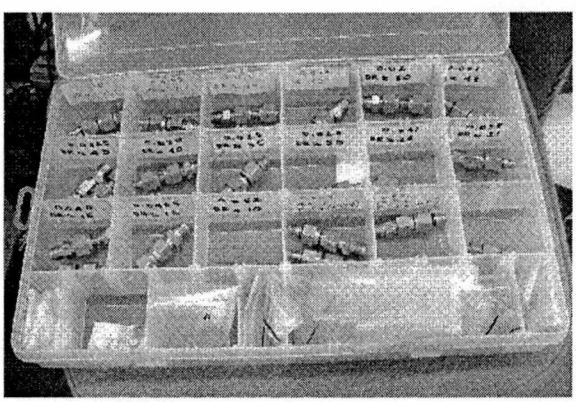


Figure D3 Orifice box with different orifice samplers

E UNITS OF GAS

Quantities of pollutants may be expressed of either a volumetric or a mass basis. For the mass basis appropriate units would be grams per cubic meter or pound mass per cubic foot. The volumetric unit normally employed is parts per million (ppm), which is defined as

1 ppm = 1 volume of gaseous pollutant/ 10^6 volumes (air + pollutant)
or 0.0001 percent by volume = 1 ppm.

Assuming ideal-gas behavior, the conversions can be made with

$$\frac{m_p}{V} = ppm\left(\frac{M_p p}{RT}\right)10^{-6}$$

where m_p/V = mass concentration of pollutant
Mp = molecular weight of pollutant
p = total pressure of the air and pollutant mixture
R = universal gas constant
T = absolute temperature of the mixture

The unit for m_p/V will be kilograms per cubic meter in the SI system. A more common unit is micrograms per cubic meter, we can note: $1kg/m^3 = 10^9$ microgram/m^3

Gases: It is customary to express pollutant concentrations in volumetric terms. The concentration of a gaseous pollutant in parts per million (ppm) is the volume of pollutant per million volumes of the air.

$$\frac{1\ volume\ of\ gaseous\ pollu\tan t}{10^6\ volumes\ of\ air} = 1\ ppm\ (by\ volume)$$

At times, gaseous concentrations are expressed with mixed units of mass per unit volume such as $\mu g/m^3$ or mg/m^3. There is a relationship between ppm (by volume) and mg/m3 depends on the density of the pollutant which depends on its pressure and temperature and molecular weight (mol wt).

$$mg/m^3 = ppm \times \frac{1m^3 pollu\tan t/10^6 m^3 air}{ppm} \times \frac{mol\ wt\ (g/mol)}{22.4\times10^{-3} m^3/mol} \times 10^3 (mg/g)$$

$$mg/m^3 = \frac{ppm \times mol\ wt\ (g/mol)}{22.4} (at\ 0^0 C\ and\ 1atm)$$

$$mg/m^3 = \frac{ppm \times mol\ wt}{22.4} \times \frac{273}{T(K)} \times \frac{P(atm)}{1\ atm} (at\ other\ temperature\ and\ pressures)$$

Masters, M. Gilbert, Introduction to Environmental Engineering and Science, Prentice Hall, Inc., New Jersey, 1991, pp. 4

Table E1 Mass concentration of several main pollutants at different temperatures.

Pollutant	Mass Concentration (microgram/m^3) at 0^{0}C	Mass Concentration (microgram/m^3) at 25^{0}C
Carbon monoxide (CO)	1250	1145
Nitric Oxide (NO)		1230
Nitrogen Dioxide (NO_2)		1880
Ozone (O_3)	2141	1962
PAN [$CH_3(CO)O_2NO_2$]	5398	4945
Sulfur dioxide (SO_2)	2860	2620

VITA

Thang Dam was born in Sai Gon City, Vietnam. He studied in Hoang Hoa Tham high school from 1976-1979. After arriving in the United States on October 17, 1989, he worked as a beekeeper for 3 years. Then, he studied and got work-study as a biology and chemistry laboratory assistant in Cypress College, California from 1993-1996. Mr. Dam began his undergraduate studies in the University of California, Riverside from 1996-1999. In Riverside, he joined three vehicle challenges: propane challenge, Ethanol challenge with Chevrolet Malibu and Silverado in CE-CERT. He received his Bachelor of Science degree in Environmental Engineering in May of 1999 from the University of California, Riverside. His academic focus was in air quality control technologies and emissions modeling. As an undergraduate, Mr. Dam worked part-time at CE-CERT from 1996 through 1999. His work experience has included research and data acquisition in renewable energy and fuels, particularly partial oxidation reformer as a fuel conversion device. In the summer of 1998 he was employed at Ford Motor Company, Division of Environmental Engineering, where he performed vehicle emissions research. After graduation, he continued to pursue a Master of Science degree in Engineering Science in the University of Tennessee Knoxville and received graduate research assistantship at Oak Ridge National Laboratory from 1999 to 2001. Finally, he graduated and received his Master of Science in Engineering Science and additional certification in hybrid electric vehicle in December 2001.